Soft Lithography applied to the construction of a low-cost bioassay system

DISSERTATION

zur Erlangung des Grades eines Doktors

der Naturwissenschaften

der Fakultät für Mathematik und Physik

der Eberhard-Karls-Universität zu Tübingen

vorgelegt von

SEBASTIAN LANGE

aus Tübingen

2004

Tag der mündlichen Prüfung: 26.11.2004

Dekan: Professor Dr. P. Schmid

1. Berichterstatter: Professor Dr. D. Kern

2. Berichterstatter: Professor Dr. S. Dübel

3. Berichterstatter: Professor Dr. J. Wachtveitel

Abstract

The importance of simple, fast, and inexpensive analysis tools for diagnostic marker molecules in patients' sera will increase in the near future. Today's analysis devices for immuno diagnostics or DNA tests are by far too expensive and are thus rarely found in doctors' offices and hospitals. Furthermore, the disposables and carriers for the biotests are fabricated in complicated and cost-intensive processes.

It was the goal of this work to setup an analysis device for the detection of molecular binding events employing a CD-pickup from conventional CD players. Additionally, simple and fast methods for the structured immobilization of biomolecules such as proteins or DNA were created, evaluated and improved.

These developments aim at establishing a low-cost platform technology for the analysis of patients' sera, which includes a fabrication method for affordable test carriers such that they could be used on a routine basis in doctors' offices and hospitals.

Zusammenfassung

Die einfache, schnelle und billige Analyse von diagnostischen Markermolekülen in Patientenseren wird in den kommenden Jahren eine immer größere Bedeutung gewinnen. Aktuelle Analysegeräte zur Messung von Immunoassays, d.h. molekularen Bindungsreaktionen und zur DNS Analyse, sind noch unverhältnismäßig teuer und daher nicht umfassend einsetzbar. Weiterhin werden die Analyseträger derzeit in komplizierten und Kosten intensiven Verfahren hergestellt, was natürlich den damit durchgeführten Test stark verteuert.

Ziel der vorliegenden Arbeit war die Entwicklung eines Prototyp Analysegerätes, aufbauend auf einem einfachen CD-Lesekopf, zur Erkennung biomolekularer Interaktionen. Des weiteren wurden Methoden zur einfachen strukturierten Aufbringung von Proteinen, sowie DNS Molekülen gefunden, weiter entwickelt und verbessert.

Auf diese Weise sollte so eine low-cost Plattform für die Analyse von Patientenseren auf Immunmarker oder genetische Defekte sowie eine Methode zur Herstellung von geeigneten Testträgern entstehen. Diese low-cost Plattform eignet sich für den Einsatz in Arztpraxen und Krankenhäusern.

Learn from yesterday, live for today, hope for tomorrow.

The important thing is not to stop questioning.

- Albert Einstein -

Table of Contents

Abbreviations

Ab	-	antibody
AFM	-	atomic force microscope
AP	-	alkaline phosphatase
APTMS	-	amino propyl tri methoxy silane
APTS	-	amino propyl tri ethoxy silane
BSA	-	bovine serum albumin
bBSA	-	biotinylated BSA
CD	-	compact disc
CRP	-	C - reactive protein
DAB/Co	-	diaminobenzidine / cobalt
ddH$_2$O	-	double distilled water
DI-water	-	de ionized water
DNA	-	Deoxy nucleic acid
dsDNA	-	double stranded DNA
DVD	-	digital versatile disc
ECT	-	eicosane thiol
ELF	-	ELF-97 fluorescent substrate
ELISA	-	enzyme linked immunosorbent assay
EM	-	electron microscope
FITC	-	fluorescein iso thio cyanate
FWHM	-	full width at half maximum
GAPS	-	gamma amino propylsilane
HDT	-	hexadecane thiol
HPLC	-	high performance liquid chromatography
HRP	-	horseareadish peroxidase
IgG	-	immuno globulin G
μCP	-	microcontact printing
μFN	-	micro fluidic network
μTAS	-	micro total chemical analysis system
NHS	-	n-hydroxy succinimide
Oligo	-	oligonucleotide
PBS	-	phosphate buffered saline
PCR	-	Polymerase Chain Reaction
PDMS	-	Polydimethylsiloxane
PLL	-	poly-L-lysin
POD	-	peroxidase

RNA	-	ribo nucleic acid
SAM	-	self assembled monolayer
SDS	-	sodium dodecyl sulfate
SSC	-	saline sodium citrate
TE	-	Tris EDTA
TRITC	-	tetra methyl rhodamine iso thio cyanate
v.d.W.	-	van der Waal

1. Introduction

1.1. Motivation

Bioanalytical tools have become increasingly important in recent years. For example, advancements in biochip technology and increasingly sophisticated applications in molecular biology, especially in the pharmaceutical industry, have driven demand for high-throughput screening of molecular targets. Various research and investment reports published by Frost & Sullivan[1], Front Line Strategy Consulting[2], and Ernst & Young[3] predict a several billion dollar market for Deoxyribonucleic acid (DNA) and protein chips within the next few years.

These sources suggest that biosensors, bioassays, and bioanalyzers, will become even more important as the scientific advance steadily reveals functions within the complex human organism. With the increasing knowledge of molecular and chemical processes and, similarly, improved understanding of disease, the ability to find cures for menacing diseases grows. To locate new pharmacologically active molecules, nowadays a huge number of chemical compounds has to be screened for interactions with potential disease-related molecules or cellular compounds. One way of speeding up this screening procedure is to use arrays of thousands of molecules immobilized to the surface of solid substrates and to screen them for specific interactions with disease related molecules extracted from cell or tissue samples. This potentially more effective search technique has generated attention among researches and pharmaceutical companies. As a result, there has been increasing demand for such high-throughput applications at the beginning of the new millennium. Accordingly, investigations into new screening technologies have increased with no indication that demand for such applications has abated.

It is not only the search for clinically relevant substances that drives the development of assay platforms, but also the elucidation of the genetic information, that is, the genes and their sequence, involved in the diseases. Since the unveiling of the human genome in 2001 by the International Human Genome Project [Lander, 2001] and C. Venter et al. [Venter, 2001], great interest has developed in the effort to attribute gene sequences to the function or dysfunction of proteins and to specific expression patterns. With the use of microarrays, that is, arrays of thousands of DNA probes

---

1) Frost & Sullivan, www.frost.com

2) Frontline Strategy Consulting, www.frontlinesmc.com

3) Enst&Young, www.ey.com

attached to carrier substrates, differences in genetic expression patterns can be investigated in various organs, tissue or fluid samples from a diversity of species.

In contrast to the high-density molecule arrays that are used for pharmacological screening purposes or genetic expression studies, low density arrays of molecules are increasingly used for the development of diagnostic platforms. These platforms target improved diagnosis in patient care as increasingly demanded by contemporary physicians and other, hospital based, practitioners. Of special interest are particular parameters for optimal diagnoses of immunologic and cardiac disorders, as well as bacterial infections.

Microarrays of DNA molecules or proteins can be fabricated by a number of different techniques. Developed early and still the major technique for arraying DNA molecules (as well as proteins) is the ordered deposition of DNA molecules from micro drops by either solid pin printing or by piezo nozzle dispensing. A different approach for the production of DNA arrays is the in-situ-synthesis of short DNA molecules (oligonucleotides) by light directed deprotection of reactive end groups of the molecules using photolithographic masks [Fodor, 1991]. Newly developed techniques rely on the flexible concept of digital light processing mirrors (DLPs) to direct the light to the site of deprotection [Baum, 2003; Singh-Gasson, 1999]. Although developed to a high standard, these microarrays still await an inexpensive production technology such that they can be used routinely in clinical diagnostics.

Furthermore, a weakness in modern day molecular diagnoses is the detection technology in use. Detection is most often based on using fluorophores as labels to visualize binding events for the detection with confocal fluorescent scanners or microscopes. Fluorescence is sensitive yet prone to errors due to bleaching of the fluorophores. Other methods employ electronic or label-free detection schemes. Problems common to all these detection techniques include their relatively high expense, their usefulness only in low-density applications, and their intrinsic difficulties in handling.

The development of a low cost solution for the production of molecule arrays as well as a reliable detection method combined with an inexpensive readout technology could help improving clinical and patient based diagnoses as well as future drug development.

1.2. Goals of this work

For the reasons given, it was the goal of this thesis to find new strategies for setting up an assay system that circumvents the shortcomings of currently available technologies and present a less expensive and faster alternative of performing biomolecular and diagnostic testing.

The protocols suggested in this work setup include methodologies for the rapid patterning of surfaces with relevant biomolecules and the use of a novel detection and readout device, including new ways of labeling molecular binding events. Together these components constitute a reasonably cheap assay system that could potentially be used in diagnostic testing.

In the first approach, a recently developed technique called "softlithography" was chosen for patterning of the substrate surfaces with molecules of interest. In this work a special focus was set on establishing a novel method for patterning DNA molecules. In addition to that, this novel method was developed further and made "intelligent" in order to reduce array fabrication time and, hence, costs.

The goal of using a completely novel detection method was to be achieved by using the core element of a conventional compact-disc (CD) player, the CD-pickup head, as the detection unit for micrometer sized molecular recognition events. To fit the needs of the detection apparatus, new labeling methods had to be evaluated. The focus in this investigation was set on labeling strategies resulting in solid precipitates detectable by the CD-pickup.

The objective of this thesis is to contribute to the challenging task of developing an inexpensive and easy-to-use assay system for detecting biomolecular interactions, including the setup of a prototype readout device and the performance of initial tests. Integrating nano- and bio-technological methods as well as using well-established and thoroughly tested technologies from the entertainment industry might be a way of creating synergies and thus combine the advantages of the different fields.

2. Background & Theory

This chapter is dedicated to the presentation of basic principles, methods and technologies as well as theoretical considerations important for the understanding of the experiments performed during this thesis.

At first, the method of "soft lithography" for patterning surfaces with biomolecules is introduced (Section 2.1.). Furthermore, emphasis is put on illuminating the physical, chemical, and biochemical aspects of soft lithography. In Section 2.2. a novel concept for building an inexpensive but high-resolution surface-imaging tool is presented and the basic physical and technical features of this device are discussed. The biochemical and biophysical concepts for modifying or functionalizing surfaces as well as fundamental biomolecular concepts are introduced in Section 2.3. Finally, the strategy and the theoretical background for detecting and measuring the binding of molecules to specific surfaces is presented in Section 2.4. Together, these chapters are intended to give the reader a profound understanding of the experiments discussed in Chapter 3.

2.1. Softlithography of biomolecules

The word lithography is derived from the two Greek words *lithos = the stone* and *graphein = to write*. Lithography was invented in 1798 by A. Senefelder who found out that after patterning a limestone with oily chalk and subsequent inking this same wet stone, the black color only remained at places where chalk served as an "adhesion promoter". He was then able to transfer the such created pattern to a piece of paper by pressing the stone firmly onto that paper.

Since this initial demonstration many different variants of the original lithographic method were developed. Lithographic techniques are nowadays extensively used in the printing industry as well as in the semiconductor industry. For the latter, a photosensitive resist on top of semiconducting substrates is illuminated through a photolithographic mask. After developing the activated resist structure and subsequent etching the underlying substrate the mask pattern is transferred into the semiconducting material. Today, circuits with structures down to the size of a few hundred nanometers and even below are manufactured using photolithography.

Instead of using "hard" lithographic masks to shield the resist from being exposed by the light, soft lithography employs an elastic, that is, "soft", material to transfer and reproduce a pattern. Soft lithography as a method to pattern molecules onto surfaces was originally developed by the group of Prof. G. Whitesides at the Harvard Medical School in Boston [Kumar, 1993] and was further worked

on by the IBM research group at the IBM research lab around Dr. B. Michel. These groups used the soft, elastomeric, and transparent polymer poly(dimethylsiloxane) (PDMS) to transfer molecules from an inking solution to specific sites on a target surface [Biebuyck, 1997].

PDMS is polymerized from its liquid precursors (Compound A and B) either thermally using a platinum catalyst (Figure 1) or under UV light through radical initiator compounds. The polymer can be cured against a solid surface (master), resulting in a very accurate inverted replica of the surface topography (relief structure) of this master. A PDMS replica, also called a "stamp", cast from a 3D-master can be used quite similar to a common office stamp that delivers ink as a pre-defined pattern to a target surface. Various blends of PDMS found widespread use in the contact lens industry and also served as a base material for surgical implants.
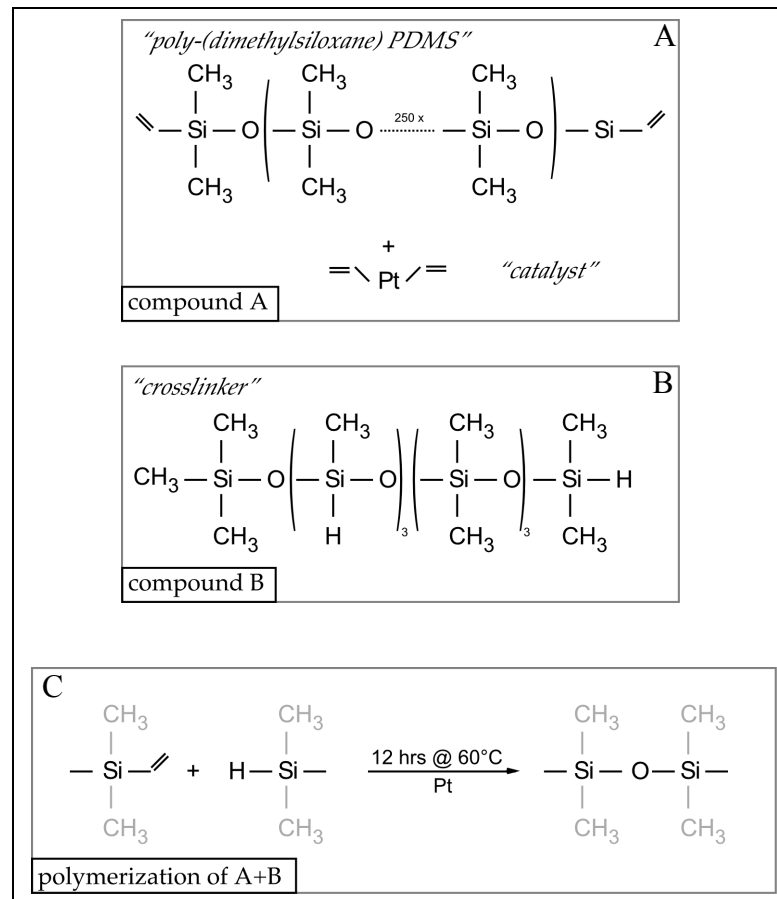
Figure 1: Chemical structure of the two compounds of poly(dimethyl-siloxane) (A,B) and schematic diagram of the polymerization process (C)

The key property of PDMS for soft lithography is its ability to come into a very close and intimate contact to the target surface onto which it is applied. A so-called "conformal" contact takes place (Figure 2 A, B). The molecules from the ink solution, with which the stamp is decorated, are sandwiched between the PDMS and the target surface. The definition of this conformal contact in high-resolution printing goes beyond contact between two hard, macroscopically flat but microscopically

rough, surfaces (that is, when a glass mask is pressed onto a resist surface). Conformal contact comprises first, the macroscopic adaptation to the overall shape of the substrate and second, the microscopic adaptation of a soft polymer layer to a rough surface, leading to an intimate contact without voids. Adhesion forces mediate this elastic adaptation, and even without applying external pressure, an elastomer can spontaneously compensate for some degree of substrate roughness, depending on the material's properties.
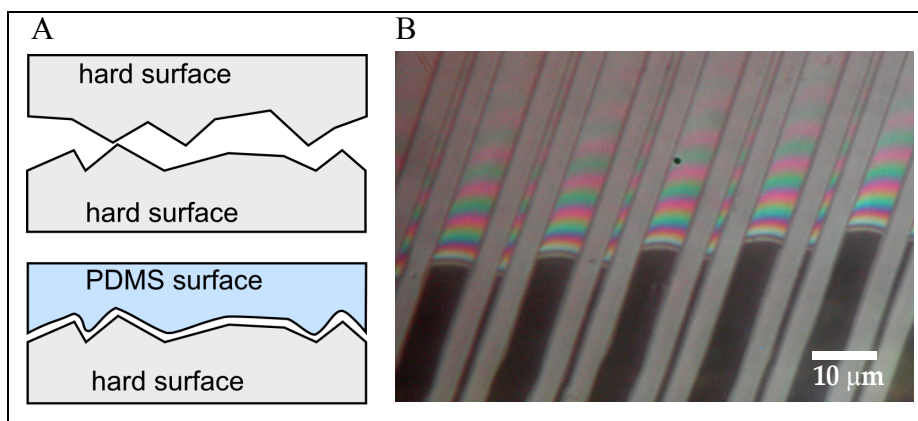
Figure 2: (A) Hard contact vs. conformal contact on a molecular level. (B) Micrograph of stamp forming intimate molecular contact. The lower part of the stripes showing the dark color is already in contact with the surface, whereas the upper part of the stripes is very close to the surface but not yet in contact. This vicinity leads to the phenomenon of colored Newtonian Rings visible where two surfaces come in close contact.

As PDMS is a chemically rather inert polymer (siloxane chemistry), it does not react with many other materials. However, during the polymerization process, reactive groups are present and therefore the materials used as templates (masters), such as silicon, metals or plastics, must have low energy and appropriately rendered hydrophobic surfaces using fluorination methods. Fluorination is typically done by exposing a master to the vapor of perfluorinated alkylchlorosilanes (such as CF_3-CF_2-CH_2-$SiCl_3$ or similar).

2.1.1. Properties and characteristics of PDMS

Reliable and repeatable conformal contact and defect-free separation of the elastomer from the surface requires the following three features:

i) a relatively low and defined Young's modulus and high toughness to avoid local overload and defects caused by brittle failure of vulnerable features

ii) a rubber-elastic behavior to allow stamps to recover their original shape even after having undergone significant strain (>25%)

iii) a low work of adhesion to allow the stamp to separate from the substrate at low force and to prevent the sticking of particles to the substrate.

The commercially available PDMS material of choice for µCP is Sylgard 184 from Dow Chemicals. It has a Young's modulus of 2.5 MPa and a work of adhesion of 0.1 J/m^2 [Michel, 2001; Bietsch, 2000].

PDMS is a remarkable and versatile chemical and has a further useful quality: Channels molded in the polymer material, initially open, are self-sealing and thus form closed channel structures that can be used to guide fluids over surfaces. This sealing is reversible such that a network of channels can be reused to flow fluids across several surfaces.

It has been shown that it is possible to replicate features as small as 60 nm and use them to transfer molecules onto surfaces [Bernard, 1998]. One has to bear in mind, however, that for a successful transfer of the desired pattern of molecules, the stability of the three dimensional structure of the stamp is vital. The intrinsic elasticity of the elastomeric stamps is responsible for a feature that can be observed during the application of a stamp to a surface. Once brought into contact with the target surface due to the adhesive forces the three dimensional patterns undergo certain deformations. Thus stamps are only stable to some extent. The elasticity of the polymer can be modulated in a wide range: The ratio of base and crosslinker, the chain length of the pre-polymer and the addition of filler materials such as small nanometer sized glass beads or fibers are handles to fine-tune the rubber-elastic properties of the elastomer. However, beyond a certain aspect ratio (AR) the structures tend to collapse during conformal contact establishes. The AR is defined by the ratio of the structure width to the structure depth. For the material used in this work the maximum aspect ratio is roughly 10:1. This number could be improved by making the elastomer mold more rigid by either using harder material or by improving the rigidity of the supporting structure e.g. by adding a solid backplane to the thin elastomer layer. Furthermore, to avoid the contact of larger areas of the stamp's recessed structures with the target surface, a low aspect ratio (<10) pattern can be designed such that pillars or ridges have supporting character and hence do not collapse during contact. Figure 3 shows an optical micrograph of a collapsed stamp structure. It is clearly visible that parts of the stamp ("collapsed area") not intended to form contact are actually touching the surface. Only the lines to the right, the dots at the bottom and the alignment crosses were supposed to undergo conformal contact. However, due to the high AR of the design the large unsupported structures collapsed.

In the following chapters two strategies for patterning biomolecules such as proteins (e.g. enzymes or antibodies), or DNA onto specially tailored surfaces using PDMS will be described.
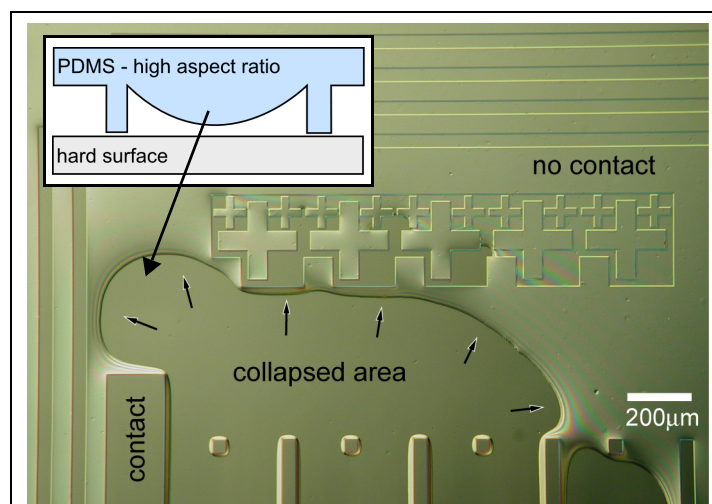
Figure 3: Micrograph of a partially collapsed elastomeric stamp. The darker areas in the lower part of the stamp are already, but unintended, in contact with the substrates' surface. Newtonian Rings indicate the proceeding contact line (arrows).

2.1.2. Microcontact Printing (µCP)

Printing approaches regained attention when in 1993, Kumar and Whitesides discovered that an elastomer (polymer) inked with an alkane thiol and brought into contact with a gold-coated surface can form a monolayer of these molecules in the areas of contact [Kumar, 1993; Kumar, 1995]. This printing process, called microcontact printing (µCP), prints directly off a patterned elastomeric stamp (Figure 4).
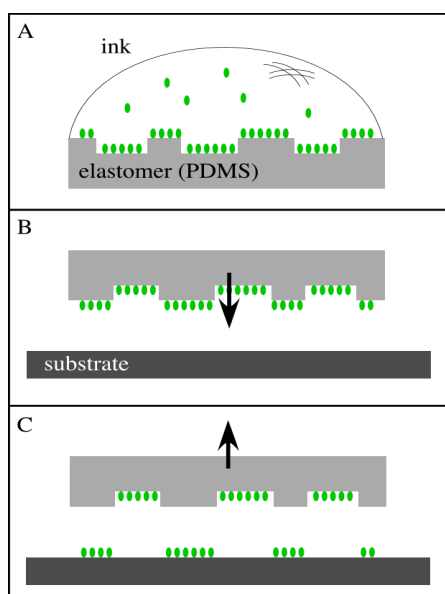
Figure 4: Schematic representation of the steps characterizing µCP. (A) Inking the stamp surface with the molecule-containing solution, thereby forming a monolayer of molecules on the surface. (B) Application of the blown-dry stamp to the target surface forming intimate conformal contact of the protruding features. (C) Removal of the stamp from the surface, thereby leaving behind a pattern of molecules on the surface.

The revolutionary new concept of this process is that it only transfers a molecular monolayer of ink to a surface. The latter renders it insensitive to detrimental wetting and squeezing effects of macro-

scopic amounts of viscous ink between stamp and substrate, and allows the size of printed patterns to be reduced dramatically. Microcontact printing gave rise to the development of a set of related patterning approaches now summarized by the term "soft lithography" [Xia, 1998; Bernard, 2000].

Thiols strongly adsorb to gold surfaces at areas of contact between stamp and surface through the high binding affinity of sulfur to gold. µCP was and still is intensively studied and it has become an important tool for microfabrication purposes. µCP has been applied to:

i)   pattern replication with thiols as etch resists [Biebuyck, 1997],

ii) controlling the deposition of metal films and clusters [Geissler, 2003],

iii) crystal nucleation [Aizenberg, 1999],

iv) wetting [DiMilla, 1994],

v)   protein adsorption [Prime, 1993],

vi) cell growth and guidance [Singhvi, 1994; Mrksich, 1996].

Apart from alkanethiols for transfer onto gold surfaces, other molecules were suggested as candidates to form quasi self-assembled monolayers (SAM) and to be microcontact printed, e.g. alkylsilanes, aldehydes, lipids, or etchants [St. John, 1996].

In the course of an intense research in the field of patterning techniques, the use of µCP has been expanded to printing protein-like polymers such as poly-L-lysin (PLL) onto hydrophillic glass slides [James, 1998] or PLL and poly-D-lysin onto glutaraldehyde-activated amino-silanized glass substrates for patterning in neuronal cell culture [Branch, 1998]. Further development proved µCP to be useful for depositing antibodies onto oxidized silicon [St. John, 1998]. In all these reports, hydrophillic or chemically activated substrates were used as target surfaces to ensure the successful transfer from the stamp. The contact time between stamp and surface was long, from several minutes to one hour. That µCP can be an universal approach to pattern proteins of almost any kind on surfaces without being specifically tailored was shown by Bernard et al.[Bernard, 1998].

An overview of the processes governing the transfer of biological molecules will be given in Section 2.1.5., Section 2.1.6., and Section 2.1.7.

2.1.3. Microfluidic Networks (µFN)

Microfluidic networks are miniaturized channels molded into polymer slabs. The relief structure in the mold forms a network of empty channels. Here, the elastomer constitutes three sidewalls of the conduits that guide a solution, the fourth sidewall being the solid substrate to be patterned. These channels exhibit unique properties and enable new ways of fluid handling and probe delivery. A prerequisite for such a channel is that the elastomer placed on the substrate seals perfectly at the inter-

face between the two materials. As outlined above (2.1.1.), PDMS is such a material forming intimate (conformal) contact to a macroscopically flat substrate. The driving force promoting a flow inside a µFN can be:

    i)   capillary action through the wetting of the sidewalls,

    ii) electroosmotic pumping,

    iii) pressure (positive or negative) at the entrance of the channels,

    iv) surface acoustic waves.

Inside the small channels that can have practical dimensions from about half a micron to millimeters, liquids are transported in a laminar flow regime (low Reynold's number). Mixing occurs only through (lateral) diffusion. The flow profile exhibits a Poisseuille[4] shape, leading to zero flow velocity at the borders and highest in the middle. Flow speeds of aqueous fluids reach a few centimeters per second inside a hydrophillic channel [Delamarche, 1998].

Microfluidics has been used extensively to guide chemical and biological solutions to reaction sites in miniaturized chemical analysis chips (µTAS, micro total chemical analysis system) and biosensors [Gopel, 1996]. µFN's made of PDMS were first used by Delamarche et al. in 1997 [Delamarche, 1997] to pattern surfaces with different biomolecules in a parallel manner. Careful design of the µFN structure is necessary to ensure successful delivery of biomolecules over a long path. Clogging of the channels, depletion of target molecules in the guided solution, and leakage under the sidewalls of the PDMS conduits have to be prevented. However, in certain applications, the depletion of reactants in such flowing fluids and the mixing of different fluids in combined channels can have useful effects, e.g. for generating surface gradients of molecules [Caelen, 2000]. µFNs were widely applied to biosensor instruments, either to deliver the sampling fluids to the sensing surface, or to immobilize ligands in array structure for use in multi-array biosensors [Bernard, 2001b]. In addition, µFNs can be used in sequence to increase the complexity of the patterned layers. Up to now, several applications of µFN have been published. They can be used to deliver fluid samples to specific positions on surfaces; fluids can be mixed [Stroock, 2002] in a very effective manner; particles can be sorted [Fu, 2002] or complete immunological recognition assays can be performed [Papra, 2001]. Furthermore, microfluidic structures have been designed to perform PCR reactions in micrometer sized channels [Lagally, 2001]. Even microprocessor-like large scale structures, integrating calculation and storage units, have been built that allowed for fluid computing [Thorsen, 2002]. All these efforts together will eventually be integrated into a single "Lab on a chip" analysis

---

4) The Poisseuille shape of a flow can be derived by solving the Navier-Stokes equation.

system. The advantages of µFN-based assays over common macroscopic bulk assays can be summarized as follows:

i)   Through their miniaturized dimensions diffusion driven and limited biochemical reactions occur much more rapidly.

ii) Consumption of precious molecules are low.

iii) Whole bioassays from probe purification to quantification and analysis can be integrated through the minute dimensions [Burns, 1998].

iv) Through the design of hydrophillic and hydrophobic regions in the channel the fluid flow in the network can be altered and regulated, thus creating valves and "programs" for fluid flow.

v)   Channels can be made self-filling, thus no pumps or external valves are necessary [Juncker, 2001].

In this work, µFN's are used to pattern target surfaces with different DNA probes. Two ways of achieving this exist. First, an elastomeric µFN can be sealed to a glass surface. Sample fluid is then injected into the filling pad areas and by capillary forces guided through the channel, thereby depositing proteins, DNA or other molecules to the surface (Figure 5A). The second possibility is to use a µFN micromachined in a hard material (e.g. silicon) and cover the channels with a flat slab of PDMS. Then again the fluid is passed through the channels and deposits its load in the form of stripes onto the flat elastomer. The such patterned flat stamp can then be used to transfer the molecules to the target surface by means of contact printing (Figure 5B and Section 2.1.7.)
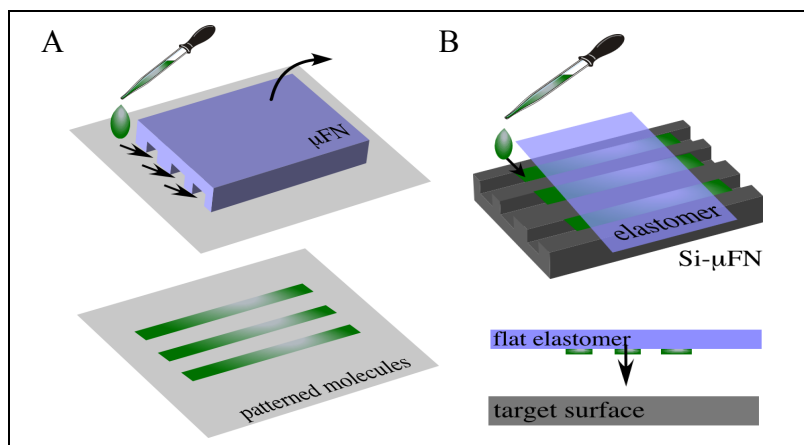

Figure 5: Using two different types of µFN's to pattern surfaces with molecules. (A) Channels molded into elastomer guide fluid directly on target surface. (B) Flat elastomer slab is patterned by guiding fluid through micromachined silicon µFN. Then patterned molecules on elastomer are microcontact printed onto target surface.

2.1.4. Intermolecular forces acting on molecules at the solid liquid interface

The characteristic of the adsorption of molecules from a solution onto a solid substrate at the solid liquid interface depends very much on the forces acting on these molecules. Due to the variability of the chemical structure of the molecules and their physico-chemical properties these forces can be of very different natures. In this section, some of the forces involved in the adsorption process are discussed and the underlying physical principles are outlined.

2.1.4.1. Covalent chemical bonds

Covalent bonds that form during chemical reactions have their origin in the complex quantum mechanical interactions between atoms. They are highly localized and specific. In the liquid environment though and without reactive groups present they do not form spontaneously and thus play a secondary role for adsorption of molecules to surfaces. Binding energies of covalent bonds reach from 350 kT[5] for the C≡N triple bond in e.g. KCN, 276 kT for the a C=O double bond, 144 kT for a C-C single bond to 60 kT for the F-F bond in F_2 [Israelachvili, 2000].

2.1.4.2. Electrostatic charge-charge interactions (Coulomb interaction)

Molecules strongly interact with surface bound charges according to their own local charge distribution. Especially in solution the electrostatic interactions play a major role for the adsorption of molecules. The strength of the interaction is governed by the Coulomb law, which states that the force between two oppositely charged entities decays with the square of the distance to each other (Eq. 1). These forces are by far the strongest forces to be considered when looking at surface interaction forces. They are even stronger than some of the chemical binding forces.

$$F_{el}(r) = \frac{q_1 q_2}{4\pi\varepsilon_0\varepsilon_r} \frac{1}{r^2}, \tag{1}$$

where q_1 and q_2 are the charges of the two objects, ε_0 and $\varepsilon_0\varepsilon_r$ are the permittivities in vacuum and in medium and r is the distance between the two charged objects. The potential is given by the integral of Eq. 1,

$$U_{el}(r) = -\int_\infty^r F_{el}(r)dr' = \frac{q_1 q_2}{4\pi\varepsilon_0\varepsilon_r} \frac{1}{r} \tag{2}$$

The attractive energy between two oppositely charged ions can be as big as *200 kT*. This compares well with the strength of covalent bonds which have binding energies from *100* to *500 kT*. The topic

---

5) kT is the abbreviation for k_BT the energy equivalent to 1/40 eV at 293 K further conversions are:
(1kJ/mol ≈ 0,4 k_BT ≈ 1/100 eV); (1eV ≈ 40k_BT ≈ 100kJ/mol); (1k_BT ≈ 1/40eV ≈ 2,5 kJ/mol) for T=293 K

of electrostatic interactions also includes dipole-dipole, or charge-dipole interactions. However, these interactions are much weaker and are most often superimposed by the stronger charge-charge interactions and are thus omitted in this overview.

2.1.4.3. Van der Waals forces and Lennard-Jones potential

The van der Waals (v.d.W.) forces are rather complex to describe, yet important, as they are involved in many biological processes such as protein folding, DNA hybridization or molecular recognition. They can act over large distances (nanometers) or only have small reach (Ångstrom) and they can be attractive or repulsive depending on the partners involved. For polar molecules there are three forces that contribute to the v.d.W interaction. These are the induction force[6], the orientation[7] and the dispersion force[8]. Each of them follows a power law, depending on the inverse of the sixth power of the distance between the interacting molecules r. Thus, the combined attractive potential can be written as [Israelachvili, 2000]:

$$U_{vdW}(r) \sim -\frac{1}{r^6} \tag{3}$$

Combining this relation with the assumption that molecules or atoms can be treated as hard spheres with a certain radius σ, often called the v.d.W radius, and the minimum of the energy $-\varepsilon$, Eq. 3 can be written as

$$U_{LJ}(r) = 4\varepsilon\left[\left(\frac{\sigma}{r}\right)^{12} - \left(\frac{\sigma}{r}\right)^6\right] \tag{4}$$

This is known as the Lennart-Jones potential and is a more general description for the pair potential between atoms or molecules. It combines the repelling atomic potential (hard sphere model) and the attractive van der Waals potential. Figure 6 gives an impression of the behavior of this potential with regard to the separation between two molecules.

2.1.4.4. Hydrogen bonds

Polar molecules with an inhomogeneous electron distribution depending on the electronegativity of the constituting atoms, such as e.g. water molecules, have a weak, partial negative charge in one part of the molecule (the oxygen atom in water attracts electrons) and a partial positive charge elsewhere (the hydrogen atoms in water donate electrons). Thus, when water molecules are close together, their

---

6) The induction forces result from the interaction between a permanent dipole of one and a temporary dipole of another molecule.

7) The orientation forces are initiated by the interaction between permanent dipoles.

8) In molecules the electron distribution can be distorted and thus induce a dipole moment, which in return can assert a force on other molecules. With increasing size of the molecule the polarizability increases and so does the dispersion force. It is thus a force induced by the interaction between temporary dipoles and induced dipoles.

positive and negative regions are attracted to the oppositely charged regions of nearby molecules and form so called hydrogen bonds. In the liquid state, for example, each water molecule is sharing hydrogen bonds with four others.
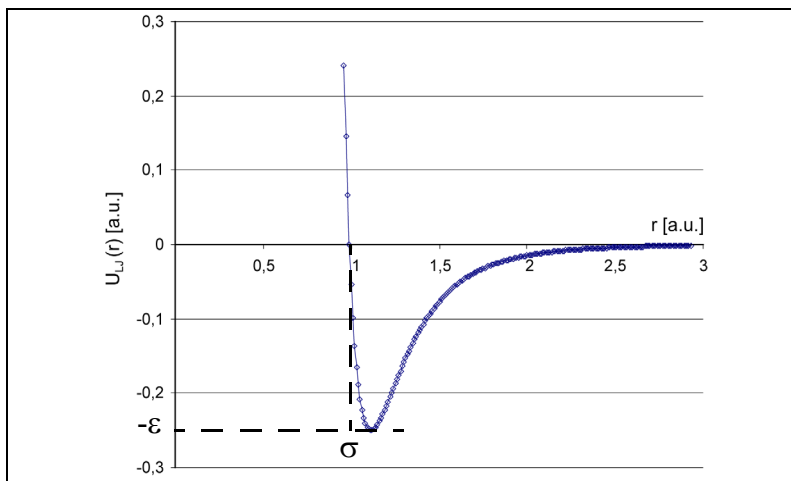

Figure 6: Graph of the Lennard-Jones pair-potential (calculated from Eq. 4). Characteristic values for this potential are $U_{min}=-\varepsilon$ and $U(\sigma)=0$.

Hydrogen bonds in general have binding energies varying from 4 to 16 kT (10 - 40 kJ/mol). The exact description of the interaction free energy, that is, the potential, is difficult but it was found that the potential is roughly proportional to the inverse square of the radius [Israelachvili, 2000]:

$$U_{OH}(r) \sim -\frac{1}{r^2} \tag{5}$$

Hydrogen bonds play a major role in the binding of two complementary DNA strands. Each nucleotide is capable of forming hydrogen bonds with its appropriate counterpart. Hence, base pairing is in fact mediated by hydrogen bonds between the nucleic acids. The nucleic acids adenosine (A) and thymine (T) form two hydrogen bonds; cytosine (C) and guanine (G) form three hydrogen bonds. Adenosin and cytosin, respectively guanine do not form hydrogen bonds at all. Therefore, with its three hydrogen bonds the G-C bond (6 kT) is stronger than the A-T bond (4 kT).

Hydrogen bonds are also involved in forming the secondary structure of proteins, such as alpha helices and beta sheets, and are the major driving force for inter-molecular interactions (e.g. antibody antigen recognition or enzyme - substrate interaction). When it comes to the adsorption of molecules to solid surfaces however, the hydrogen bond plays an inferior role, since the much stronger electrostatic forces dominate the process.

2.1.4.5. Hydrophobic interaction

Norde et al. stated in 1986: "The term hydrophobic interaction refers to the spontaneous dehydration and subsequent aggregation of non-polar components in aqueous environment." [Norde, 1986].

Interactions between polar water molecules are much more favorable than interactions between water and non-polar groups, thus non-polar groups are rejected from aqeous environment. This resembles an attraction of these groups. The hydrophobic effect is characterized by a large change of entropy in the system but merely in enthalpy. The hydrophobic interaction can thus be seen as an entropy and not energy driven effect. Due to the small size of water molecules the range over which these "forces" act is only a few Ångstroms. However, the hydrophobic interaction plays a major role in many surface related phenomena such as protein adsorption or monolayer formation on hydrophobic surfaces.

	Potential	Range [m]	free Energy ΔG [k_BT][a]	free Energy ΔG [eV][b]
covalent bonds	--	10^{-10}	100 - 350	2.5 - 8.7
electrostatic interaction	$U_{el} = \dfrac{q_1 q_2}{4\pi\varepsilon_0\varepsilon_r}\dfrac{1}{r}$	10^{-9}	<200	< 5
v.d.W interaction	$U_{LJ}(r) = 4\varepsilon\left[\left(\dfrac{\sigma}{r}\right)^{12} - \left(\dfrac{\sigma}{r}\right)^{6}\right]$	10^{-10}-10^{-9}	0.8-1.6	0.02 - 0.04
hydrogen-bonds	$U_{OH}(r) \sim -\dfrac{1}{r^2}$	10^{-10}	4-16	0.1 - 0.4
hydrophobic interaction	--	10^{-10}	<10	<0.25

Table 2.1. List of potential inter- and intra-molecular interactions (compiled from Israelachvili [Israelachvili, 2000]).

a. ΔG [k_BT]$\approx$ 0.4 $\cdot\Delta G$[kJ/mol] for T=298 K

b. ΔG [eV]$\approx$ 1/40 $\cdot\Delta G$[k_BT] for T=298 K

2.1.5. Adsorption of proteins at the solid-liquid interface

Specific or unspecific adsorption of proteins to surfaces play an integral role in biological life. Many biological processes rely on the interaction of components attached on surfaces with soluble partners. A complex interplay of forces drive and favor the adsorption to "solid objects". Since two partners are involved, their respective charge, polarity, and chemical nature govern the adsorption process, which can result in loose, reversible attachment or strong, almost covalent, bonding.

Proteins consist of one or more polypeptide chains folded into a well defined three-dimensional structure. Each polypeptide chain is built from 20 individual amino acid building blocks. The 20 amino acids vary in their side chain having different size, polarity, or charge. The sequence of the

amino acids in the chain determines the shape and finally the function of the protein. Depending on the composition of amino acids, a protein can have a certain net charge, regions of positive or negative patches and regions of higher or lower hydrophobicity (Figure 7). Furthermore, a protein is not a rigid structure but rather an object of certain elasticity.
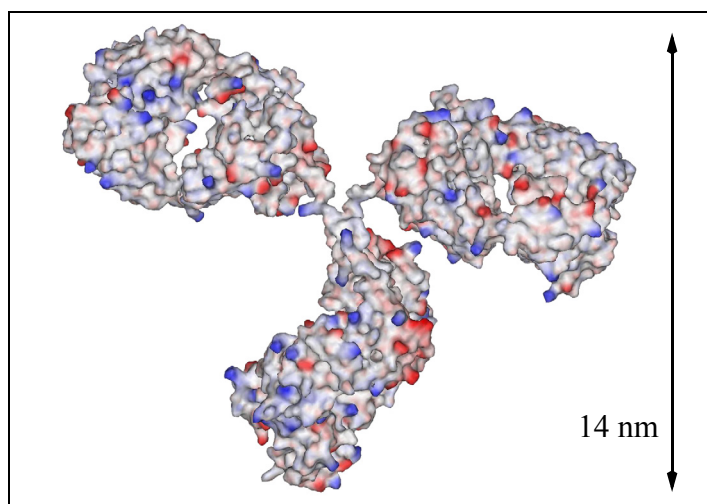

Figure 7: Molecular model of an antibody. Areas with high positive or negative charge density are coded in blue or red, respectively.

Unspecific adsorption of proteins to solid surfaces is commonly thought to be a process where the molecule, upon contact with a surface, adapts its shape or structure to maximize the interaction energy with the surface, such that the probability of unbinding becomes very small. The forces holding the molecule attached can reach covalent strength [Alberts, 1994; Grandbois, 1999].

There are at least two different regimes for the adsorption of proteins. On glass and other hydrophillic and charge bearing surfaces adsorption is governed mainly by electrostatic interactions between molecule and surface. On hydrophobic surfaces, such as PDMS, where charge is absent, adsorption is driven by hydrophobic forces, that is, the displacement of water from the interface between protein and surface [Fragneto, 2000].

It seems as if hydrophobic adsorption is comparably faster than hydrophillic, it only takes minutes to assemble a monolayer on the elastomer surface of PDMS as was observed in experiments described later. Adsorption processes of proteins underlie a self limiting behavior, where the newly formed protein layer is hydrophillic and thus hinders any further adsorption of hydrophillic proteins on top of the first layer. Hence, multilayer adsorption is unlikely, as is corroborated by experimental results, where after long incubation of a surface with labeled proteins or after adsorption from high concentrations a saturation level equivalent to one monolayer is reached (Figure 8). Similar results are also reported by Caelen et al. [Caelen, 2000].
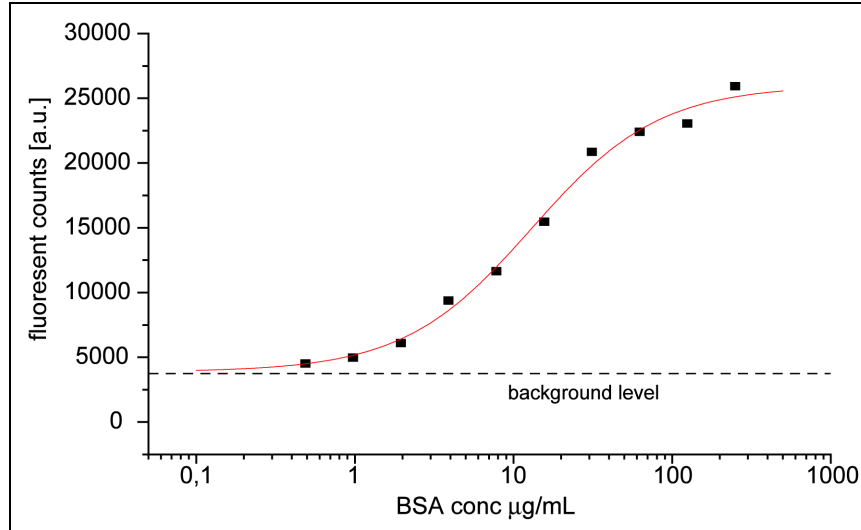
Figure 8: Adsorption curve for different BSA (fluorescently labeled) concentrations in incubating solution. The data was fitted using a sigmoid curve.

Although much slower, proteins also adsorb to hydrophillic surfaces. To be hydrophillic, a surface has to carry positive or negative or both, positive and negative, charges. This charge distribution very much effects how proteins can adsorb to such a surface. To adsorb a protein has to adjust its own charge distribution such that the electrostatic interaction energy is maximized. This structural deformation of proteins (that is, unfolding) during adsorption can have dramatic effects on the functionality of the proteins. Antibodies upon adsorption can loose the ability to bind their target antigens or enzymes can loose their enzymatic activity. It has nevertheless been shown that during μCP proteins or enzymes mostly retain their specific functionalities [Bernard, 2000]. This effect might be attributed to the residual water present on the elastomer surface.

The adsorption rate of proteins to a surface can be modeled assuming an adsorption and a desorption rate. The kinetic equation for this process is

$$\frac{\partial}{\partial t}D_s(t) \ = \ k_a C(t)D_{free}(t) - k_d D_s(t) \tag{6}$$

where $D_s(t)$ is the surface density of adsorbed proteins, k_a and k_d the adsorption and desorption constants respectively, $C(t)$ the protein bulk concentration and $D_{free}(t)$ the free sites on the surface. The solution to Eq. 6 is a first order rate equation exponentially approaching saturation (see Appendix 6.1. for derivation).

$$D_s(t) \ = \ \frac{k_a C_0 D_{0free}}{k_a C_0 + k_d}(1 - e^{-(k_a C_0 + k_d)t}) \tag{7}$$

with C_0 as the initial bulk concentration of the protein and D_{0free} the initial free surface sites.

Such a predicted saturation behavior could be observed by letting fluorescently marked BSA adsorb over prolonged time intervals (Figure 9). Eq. 7 was used to fit the measured values to obtain a saturation value of $D_s(\infty) \sim 7200$ for the $C_0 = 10 mg/mL$ and $D_s(\infty) \sim 5200$ for $C_0 = 1\ mg/mL$. The different values show that for the lower concentration the solution is depleted and a full surface coverage is not reached.

To describe the adsorption behavior even better Calonder et. al. [Calonder, 2001] used a slightly different model where they assume proteins to be hard particles that are capable of undergoing abrupt changes such as unfolding or change in internal configuration upon contact with the surface. Furthermore they included diffusion into their model. However, in principle Eq. 7 is sufficient to give a first impression of the adsorption behavior of proteins on a surface.
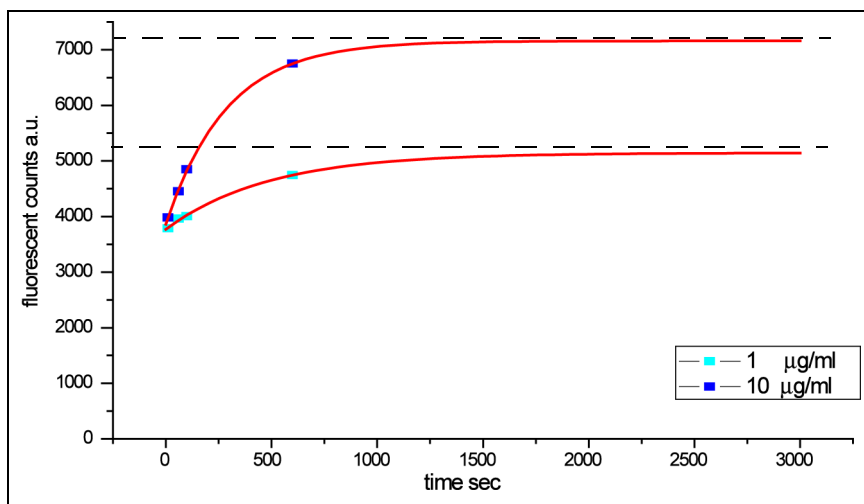

Figure 9: Saturation behavior measured for the adsorption of labeled BSA molecules from solution over time.

2.1.6. Adsorption of DNA at the solid liquid interface

In this section, the electro-chemical properties of DNA molecules and that of modified surfaces and the mechanism of the adsorption of DNA onto such surfaces will be elucidated in greater detail. With respect to that, especially the electrostatic forces play an important role. Other forces are by far smaller and are thus neglected in a first approach to model the adsorption of DNA onto charged surfaces. The models presented here primarily aim at a better understanding of the physical principles involved and mechanisms underlying the experimental findings. This knowledge will finally help to improve the initial experimental protocols for tailoring the surface properties.

2.1.6.1. Electrochemical and mechanical properties of the DNA molecule

DNA can be considered as an acidic polyelectrolyte (polyanion) built from a sequence of the four bases A, G, T, and C. When dissolved in water, a pH-dependent charge results from ionization of the

phosphodiester linkages ($pK_a < 2$) in the backbone. These are deprotonated at a pH > 1 resulting in one negative charge per nucleotide. Individual bases can have charges depending upon their chemical structure. Overall, DNA molecules or oligonucleotides are negatively charged in a wide pH range from 4 to 11 (Figure 10).
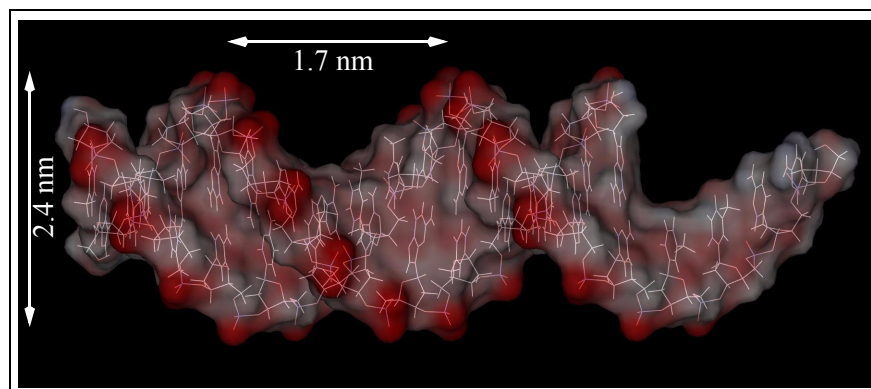

Figure 10: Model of a DNA molecule, showing the atomic isosurface with the charge distribution coded in color; red marks parts with strong negative potential, blue those with positive potential. The diameter is roughly 2.4 nm and the helical increase per base pair is 0.34 nm.

Hydrophillic surfaces present local charges but need not carry a net charge and should thus not favor DNA adsorption at all, because the molecules are not able to adjust their shape and their charge distribution such that the interaction is strong enough to bind the molecule. Adsorption rates to hydrophillic surfaces such as glass surfaces should be low. Indeed, as will be shown in the experimental section, adsorption of DNA to plain glass surfaces is low. In fact such surfaces have to be made positively charged to render them attractive to DNA binding and to increase DNA retention. For such surfaces, adsorption of the negatively charged DNA molecules is governed by the laws of the electrostatic interaction of charged particles.

Through chemical modification a glass surface can be rendered positively charged, e.g. by attaching chemical groups such as amines. In buffer solution with a pH above the surface pKa of the amines, DNA molecules will be attracted to the positive surface and adsorb firmly (Figure 11). The exact dependence of the charging with respect to the pH of the buffer will be discussed in the next section.
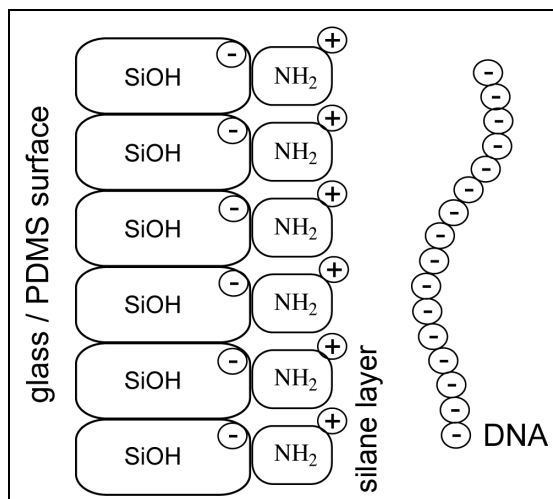
Figure 11: Schematic representation of the charge distribution of the chemical groups in the substrate- and stamp surface and the DNA molecule.

2.1.6.2. Modeling the surface charges of amine glass and PDMS surfaces

It has been reported [Carre, 2002; Carre, 2003] that a clean glass surface has a density of roughly 2.5 nm^{-2} of free SiOH groups (silanol). After O_2-Plasma treatment PDMS should have approximately the same surface density of SiOH groups, because its surface composition is very similar to that of glass.

It has further been shown that grafting amino silanes such as amino-propyl(tri-ethoxy-silane) (APTS) affects 30 to 50% of the available reactive silanol groups [Carre, 2003; Vansant, 1995]. Thus, the surface density of amine groups can be roughly estimated to be *1.25 groups/nm^2*. To put these estimated values on a more solid ground, it is useful to calculate the maximum density of amine molecules that fit onto a surface when assuming a tight packing.

The *tri-ethoxy-silane* (such as APTS) shows tetraedrical (sp³) Si configuration with bond lengths of approximately *0.18 nm* for the Si-O and Si-C bonds. The angle between the individual bonds is ~120° [Röhr, 1999]. The distance between two adjacent oxygen atoms of the silane molecule is *0.268 nm*. These values suggest a size for the minimal unit cell of *0.25 nm^2* and from that the surface density for a closely packed monolayer of silanes should be determined to be ~4 silanes per nm^2. Remembering that each silane can carry in principle one amine group and thus one positive charge, *4 q^+/nm^2* would be the maximum density of positively charged groups introduced on the surface. However, this maximum density will only be reached for a full monolayer of silane molecules on the surface. Taking into account that only *30-50%* of the silanol groups are modified the final charge density would rather be in the range of *~1-2 q^+/nm^2*. With the assumption of similar surface chemistry after equal treatment, it is plausible to expect a glass and an elastomer surface having a comparable number of charged groups. The surface pK_a of functionalized surfaces can be experimentally

determined by measuring the advancing and receding contact angle of buffer solutions at different pH [Bain, 1988; Carre, 2003].

It is important to note that only a fraction of all amine and silanol groups is deprotonated (O⁻) respectively or protonated (NH_3^+) at a given pH yielding a charged surface. The equilibrium constant for the protonation of amines is K_a=5.78x 10^{-11} and the pK_a is 9.6.

The mathematical description for this effect is given by the Hendersson Hasselbalch equation, which can be written for weak acids:

$$pK = pH - \log\left(\frac{\alpha}{1-\alpha}\right),$$

(8)

where α is the degree of dissociation. Solving Eq. 8 for the dissociation coefficient α, multiplying it with the surface density of the potentially charged groups and summing over all charged groups results in

$$\rho_{total\text{-}charge\text{-}density}(pH) = \sum_i \frac{10^{(pH-pK_{a,i})}}{1+10^{(pH-pK_{a,i})}} \rho_{surface,i}$$

(9)

Taking the dissociation values for $SiOH \rightarrow SiO^-$ ($pK_a \approx 6$) and that for $NH_2 \rightarrow NH_3^+$ into account the total charge density will be

$$\rho_{total\text{-}charge\text{-}density}(pH) = -\left|\rho_{SiO^-}\right| + \left|\rho_{NH_3^+}\right|$$

(10)

The total charge density will be zero at approximately pH 8. Hence, below pH 8 the surface charge will be dominated by the amonium ions and leads to a net positive charge of the surface. For pH 6 the total net charge density will be approximately *+1.5 q⁺/nm²*. The calculated behavior of the net charge of an amine modified surface is depicted in Figure 12 and is confirmed by measurements done by Carré et al.
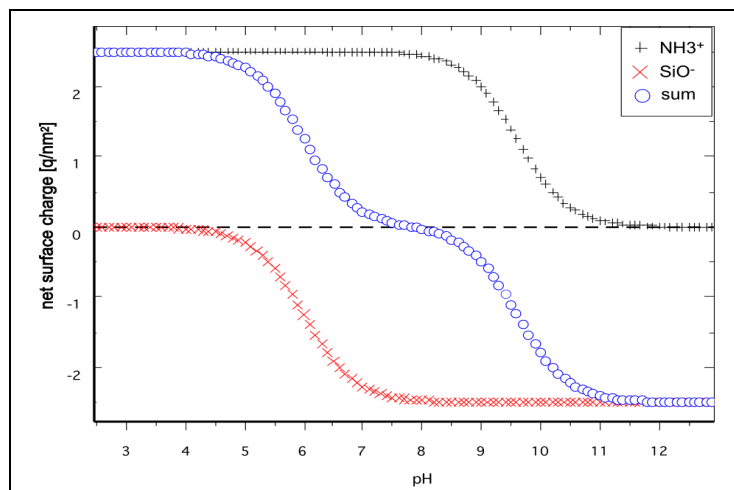
Figure 12: Evolution of the total net charge of an amine surface with rising pH. (calculated from Eq. 10)

2.1.6.3. Calculating the charge density of densely packed DNA

The helix structure of a double stranded DNA molecule (dsDNA) has a diameter of *2.4 nm*. A single stranded molecule lying flat on a surface can thus be approximated by a rod with a diameter of *1.2nm*. Hence, a single oligonucleotide of 20 bases occupies an area of *19 nm²*, assuming a length of *8.2nm*. For a densely packed monolayer of single stranded oligonucleotides the surface density can be calculated to be *~0.05 molec/nm²* respectively *5·10⁴ molec/μm²*. Assuming one negative charge for each base this molecule density results in a charge density of *-1 q⁻/nm²*. dsDNA carries two negative charges per base pair (bp) and thus leads to a charge density of twice the value determined above.

	surface density [*molec/nm²*]	charge density at pH 6 [*q/nm²*]	charge density [*C/m²*]
density of NH$_2$-groups after silanization (literature)	<1.5	+0.75	+0.12
max density of APTS molec. (tight packing)	4	+3.4	+0.54
dense layer of 20 b oligos	0.05	-1	-0.15
density of SiOH-groups on glass surface	2.5	-1.25	-0.20
density of SiOH-groups on PDMS surface	<2.5	<-1.25	<-0.20

Table 2.2. Overview: surface densities and surface charges.

2.1.6.4. Adsorption of DNA fragments on charged surfaces

Contrary to protein adsorption, DNA adsorption to surfaces is very much governed by the electrostatical properties of the target surface. To elucidate the behavior of DNA molecules in the vicinity

of a charged surface, Vainrub et al. [Vainrub, 2000] set up a model taking into account the most important factors such as surface charge, molecule charge and ion concentration in the surrounding solution. In the following paragraphs this model and its predictions will be outlined followed by a brief discussion on the impact on explaining experimental findings.

In order to determine the potential between the charged surface of the substrate and a DNA molecule, the DNA molecule is treated as an *ion-penetrable* sphere *S* of radius *a* in front of a charged ion-impenetrable plate *P*, where the charge density in the sphere is ρ*(r)* and the separation distance is *d* (Figure 13).
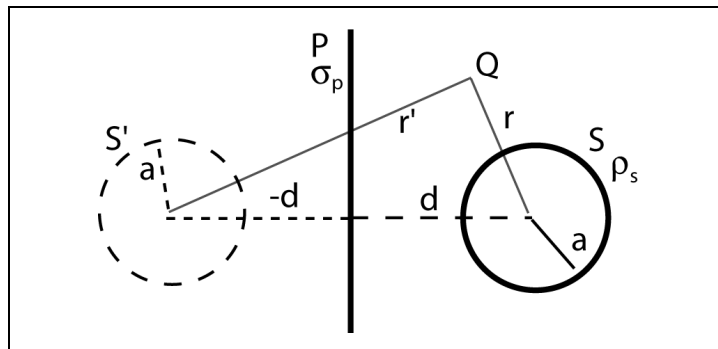

Figure 13: Model for a charged DNA fragment in the vicinity of a charged surface: charged sphere S, charged ion-impenetrable plate P, separated by distance *d*.

Following the calculations from Ohshima et al. [Ohshima, 1993] and Vainrub et al. the linearized Poisson-Boltzmann[9] equation can be used to determine the potential ψ in the above defined system:

$$\Delta\psi \; = \; \kappa^2\psi \quad \text{outside the sphere and the plane} \tag{11}$$

$$\Delta\psi \; = \; \kappa^2\psi - \frac{\rho}{\varepsilon_r\varepsilon_0} \quad \text{inside the sphere} \tag{12}$$

where κ is the Debye-Hückel[10] parameter, ε_r and ε_0 are the permittivities in medium or vacuum, respectively. The boundary conditions for such a system are:

$$\psi \text{ and } \frac{\partial\psi}{\partial n} \quad \text{are continuous at the sphere's surface,} \tag{13}$$

---

9) The linearized Poisson-Boltzmann equation extends Poisson's equation to the field of ionic solutions, that is, solutions with electrolytes dissolved. These electrolytes act as additional field sources and have to be considered calculating interaction energies and fields [Gilson, 2000].

10) The Debye-Hückel parameter k is the inverse of the Debye-length ($r_{Debye} = \kappa^{-1}$), which is the characteristic distance of the exponential electrostatic screening.

the derivative of ψ being taken along the normal n to the surface of the sphere and assuming the surface charge density σ_P on the plate to be constant (instead of a constant surface potential, which would be the case for a metal plate),

$$\frac{\partial \psi}{\partial n} = -\frac{\sigma_P}{\varepsilon_r \varepsilon_0} = const \quad \text{on the surface of the plate.} \tag{14}$$

By applying these boundary conditions to Eq. 11 and Eq. 12 it is possible to derive an expression for the potential ψ (a more detailed derivation of this potential is described in Appendix 6.2.).

The solution to the Poisson Boltzmann equation is at any point Q outside of S and P with r and r' are the distance to the center of the respective sphere:

$$\psi(Q) = \psi_{p0}e^{-\kappa z} + \psi_{s0}\frac{a}{r}e^{-\kappa(r-a)} + \psi_{s0}\frac{a}{r'}e^{-\kappa(r'-a)} \tag{15}$$

where ψ_{p0} and ψ_{s0} are factors, which can be derived from the boundary conditions.

Subsequently it is now possible to setup a relation describing the Electrostatic Double Layer Interaction[11]. The interaction energy can be written as the free energy of the system of the sphere S and the plate P at separation h minus the energy of the system at infinite separation which is 0 at any time and

$$U(h) = F(h) - F(\infty) = F(h) \tag{16}$$

To solve this equation a method of Verwey et al. [Verwey, 1948] is employed and *F(h)* can be written as:

$$F(h) = +\frac{1}{2}\int_A \sigma_P \psi_{tot} dS + \frac{1}{2}\int_V \sigma_P \psi_{tot} d \tag{17}$$

By taking into account that the surface charge $\sigma_P = \varepsilon_r \varepsilon_0 \kappa \psi_{p0}$ is constant Eq. 17 can be rewritten as

$$F(h) = +\frac{1}{2}\varepsilon_r \varepsilon_0 \kappa \psi_{p0}\int_A \psi_{tot} dS + \frac{1}{2}\int_V \rho \psi_{tot} dV \tag{18}$$

With the help of Eq. 15 and after integration the interaction free energy is obtained:

---

11) The Electrostatic Double Layer Interaction results from the interaction of the electrolyte molecules present in the solution and the potential of the charged surfaces. This interaction can be either repulsive or attractive depending on surfaces, the electrolytes involved and the pH of the surrounding medium.

$$U(h) \;=\; 4\pi\varepsilon_r\varepsilon_0 a\psi_{p0}\psi_{s0}e^{-\kappa h} + \pi\varepsilon_r\varepsilon_0\frac{a^2}{a+h}\psi^2{}_{s0}e^{-2\kappa h} \tag{19}$$

In Eq. 19 the first part describes the interaction energy resulting from direct interaction of sphere and plate, the second part is due to the interaction of the sphere and its virtual image.

With the help of this mathematical description it is now possible to model the interaction of a DNA molecule with a charged surface. A short 8 base long DNA molecule can be treated as a charge-penetrable sphere with a radius $a=1nm$. The amine surface presents a surface charge $\sigma_P=+1\ q/nm^2$. In Figure 14 the calculated potential acting on a 8 base long DNA fragment in the vicinity of such a positively charged surface is depicted.
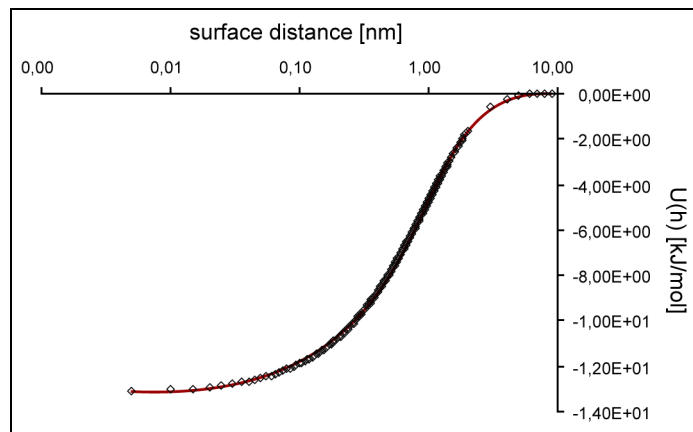

Figure 14: Potential of DNA fragment in electrolyte solution close to a charged surface. (T=293K; C_{ion}=0,1 mol/l; length=8 bp, σ_p=1 q$^+$/nm^2)

Clearly the attractive potential created by the charged groups becomes visible. Nevertheless, the potential drops rapidly to zero within one nanometer distance from the surface. Varying the different parameters showed a great instability of this calculated potential. In the simulation performed, the potential depth as well as its reach varies strongly upon changing parameters like e.g. the buffers ionic concentration or the pH. For e.g. *a=1nm, h=0 nm* (which means direct contact with the surface) sample calculations for an actual potential assuming real DNA fragments resulted in *~14 kJ/mol* maximum free binding energy. However this value is also strongly dependant on the parameters assumed and can only be seen as a rough benchmark.

Using the formulas derived above for the interaction potentials one can now estimate the amount of surface coverage of DNA on a charged surface that can be obtained by incubating the surface with a solution of molecules of defined concentration. It is important to note that once adsorption of the negatively charged DNA molecules starts the positive charge of the target surface is reduced and thus adsorption velocity is reduced. This is called the screening effect and has to be considered.

The fractional occupation of surface binding sites θ ($0<\theta<1$) can be determined by applying the Stern layer equation as proposed by Adamson et al. [Adamson, 1997]:

$$\frac{\theta}{1-\theta} = Ce^{\frac{\Delta G}{kT}} \tag{20}$$

The Stern layer equation describes the fractional adsorption of electrolytes or polyelectrolytes to a surface depending on the free energy ΔG, the Boltzman constant k, the temperature T and the bulk concentration C of DNA molecules in solution. It is valid to take the interaction free energy previously determined in Eq. 19 as ΔG and together with Eq. 20 one gets for the fractional occupation:

$$\frac{\theta}{1-\theta} = Ce^{\frac{4\pi\varepsilon_r\varepsilon_0 a\psi_{p0}\psi_{s0}e^{-\kappa h} + \pi\varepsilon_r\varepsilon_0\frac{a^2}{a+h}\psi^2_{s0}e^{-2\kappa h}}{kT}} \tag{21}$$

After rearranging Eq. 21 it is possible to calculate $C(\theta)$. Figure 15 depicts the adsorption behavior of a 20 bp long oligonucleotide with respect to different bulk concentrations. The ionic concentration $C_{ion}=0.1$ mol/L, $T=293$ K and the surface charge was set to $\sigma=1$ q/nm^2. In order to reach full surface coverage a bulk concentration of almost *1 mol/L* of oligonucleotides has to be applied, otherwise θ will not reach its maximum value. This explains why full surface coverage with molecules is hardly feasible. A *1M* solution of oligos is extremely concentrated compared to concentrations of a few *mmol/L* or even lower commonly used in DNA experiments. However, this relation is very sensitive to the internal parameters such as surface charge density, electrolyte concentration, and other parameters. Diffusion effects are also not considered in this model. By only changing the concentration or the surface potential by minute amounts the curve is shifted by orders of magnitude to the left or right. Therefore, it is difficult to make exact predictions for obtainable surface coverages, but it is conceivable, that through self limiting adsorption a perfect monolayer of DNA fragments can hardly be reached.

From the above theoretical findings one can conclude that it is very important to carefully control the experimental conditions in order to obtain useful results. The right ion concentration as well as the right pH of the buffer solution and a sufficiently charged surface can decide whether an experiment is successful or a failure.
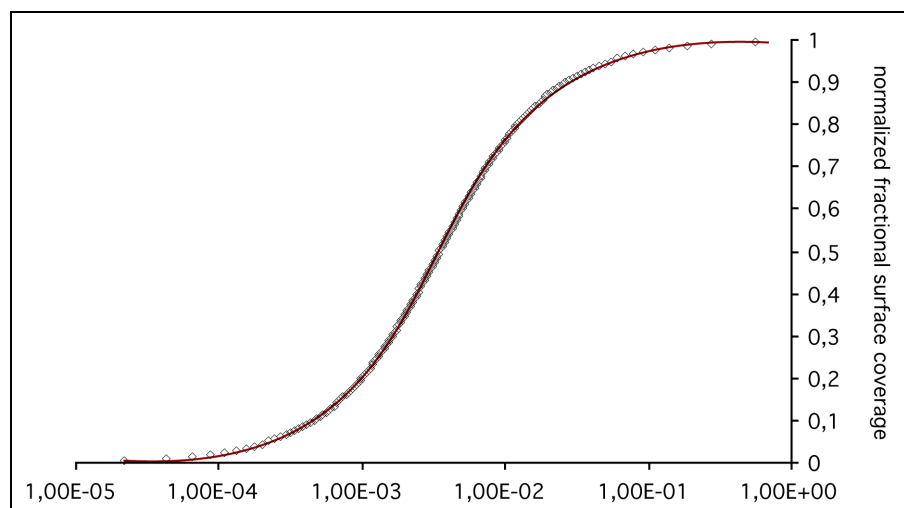
Figure 15: Calculated surface coverage of 20 bp oligos obtainable by adsorption from a solution with concentration *C*.

2.1.7. Mechanism of μCP: Transfer of molecules using elastomeric materials

In order to understand the mechanism of the observed, yet counterintuitive transfer of biomolecules underlying the concept of microcontact printing, it is necessary to have an understanding of the behavior of biomolecules at surfaces. The parameters of adsorption strength, water content, and elasticity are key to elucidating the remarkable process of monolayer printing.

Though not fully understood, one way of explaining the transfer of molecules from a material's surface to another is to assume different adsorption strengths of the molecules on the various surfaces and different elasticities. It has been observed that the transfer usually occurs from the softer to the more rigid and from lower to higher binding forces. Binding forces are strongly dependent on the sort of molecule, its internal charge distribution and the hydrophillicity or hydrophobicity of the surface exposed chemical groups. Not only the molecules characteristics but also the surface properties strongly influence the adsorption and transfer behavior. The next paragraphs will outline the basic physical and chemical concepts thought to be involved in the transfer of proteins and DNA molecules representative for two different classes of biological molecules.

2.1.7.1. Microcontact printing of proteins

A key feature of a successful and benign transfer of proteins from the stamp to a substrate is, first, the elastomeric property of PDMS and, second, the ability to incorporate traces of water into the bulk of the stamp. This feature is, as already mentioned before, probably the key feature to a successful molecule transfer. During printing, the stamp establishes contact with the target surface on a molecular level. Thereby, proteins adsorbed to the stamp surface are sandwiched at the interface between stamp and substrate and may equally adsorb to the surface of the substrate or to the stamp. However,

when the stamp is released from the surface, the proteins remain on that surface where the sum of all energies of interaction between protein and surface is highest. It is believed that the work of adhesion between protein and PDMS can be dissipated as the stamp is removed from the substrate due to the viscoelasticity and the "fluidic" behavior of the stamp surface. This leads to the dissociation of intact molecules, rather than to unfolding or breaking of covalent bonds within the stamped molecules. This means that the protein simply dissociates from the stamp surface and remains bound to the target surface.

The importance of the water content on the surface for a successful transfer has to be stressed. Letting an adsorbed layer of proteins on a stamp surface dry for a longer time (several minutes depending on the humidity), decreases the probability of a successful transfer of a monolayer. It is suspected that drying of the proteins denatures their secondary structure on the surface and lets them bind stronger to the elastomer surface. Furthermore, it might be the fluid layer that mediates the electro-static and hydrophobic interactions to the target surface. When water is missing on the stamp surface the target surface seems not to be able to exert strong attraction on the molecules bound to the stamp surface. (For adsorption of proteins on surfaces see Section 2.1.5..)

2.1.7.2. Microcontact printing of DNA

DNA molecules are, as has been described in Section 2.1.6., predominantly bound merely through electrostatic attraction to the stamp surface. In the presence of two similarly charged surfaces (the glass surface as well as the PDMS surface) during contact, the sandwiched molecules feel the same forces acting from both sides. The probability of one molecule being transferred in an ideal case should thus be roughly 50%. Any deviation from this value indicates that one of the attractive forces asserted by the two surfaces is higher than the other. This consideration immediately implies a further property of the microcontact printing of DNA molecules. If only 50% of the molecules are transferred, half of the initial amount of molecules remain on the elastomer surface. These remaining molecules should be readily printable in another printing step to a further surface. Therefore one can expect an exponentially decreasing density of molecules being transferred on different target surfaces with every new stamping step. The relation between the amount of transferred molecules $I(n)$ and the number of the stamping step n assuming a transfer probability p is best described by

$$I(n) \;=\; I_0 p^{-n} \tag{22}$$

Plotting equation (22.) for $p=0.5$ and scaling the y-axis logarithmically reveals the expected exponentially decaying behavior with a slope of 0.5 (Figure 16).

Experiments performed in the course of this work suggest that the length of the DNA molecules, the surface modification of the elastomer and that of the target surface, and the amount of water incorporated on the surfaces are further important factors determining the transfer probability.
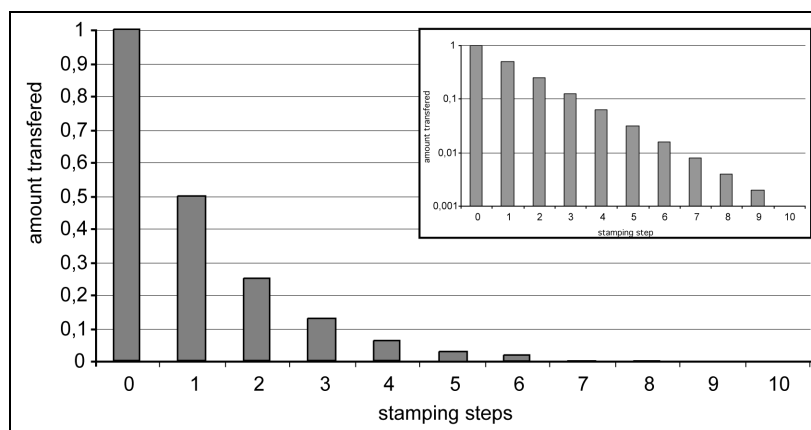

Figure 16: Ideal transfer behavior simulated for short DNA molecules with an intrinsic transfer probability of 50% (p=0.5). Inset: logarithmic scaling.

The ideal behavior showing a transfer probability of 50% is expected only for short molecules and equally charged surfaces. In conclusion, experimental data showing a deviation from the simulated curve for a transfer rate of 50% could then be attributed to an unequal charge density on the two surfaces. Alternatively, the deviation from the predicted behavior might also be explained by the formation of meshworks of molecules (Figure 17). This meshwork formation might become increasingly important for longer molecules that are more likely to intersect each other. During the contact of the stamp to the target surface, it is then possible that a whole layer of molecules intersecting each other is transferred simultaneously, leading to higher than predicted transfer rates. For long DNA molecules it is possible that during transfer only part of the molecule comes into contact with the target surface and thus the attractive force to remove the long molecule from the stamp surface might not be high enough. This in fact, would reduce the transfer probability. The above given explanations of processes taking place on DNA loaded stamp surfaces during transfer might elucidate experimental findings presented in Section 3.4.. Further experiments have to be performed to strengthen these theoretical considerations.
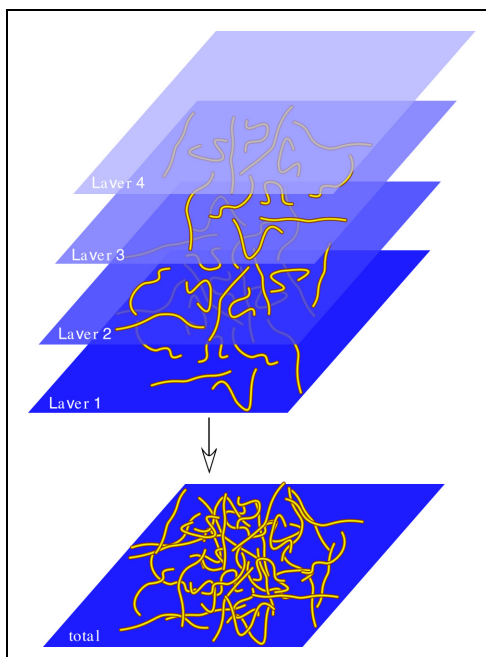
Figure 17: Schematic drawing of the formation of meshworks of DNA molecules. It is believed, that adsorption of longer DNA molecules on the stamp surface occurs in a layered fashion. Upon contact with the target surface these layers are transferred individually.

2.1.8. Affinity driven transfer of single stranded DNA molecules

This section is intended to present an overview of processes and properties important for the successful implementation of the novel PCR-on-stamp method, which was developed in the course of this work. The underlaying idea of PCR-on-stamp (Experimental part see Section 3.5.) shares some similarities with the method of "affinity contact printing" published by Bernard et al. [Bernard, 2001a] but expands its capabilities to the field of DNA microarray printing.

The term affinity contact printing (αCP) is attributed to the mechanically induced dissoctiation and contact printing of molecules, which are captured from a crude solution by e.g. antibodies firmly attached to the elastomer surface. During the contact of the stamp and the target surface the captured molecules are strongly attracted by the target surface and dissociate from their binding partners if the attractive force between target substrate and captured molecule is bigger than between capturing and captured molecule (Figure 18 A).

A similar principle is exploited for the newly developed PCR-on-stamp method. Here the two hybridized strands of a dsDNA molecule, instead of an antibody - antigen pair, are to be separated by surface contact. One end of the double stranded DNA molecule is firmly attached to the stamp's surface. Upon contact to a target surface, the second strand is strongly attracted. If forces are high enough, the inter strand bonds can be broken upon removal of the elastomer, thus leaving the second strand attached to the target surface. The first strand bound covalently to the elastomer remains on the stamp surface (Figure 18 B).
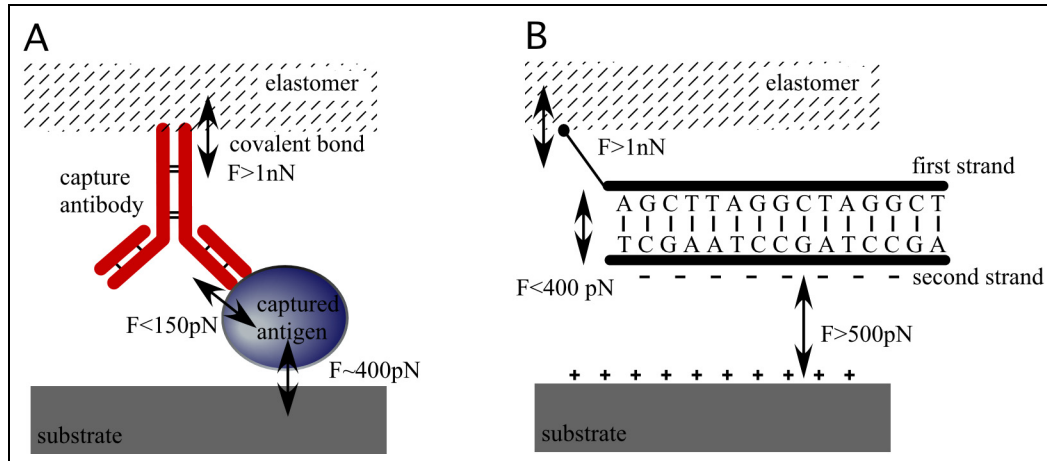
Figure 18: (A) Affinity contact printing of proteins. (B) Separation of the strands of dsDNA molecules by microcontact printing.

For the setup of the experiments investigating the possibility of tearing dsDNA molecules apart by microcontact printing it was important to consider all forces acting on the molecules, the bonds and the surfaces. The following paragraphs will give a brief overview of the forces involved.

Covalent bonds between molecules can have binding energies of up to *350 kT (850kJ/mol)*[12] as has already been described in Section 2.1.4.. The average bond length is *0.12-0.16 nm*, but the actual forces that these bonds can withstand depend strongly on the loading rate, that is, the velocity with which the force is applied. For a loading rate of *10 nN/s* forces between *2 to 4 nN* for Si-C to C-O bonds were measured [Florin, 1994; Albrecht, 2003].

The binding energies of the two strands in a dsDNA molecule depend strongly on their sequence and can be determined by counting the number of C-G and A-T bonds and multiplying it with the respective bond energies. A-T-rich regions contribute a (Gibbs) free energy of about *2kcal/mol=8,37kJ / mol= 3kT* per base pair, while G-C-rich regions contribute roughly *3-4kcal/mol = 16,7kJ/mol=6kT* per base pair [Breslauer, 1986]. The forces acting during unbinding of DNA have been measured by various research groups [Bockelmann, 2002; Smith, 1996]. These groups found a value of approximately *400pN* for breaking the backbone of a dsDNA molecule and *10-15pN* for the separation of two strands base by base in thermodynamic equilibrium[13] with a separation velocity *20nm/s*. By assuming that each negative charge in the backbone of the second DNA strand interacts with one positive charge on the surface, the maximum force attracting the second strand upon surface contact can be approximated by Eq. 1. The distance between the two interacting charges can be assumed to

---

12) (1kJ/mol $\approx$ 0,4 k_BT $\approx$ 1/100 eV); (1eV $\approx$ 40k_BT $\approx$ 100kJ/mol); (1k_BT $\approx$ 1/40eV $\approx$ 2,5 kJ/mol) for T=293 K

13) If separation velocities are below 200 nm/s unzipping occurs in thermodynamic equilibrium, that is, unbinding of the single bases takes place on a much faster time scale than the experiment and hence forces do not depend on the speed of separation [EssevazRoulet, 1997; Bockelmann, 1997].

lie between *0.2nm* and *1nm* (a covalent bond has a length of approximately *0.15nm*). Thus, for a 20bp long DNA fragment the theoretical surface binding force will be in the range from *4nN* to *100nN*. Although the values presented above are only approximate they give a sense for the forces acting during the process of separating DNA strands by contact printing.

Unzipping the two strands of a DNA molecule base by base should result in little strain on the covalent bonds keeping the first strand attached to the stamp surface, as energies as low as only *6kT* have to be withstood. However, trying to break all bonds between the two strands simultaneously as it would occur in a shear force type arrangement, should be difficult, because binding energies add up to values higher than covalent binding energies. Hence, the covalent bonds keeping the first strand attached to the stamp surface could break first.

By using the so called GC-rule, the dissociation or melting energy for the DNA fragments used in the experiments in Section 3.5. can be calculated. For the 24 bp long RS3/RS4 double stranded oligo (for sequence definition see section 4.7.3.) a value of *47 kcal /mol=196 kJ /mol≈80 kT* and for the 20 bp long SL1/SL-1 oligo *33 kcal /mol=138 kJ /mol≈55 kT* was determined. These values come very close to the bond strengths found for the covalent C-C bonds, which are the main bonds keeping the first strand attached to the stamp surface. As it is always the weakest bond that breaks first, it becomes increasingly probable that with increasing length and thus intramolecular bond strength the whole molecule is lifted from the stamps surface instead of breaking the intramolecular bonds between the two strands. However, increasing the temperature of the surrounding media should be one way to reduce the binding energies between the two strands and facilitate the transfer of the second strand even for longer DNA molecules.

With these theoretical predictions in mind, it was possible to successfully develop an efficient protocol for transferring the second strand to the target surface. The experiments performed to prove this achievement will be described in Section 3.5.

2.2. Compact Disc (CD)-Pickup Imager

During its 20 years history, the Compact Disc (CD) had a very big impact on the entertainment market and later on the computer industry. Once developed at Philips and Sony and specified in the Red and Yellow book[14], this technically sophisticated system is a very robust and easy-to-use medium allowing to store and transport a tremendous amount of data such as music, movies or computer information. The storage principle relies on tiny impressions in the surface of a plastic disc digitally encoding the information content. These impressions are sampled by a laser beam and reflections are read by a detection system. By reducing the size of these impressions, using different laser diodes, and shrinking the track distance, it was possible to even increase the data density. This new type of disc format, called Digital Versatile Disc (DVD), finds its main application in storing the vast amount of information necessary for digital movies.

It was the goal of this work to use this highly integrated and optimized technology to detect biological binding events on surfaces. Therefore, a prototype tool, the CD-pickup imager, was built.

This section will give a brief introduction into the principal concepts in CD technology and will further elucidate the physical properties and limitations of the technology and its impact on the detection of biological binding events.

2.2.1. The CD - principle

The reading principle of a CD and DVD apparatus relies on a light intensity measurement on a reflective surface. The remarkable key element of every CD Player is the CD pickup (Figure 19 A), that contains a semiconductor laser as light source, a few optical elements such as lenses and filters that focus the laser beam onto the surface of the CD and a photo detector to collect the reflected light.

The data storage medium is a metal-coated plastic disc that encodes data in small impressions or "pits" (Figure 19 B), which are of the same length scale as the focused laser beam, following a spiral. These discs are fabricated by injection molding, a very cost and time saving process. A master structure, the shim, is pressed into the liquid thermoplast PC, which is heated above the glass transition temperature T_g (~140°C). While impressing the shim, the mold is cooled down below T_g and separated from the shim. The released plastic disc now contains an exact replica of the master's structures.

---

14) The Red Book documents the specifications for the audio CD standard, whereas the Yellow Book contains the specifications for the data CD standard. These specifications were published jointly by Philips and Sony.
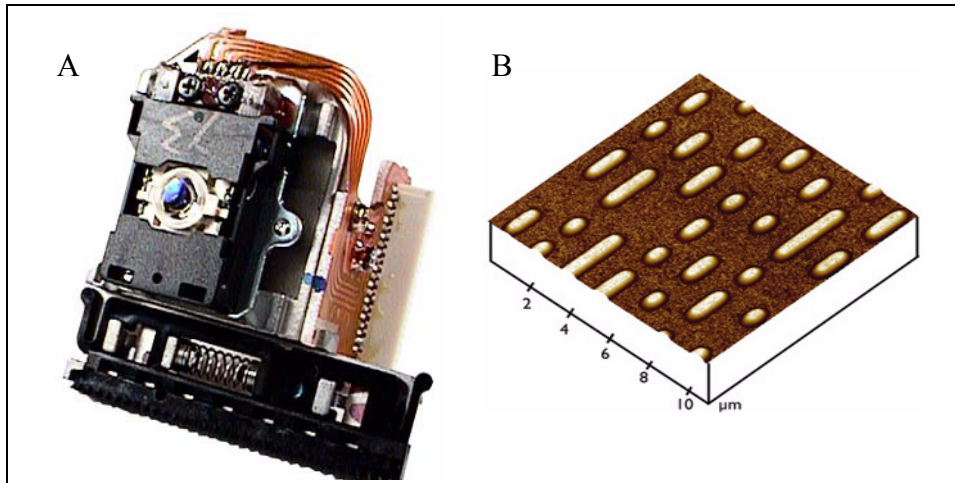
Figure 19: (A) Photograph of a conventional CD pickup head. (B) Three dimensional representation of AFM image of a CD surface. Structures are between 1-4 μm long and 1 μm wide.

A pickup commonly used in CD-players (Figure 20) contains a laser diode with a wavelength of 780 nm (e) and approximately 1 milliwatt output power, which is focused through an adjustable lens hovering inside the magnetic field of a coil (c) onto the surface of the sample (d). The back-scattered or reflected light is collected by the same lens and projected via a beam splitting mirror (b) onto a photo detector (a).
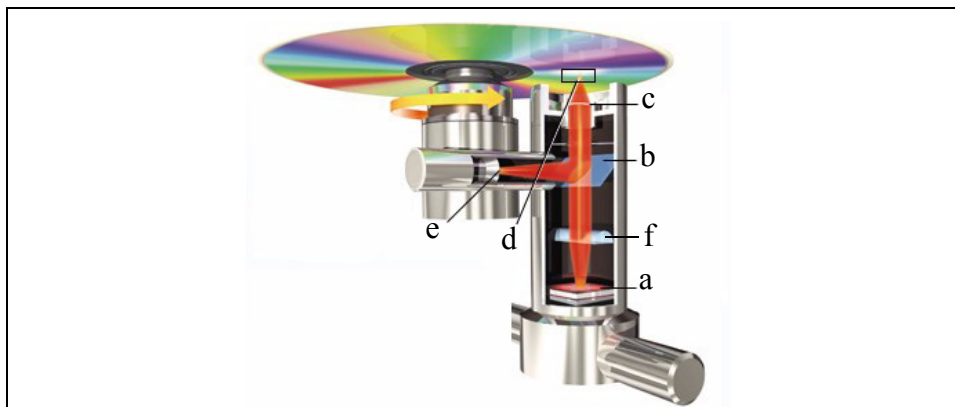
Figure 20: Working principle of a compact disc pickup. The light of a laser diode (e) (standard wave length of 780 nm) is passed through a beam splitter (b) and focused through an auto movable lens (c) onto the disk surface (d). The backreflected or scattered light is collected by the same lens (c) and directed through a cylindrical lens (f) onto the photodetector (a).

Whenever the beam of the pickup hits the rims of the pits the reflected light intensity experiences a drop due to scattering. These changes in reflectivity are recorded and translated into digital information. If the focal point of the laser is outside the plane of the surface an additional cylindrical lens (f) in the light pathway deforms the reflected laserspot into an oval. This deviation from its circular shape is detected by the 4 quadrant detector (Figure 21). An electromagnetic actuator within a feed-

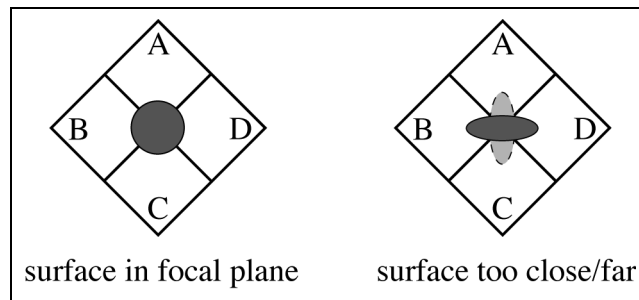back loop is then employed to correct the focus position such that it again lies exactly in the plane of the pits.

Figure 21: Autofocus: The image shows the deformation of the reflected beam on the 4 quadrant detector by the cylindrical lens with respect to the surface position. If the surface is to far or too close, the quadrants will measure different intensities.

The robustness of the CD system for everyday's use (e.g. in a portable Discman) is facilitated by an ingenious function called auto-tracking, which is built into the pickup. It helps keeping the laser-beam on track and correcting any deviation from the line of pits.

Auto-tracking is achieved by using two side-maxima of the laser beam generated by a special grating. During normal operation the two side-maxima of the laser beam lie exactly between two tracks and are not back-reflected. These side-maxima are detected by two additional photo diodes. Any out-of-track position is detected in the change of the reflected signal of these side maxima as now parts of the side-maxima are reflected by the pit structures. In order to correct the focus position the signal from the two additional detectors can be employed as a measure for the deviation from the ideal focus position. Using a stepping motor that controls the radial position of the pickup the position of the focus is then adjusted.
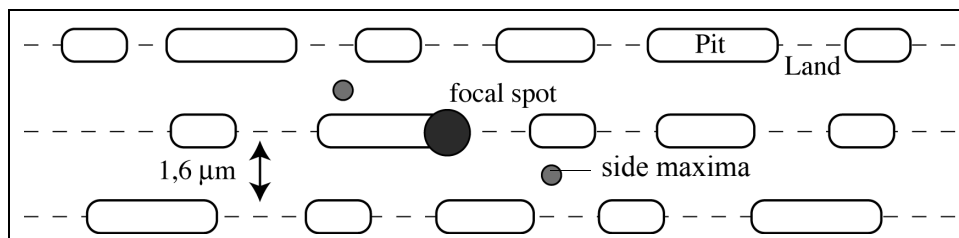
Figure 22: Image of pickup laser focus spot on pit-track (adopted from Kuhn K.J. [Kuhn, 2001]).

2.2.2. The CD-Pickup imager - A reader for bioassays

The key part of the CD pickup imager consists of a standard CD pickup (Philips CDM12.4) found in commercial audio CD players (Figure 20 B). This pickup is positioned in the optical axis of an inverted microscope (IM-20, Zeiss) above the sample stage. This allows for an easy initial focusing and positioning of the laser beam on the sample surface. A micro actuated stage is used to scan the sample surface by moving the probe in x and y direction (see also Section 4.2.).

The photo detector is connected to a sophisticated electronic circuitry that controls the automatic focusing of the adjustable lens. The optical resolution of this setup is limited by the wavelength of the laser diode employed and the size of the focal point. For the pickup described and used here the focal spot has a diameter of approximately 1 μm. During the experiments also a DVD pickup employing a laser diode with a wavelength of 650 nm was tested. However, the smaller focal spot only resulted in a slightly increased resolution of the recorded data.

The autofocus feature of the pickup proved to be very useful for the standalone application of the pickup as a surface scanner, because exact positioning of the pickup with respect to the surface is not necessary. The setup is able to find its own working point within a certain range. The only prerequisite is that the surface is slightly reflective (above 4% reflection); otherwise the autofocus loop would not receive any useful signal intensity and could not find the correct focus position. A bare glass slide surface, however, has already a high enough reflectivity to produce a signal intensity satisfying the auto-focus mechanism.

In order to get a better idea of the optical resolution of such a pickup imager and to better understand the physical meaning of the measurements performed, the maximum achievable resolution of the developed instrument will be investigated in the following section. Furthermore, the behavior of small particles within the laser focus of a pickup will be modeled.

2.2.2.1. Optical resolution of the CD-pickup

The resolution of optical instruments is defined by the Rayleigh criterion:

$$dx \geq 0{,}61 \frac{\lambda_0}{n \sin \Theta} \qquad (23)$$

where λ_0 is the wavelength of the laser light and $NA{=}n sin\Theta$ the numerical aperture of the setup. Eq. 23 states that with light of the wavelength λ_0 two features have to be dx apart to be clearly distinguishable. The numerical aperture specified for CD pickups is $NA{\approx}0.45$.

Thus for the laser wavelength $\lambda_0{=}780\ nm$ the maximum resolution will be $dx{=}1060\ nm$. The full spot diameter which is defined by the first minimum of the airy pattern is $d{=}2.1\ \mu m$ with an effective

spot size at the FWHM of $d_{eff}=0.88 \cdot 2.1 \mu m \approx 1.9 \mu m$. When using the CD pickup as bioimaging tool for measuring the reflectivity of a test spot the laser beam only travels through ambient air before it reaches the test spot area. Thus, the maximum resolution will be limited to $dx \approx 1 \mu m$ as calculated above.

Compared to a conventional optical microscope with a best resolution of ~0,4 µm the value of 1µm seems to be low and not worthwhile using it in an imaging tool. However, this slightly worse resolution can be neglected comparing the price of 10 Euro for a CD-pickup, and e.g. 500 Euro for a full imaging tool that might possibly be developed and commercialized in future, to 10000 Euro for a simple commercial light microscope.

2.2.2.2. Detection of particles in the laser focus

To interpret the experimental data obtained with the pickup imager from imaging surfaces covered with small particles correctly it is important to understand the physical behavior of a small particle in a laser focus. Especially the reflected or back-scattered intensity of laser light is of great importance.

In principle there are three different regimes that describe the interaction of an incident light beam of wavelength λ with a particle of size d. These regimes are the scattering or Raman-regime ($\lambda << d$), the diffraction- or the Mie-regime ($\lambda \sim d$), and the refraction- or Rayleigh-regime ($\lambda >> d$, $I \propto d^6$) [Török, 1998]. As already discussed before, optical instruments using light of wavelength λ are only capable of separating objects that are further apart than approximately $\lambda/2$. However, if objects are smaller than $\lambda/2$ but are further apart it is still possible to detect them.

Because the dimensions of the particles used in the presented experiments are of the order of λ, Mie theory qualifies best to be used to describe the interaction of the particles with the focused laser beam. The interesting question to be answered here was, how the particle size is related to the amount of light reflected back into the pickup detector. This correlation helped to analyze reflection data from the pickup imager correctly.

Mie theory in general provides a solution to the problem of a linearly polarized plane wave illuminating a spherical scatterer. By expressing the incident plane wave through spherical functions and then applying the appropriate boundary conditions for the electromagnetic field inside and outside the sphere, the scattering as well as the extinction cross sections and subsequently the efficiencies can be derived.

The physics of the interaction of an electromagnetic wave with a sphere, that is a gold or sliver particle on a glass surface in the path of an incident laser beam, is extremely complex. However, Mie theory can be applied to approximate this interaction to some extent. A theoretical solution for the posed problem is described in Bohren and Huffman [Bohren, 1983]. Figure 23 shows a graph for the scat-

tering cross section for gold particles with diameters between 0,01 to 1 μm in a beam of laser light with a wavelength of *780 nm*. This graph was calculated with the Java applet Mie-Calc by B. Michel [Michel, 2002]. The scattering crossection dramatically increases for particles with a diameter bigger than 0.2 μm. It reaches a maximum around 0.25 μm and approaches a constant value for larger particles. The oscillations between 0.2 and 0.4 μm might explain some adsorption phenomena observed during experiments and are also found in a simulation performed in Section 3.1.1.. This simulation models the backscattered intensity from a spherical gold particle of varying diameter, which is moved through the focus of a laser beam.

To perform this simulation a more complex program, LIGHTWAVE by A. Rohrbach, EMBL-Heidelberg, was used. This program takes into account, that the incident light from the pickup is not a plain wave but rather a spherical wave due to the focusing by the objective. Parameters were set such that they best met the experimental conditions.
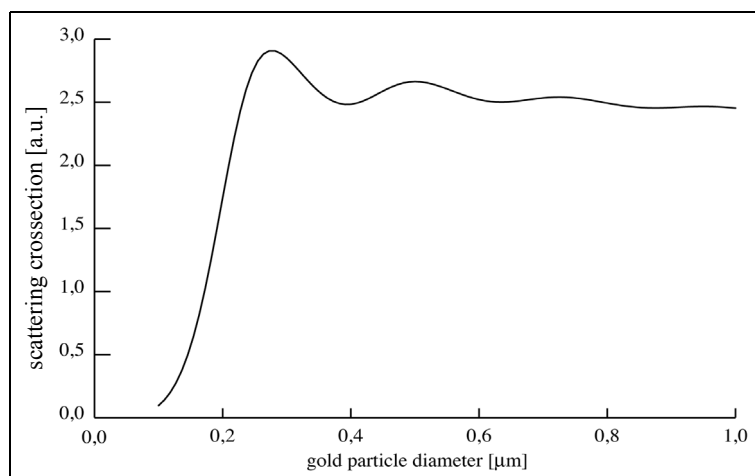
Figure 23: Mie theory: scattering crossection of particle in a laser-beam with respect to the particle size.

2.3. Biochemistry, Biophysics, and Surface Modification

This chapter is dedicated to give an overview over the biochemical and biophysical principles and methods used in the experiments performed for this thesis. The optimal adaptation of these methods to the particular problem was crucial for the success of the experiments. First, a description of the surface modification with reactive molecules necessary for altering the surfaces properties and for permanently decorating surfaces with biological molecules is given. In the next section a newly developed method for surface structuring by enzymatic digestion is presented. Finally, the polymerase chain reaction is introduced. This method is one of molecular biology's most important methods and was slightly modified and used in the experiments performed for printing DNA (Section 3.4.) and PCR on stamp (Section 3.5.).

2.3.1. Surface chemistry & physics

The subsequent paragraphs give a brief introduction into suitable chemical surface modifications. A particular interest is put on silanization to yield surface bound amine groups and on their crosslinking to other molecules. Furthermore, the formation of self-assembled monolayers on gold surface is briefly discussed.

2.3.1.1. The concept of silanization

Chemically inert surfaces such as e.g. polycarbonate or poly(dimethyl siloxane) (PDMS) surfaces need to be modified before they can be covalently decorated with biomolecules. In order to activate the surface, reactive groups (OH) can be generated by an oxygen plasma treatment. These OH groups can then serve as anchoring points for the covalent attachment of end-functionalized silanes.

The introduced functional (reactive) end groups can be e.g. amino, mercapto or carboxy groups. This nm-thin layer of reactive silanes dominates and determines the properties of the freshly modified surface. Figure 24 shows the scheme for an amino modification of the PDMS elastomer surface used in this work.
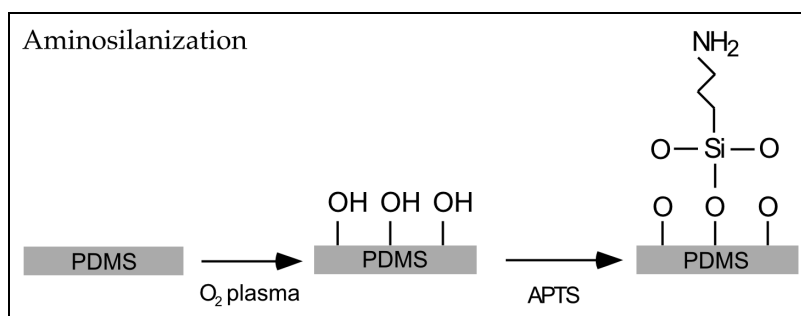

Figure 24: Scheme of the amino-silanization process

2.3.1.2. The concept of chemical cross linking

Coupling two or more molecules together is an important topic in organic- and biochemistry. There are many reasons that make linking of molecules necessary. In order to purify molecules from crude solutions, molecules can be temporarily linked to membranes. In immunological tests probe molecules presenting features from several molecules can be obtained by linking the separate compounds together. Furthermore, molecules can be labeled with specific markers or reactive groups or they can be permanently linked to surfaces to alter the properties of these surfaces. There is a vast number of protocols for fusing molecules together to form complexes, such as antibodies coupled to enzymes, antibodies coupled to dyes or others [Hermanson, 1996]. In this section a brief overview of coupling techniques used in this work will be presented.

A common way to couple molecules together is to use a "bridge" molecule that has two either identical or different reactive chemical groups. Consequently, these molecules are called "homo"- or "hetero"-functional. These "cross-linkers" are most often used in a two step process. First, the crosslinker is reacted with molecule A or surface A, then washed, and finally reacted with molecule B. The crosslinker acts with its two reactive groups at either end as a bridging unit.

Figure 25 A shows the first step of this process on the example of an amine reactive crosslinker that is covalently attached to the amine grafted surface.
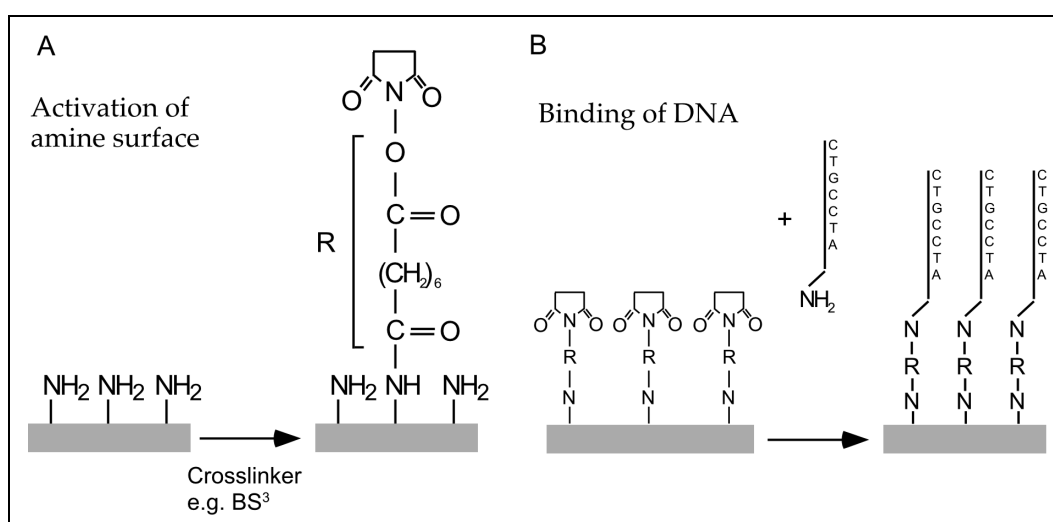
Figure 25: (A) Scheme of surface activation with a homo bifunctional crosslinker. (B) Scheme of coupling the molecule covalently to the previously activated surface.

The subsequent step of the molecule being coupled covalently to the surface is depicted in Figure 25 B. The free reactive end of the cross-linker molecule reacts with the appropriate chemical group in the target molecule. The same concept can not only be employed for aminated (NH_2) but also for thiolated (SH) molecules, which can be coupled to the amine surface by employing a heterobifunctional cross-linker containing two different reactive groups, e.g. an amine and a thiol reactive end group. In

recent years a variety of crosslinker, reactive towards many different chemical groups, have been synthesized such that the needs for almost any application can be fulfilled.

It is important to note, that the performance (reactivity) of a cross linking molecule can be strongly pH dependant. The appropriate pH influences reactivity and yield of the coupling.

2.3.1.3. Alkanethiol chemisorption at gold surfaces

Self-assembled monolayer formation of thiol molecules to gold surfaces is the consequence of the strong interaction between gold and sulfur atoms. The sulfur-gold bond has almost covalent character (*400 kcal/mol = 480 kT*). Alkanethiols were the first molecules used for contact printing (see Section 2.1.2.)and their behavior on gold surfaces is well understood.

Alkane thiols have the unique property to "chemisorb" to gold and thereby forming dense monomolecular layers of remarkable order. These self assembled monolayers (SAMs) are stabilized by lateral interaction forces between the individual alkyl chains. Indeed, they are very stable against distortion and rupture [Delamarche, 1996b; Delamarche, 1996a]. Because of their small size and their tight packing (Figure 26) these layers are impermeable to many polar and charged molecules. Using this property a SAM layer of alkane thiols chemisorbed on a gold surface serves as an excellent etch resist to common etch solutions such as buffered KCN (0.1 M). In the KCN etch bath a thin gold layer can be etched in a few minutes with an etch rate of *0.05 nm/sec*. Hence, for a typical gold layer thickness of *20 nm* the etching time was *~7 min*.

By exploiting this etch stop property of SAMs and using µCP to deliver the thiols to the target surface with high lateral resolution the fabrication of complex patterned gold or other metal surfaces became possible [Kumar, 1992].
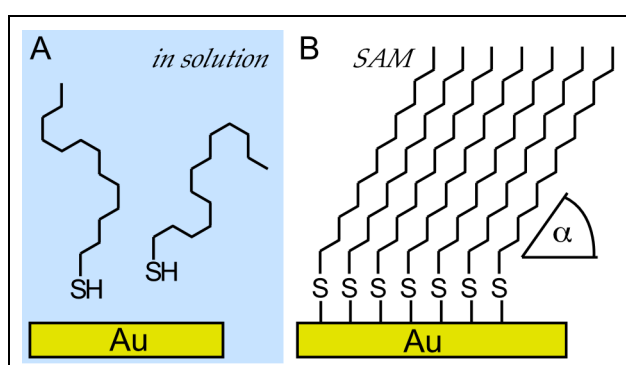
Figure 26: Scheme of self assembled monolayer formation of alkane thiols. (A) Thiols in solution before adsorption. (B) Thiols forming monolayer with α~30°.

2.3.2. Enzymatic digestion of proteins

Proteases are enzymes that digest proteins by cutting them into smaller peptide fractions and finally single amino acids in a process called proteolysis. The technologically relevant proteolytic enzymes are mainly extracted and purified from bacterial sources. They find application in a variety of fields, such as cell digestion in molecular biology or broadly as cleaning aids in modern detergents. They are used whenever it is necessary to destroy proteineous material.

In the presented experiments proteases were used for controlled enzymatic digestion of surface bound proteins, hence, allowing the target surface to be structured. Up to now the ability of protease to digest adsorbed molecules has not been exploited in research and might lead to a new set of surface structuring techniques. The feasibility of such a procedure will be experimentally proven in Section 3.2..

The two proteases used for the experiments were *Proteinase K* from Tritiachium album limber [Crowe, 1991] and *Pronase E* from Streptomyces griseus [Jehanli, 1985] (Sigma-Aldrich, USA). Proteinase K cleaves peptide bonds at carboxylic sides and works best at an elevated temperature of 65 °C. Pronase E can be used at room temperature and cleaves peptides unspecific.

Target proteins for the enzymatic digestion were BSA, casein and gelatin from cold water fish. Gelatin is usually obtained by the hydrolysis of collagen, which is the principal protein found in skin and bones. By the destruction of the intramolecular bonds between the three polypeptide chains in collagen a loosely connected meshwork of peptide chains is formed. This network is efficiently digested by the proteinases mentioned above. BSA, as well as casein are globular proteins exposing a variety of peptide sequences susceptible to enzymatic attack. Hence, the proteins are randomly cut by the enzymes and fragments or single peptides are released into the medium. To insure optimum conditions for the enzymes to work, an appropriate buffer suggested by the supplier has to be used.

2.3.3. Polymerase Chain Reaction (PCR)

The Polymerase Chain Reaction was invented in 1985 by K. Mullis. [Saiki, 1985; Mullis, 1985]. In 1993 K. Mullis was awarded the Nobel prize for the ingenious finding that small amounts of DNA molecules can be successfully amplified in a chain reaction. PCR is one of today's most frequentley applied techniques in molecular biology laboratories and other research institutes.

In the experiments described in the next chapter PCR was used for the synthesis of longer (up to 500 base pairs) DNA fragments to investigate contact printing of DNA. A modified PCR method was further used in the Section 3.5. (PCR-on-stamp) to synthesize new strands along ssDNA bound to an elastomeric stamp.

PCR nowadays employes enzymes (Taq-Polymerase) that sustain high temperatures (>90°C) where DNA molecules can be melted (separated in two strands), short DNA fragments, so called primers and single nucleotides (A,C,T,G) present in the buffer, to copy longer double stranded DNA fragments. This enzymatic process is performed in cycles, where each cycle consists of periods of different temperatures. The temperature controls the behavior of the DNA molecules as well as the action of the enzymes. First, at high temperature (95°C) dsDNA is melted into two strands, then the short primers are allowed to hybridize to the appropriate sequences on the longer target DNA fragments at lower temperature (50°C). The primers are then enzymatically elongated by sequential attachment of single nucleotides to the end of the primers at an elevated temperature of 70°C and finally the newly synthesized strand is again separated from the longer template at a temperature of 90°C. Here, a new cycle can be started and the initial strands as well as the newly synthesized strands are replicated again. The amount of identical strands is duplicated with every cycle, hence the total amount of material increases exponentially with the number of cycles. Replication can be performed as long as enough primers and single nucleotides are present in the solution and as long as enzymes are intact and functional. A common number of cycles is between 20 and 40 cycles.

2.4. Detecting the binding of biomolecules

The efficient detection of specifically bound molecules is crucial to the success of the envisioned CD-pickup imager device. The CD-pickup imager is capable of detecting the reflection or scattering properties of a target surface. To be used as a read-out device for biological tests, suitable binding-, or "reporter" elements have to be employed to mark the molecular binding reactions.

To measure binding events with the CD-pickup the sites where binding took place had to be labeled with reflective or scattering particles that are of a certain size to create a measurable signal. This section will give a brief introduction into the fields of immunoassays, signal generation and signal enhancement appropriate for being read by the CD-pickup.

2.4.1. Immunoassays

Immunology is the study of the body's immune system, which includes, besides others, the theory of antibodies and their ability to bind specifically to other target molecules (antigens). Immuno-assays [Diamandis, 1996] are diagnostic tests performed in research laboratories or clinics to check patient or animal probes (tissue or fluid samples) for the existence or absence of certain disease molecules. In common immuno-assays the specific binding of these molecules is used to visualize the molecules of interest by labeling one with a specific marker (fluorophores, fluorescent beads, radioactive isotopes, quantum dots or colloidal particles). Upon adding such a labeled specific marker to a probe solution with unknown molecular content, the labeled molecule can, if present, bind its partner such that this partner can be observed by the researcher (Figure 27 A).

Such assays have a long tradition in biological science and diagnostics and they are used to either classify and locate specific molecules in cell samples or histological thin films or to detect specific disease-related molecules in diagnostic immunoassays. In general, immunoassays are built-up as a sandwich (Figure 27 A), where a capture antibody that is firmly attached to a solid support, captures a binding partner from solution (the antigen) and thus localizes it to a certain area. An advantage of binding the capture molecule to a solid support is the fact, that once the antigens of interest are bound, the surface can be washed and thus all molecules that are of no interest are washed away. A second specific antibody is then used to visualize captured antigen if present. Finally the second antibody, which is labeled with e.g. fluorophores, radioactivity or other detectable labels, can then be observed using the appropriate label dependent detection method.
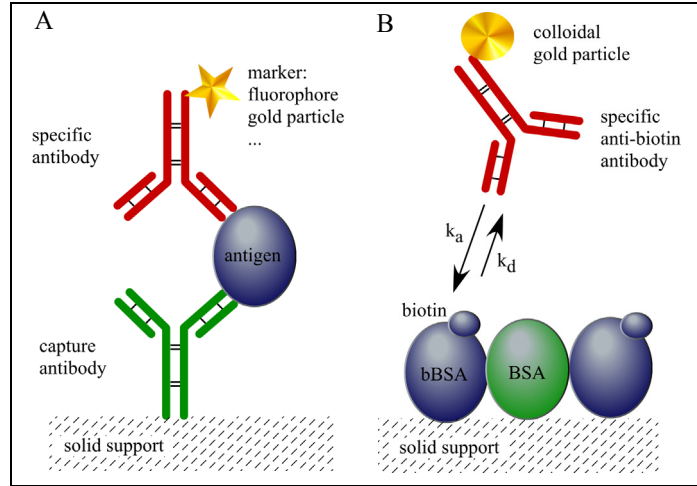
Figure 27: (A) Schematic representation of a sandwich immunoassay. (B) Binding reaction to a surface that was functionalized with specific binding regions (biotin) used for some of the experiments.

To relate antigen concentration and measured signal and to interpret the result it is important to understand the kinetic behavior of a molecular binding reaction. The thermodynamic equilibrium of a molecular binding reaction can hence be written as

$$[Ab]+[Ag] \xrightleftharpoons[k_d]{k_a} [AbAg] \tag{24}$$

Eq. 24 is the mass action law underlying the binding reaction and is the starting point for the theoretical approach to describe the binding reaction of e.g. antigen to antibodies. Eq. 24 relates the bound and unbound antigen, with the reaction rate constants k_a *[1/Ms]* and k_d *[1/s]*. In Figure 27B a schematic representation of this reaction is given.

The mass action law defines the equilibrium constant K as the quotient of the two reaction constants k_a and k_d

$$K = \frac{k_a}{k_d} = \frac{[AgAb]}{[Ag][Ab]} = \frac{c_{bound}}{c_{Ag} c_{Ab}} = \frac{c_{bound}}{(c_{0Ag} - c_{bound})(c_{0Ab} - c_{bound})}, \tag{25}$$

where c_{0Ag} is the start concentration of the antigen on the surface and c_{0Ab} is the concentration of detection antibody in solution. Eq. 25 can be solved for c_{bound}

$$c_{bound} = \left(\frac{\frac{1}{K} + c_{0Ag} + c_{0Ab}}{2} \pm \sqrt{\frac{\left(\frac{1}{K} + c_{0Ag} + c_{0Ab}\right)^2}{4} - c_{0Ag} c_{0Ab}} \right) \tag{26}$$

The units of the variables are respectively:

$$K= \left[\frac{l}{mol}\right] = \left[\frac{1}{M}\right] \qquad k_a = \left[\frac{1}{Ms}\right] \qquad k_d = \left[\frac{1}{s}\right] \tag{27}$$

Figure 28 depicts such a binding curve as it is expected for a simple immunoassay system.

The above described formulas are valid for the equilibrium state, which is only the end status of a dynamically evolving system. The kinetics within such a dynamic biochemical system are best described by a differential equation, which shows the time dependency of the analyte concentrations in solution and on the surface:

$$\frac{dc_{bound}}{dt} = k_a c_{Ag} c_{Ab} - k_d c_{bound} \tag{28}$$

By assuming $c_{Ag} \gg c_{bound}$ one can solve Eq. 28 using the same approach as has been described for surface adsorption of proteins in Appendix 6.1. and one finds:

$$c_{bound}(t) = \frac{k_a c_{0Ag} c_{0Ab}}{k_a c_{0Ag} + k_d}(1 - e^{-(k_a c_{0Ag} + k_d)t}) \tag{29}$$

This equation is describes a "steady-state" kinetics.

It should be noted here, that Eq. 29 reflects the situation only for an ideal case. To calculate the time-dependent concentration in reality the diffusion of the analytes as well as the geometry of the system has to be taken into account. However, especially the implementation of diffusion on structures with different feature sizes is complex and will not be discussed here in depth.
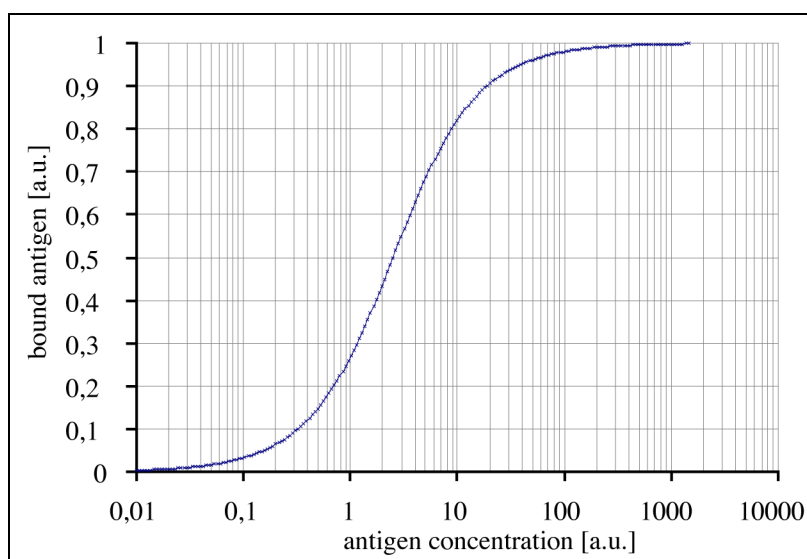
Figure 28: Binding curve for bound antigen vs. applied antigen obtained from Eq. 26.

2.4.2. Fluorescent labeling

The previous section presented ways to identify, visualize and measure molecules of interest by detecting them with labeled molecules (most often antibodies). One such label can be a fluorophore. A fluorophore is a chemical structure, that has a highly delocalized π-system and is thus able to adsorb photons from visible or UV light. Upon relaxation this color center can emit red-shifted light at a wavelength depending on the chemical structure. A fluorescence microscope equipped with the appropriate filter sets is the standard tool for inspection of such molecules.

One major drawback of fluorescence though is the intrinsic photobleaching, that is, the destruction of the color centers of the fluorophores by illuminating it with high energy photons. A fluorophore in its excited state can either dissipate energy by emitting a light quant (after stokes shift) or by chemical reaction respectively decomposition and thereby loosing its resonance structure. Hence, a stained sample can only be imaged for a certain time before the signal deteriorates and intensity drops below background.

Fluorophores used in the experiments were TRITC (Tetramethyl-rhodamine-iso-thio-cyanat) and FITC (Fluorescein-iso-thio-cyanat). The excitation wavelengths are 550 nm and 475 nm, respectively. The absorption spectra for these molecules are shown in Figure 29.
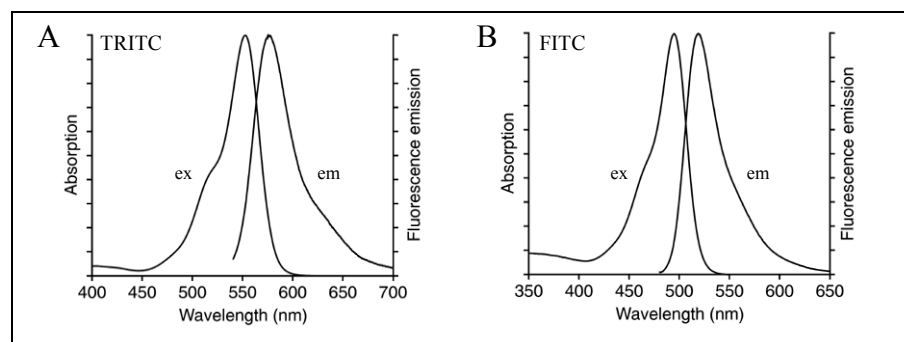
Figure 29: Excitation (ex) and emission (em) spectra of the fluorophores TRITC (A) and FITC (B). (source: Molecular Probes)

2.4.3. Colloidal Gold labeling

Another well established method for labeling molecules is immunogold labeling. Here small colloidal particles such as gold or silver with a diameter between 1 and 50 nm are conjugated to a binding molecule. These conjugates can then be used to specifically mark molecules of interest. Because of the small size of the colloidal particles this method was established and mainly used for electron microscopy to visualize the location of molecules in thin tissue samples or slices.

A variety of different methods for the fabrication of colloid gold particles can be found in literature. The one used mostly lets the particles grow around nucleation cores. For this method it is important

to carefully control the rate of formation of new nucleation cores and of the crystal growth itself. The colloidal gold particles carry a negative charge in aqueous media. This allows a firm attachment to proteins such as e.g. antibodies, thereby creating immuno-active particles that connect the selective binding capabilities of the biomolecules with the unique catalytic properties of inorganic gold. Since the 1970ies such particles are extensively used in electron microscopy. The colloidal gold particles present a high scattering cross section for the electron beam and are easily detectable in the recorded images.

2.4.4. Autometallography

For light microscopic purposes or for the use as reflecting elements for the CD-pickup imager the colloidal metal particles are too small to be detected (1-50 nm), thus they had to be enhanced. In 1985 Hacker et al. [Hacker, 1985] developed a method to catalytically deposit pure metal from its metal salt in the vicinity of a gold particle acting as catalyst. Consequently, this technique found application to enhancing the contrast of immuno-stained thin film sections for electron microscopy. Gradually, this process has been further developed [Danscher, 1993] to an easy staining and signal enhancement method. Commercial kits (Sigma, Nanoprobes) are ready to use procedures and are able to increase the size of the gold particles from 1 nm to 600-800 nm without producing high background by unspecific precipitation.

The reduction agents (such as hydrochinone or pyrogallol) induce a reduction potential, which is building up within the staining solution over time, by providing electrons. Gold particles present e.g. on the surface of a biotest can then act as reservoir for these electrons and by transferring the electrons to the metal ions catalyze the reduction of silver or gold salts into their solid state on the surface of the gold particles (Figure 30). In this process, electrons are donated by the reduction agents which are in turn oxidized (Inset to Figure 30), then collected and channeled by the gold particles and transferred to the metal salts. If no gold particles were present or if the density of latter is low, unspecific autonucleation of metal ions increases and the background of the reaction becomes high. The growth of the particles is terminated by the reduction potential present in solution. It has been observed that particles up to 1 μm could be prepared by autometallographic enhancement[15].

---

15) These observations have been made in the course of the experiments but were not further quantitatively measured.
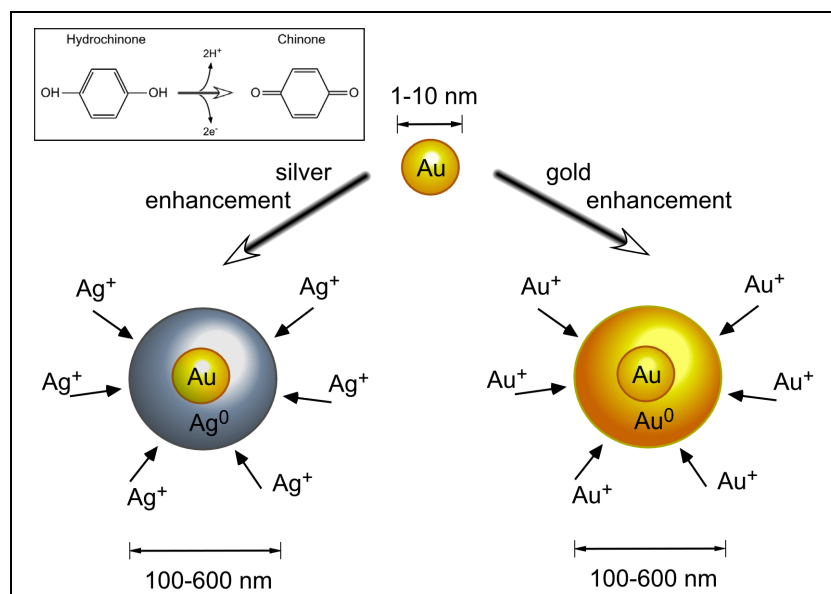
Figure 30: Schematic diagram for silver (left side) respectively gold (right side) enhancement (adopted from Nanoprobes). The inset shows the reaction of the reduction agent hydrochinone which provides the electrons for precipitation of the silver- respectively gold ions.

The schematic procedure for the use of silver or gold precipitation for signal enhancement is depicted in Figure 31, where a colloidal gold labeled specific antibody binds to a captured or immobilized antigen. Subsequently, the gold particle is enhanced as described above.

In comparison to fluorescence, autometallography has several distinct advantages. Fluorophores are usually destroyed through the excitation with light, and hence, loose their capability of emitting light. Thus it is very important to acquire images quickly after immunolabeling. With the autometallographic enhanced samples one can image over and over again, exposing the samples to high light intensities without loosing any signal.

Furthermore it is possible to detect single molecules by using autometallography. In contrast to single molecule detection with fluorophores however, no complex and expensive photomultiplier-tube and signal amplification device is necessary. If the molecules of interest are sparse enough, then single enhanced grains can be attributed to single binding events. This in turn could open up a whole new field for measuring concentrations. Now it could be feasible to count the number of binding events and relate this number to a concentration of binding partners in solution, thereby applying a "binary biochemistry".
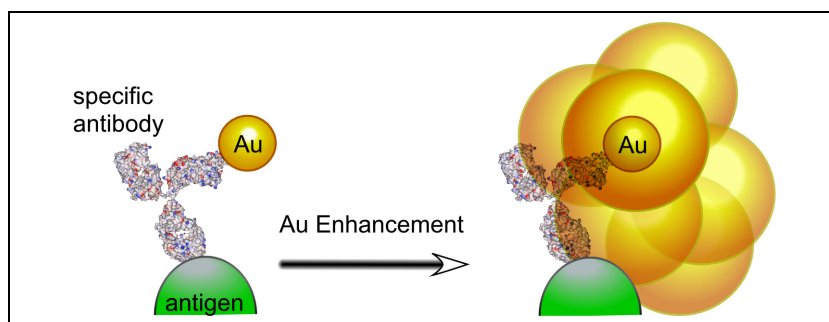
Figure 31: Signal enhancement process using autometallography. Drawing of the immunoassay and signal generation. A gold-labeled detection antibody binds the immobilized antigen and a gold grain is generated by catalysis of gold.

2.4.5. Enzyme-assisted precipitation of fluorescent or colored material

Enzymes are powerful biochemical machines that can fulfill a variety of chemical and mechanical tasks. For immuno-histochemistry and in-situ-hybridization-detection enzymes can be exploited to convert an organic colorless substance to an intensely colored, insoluble reaction product. By coupling enzymes to detection molecules such as antibodies, one can e.g. generate localized precipitation of solid colored or fluorescent reporter material.

Alkaline phosphatase (AP) and *horseradish peroxidase (HRP)* are among the most common reporter enzymes used for enzymatic precipitation of solid material. Coupled to streptavidin or to a specific antibody these hybrids become powerful tools for surface bound assays. In Figure 32 the schematic reaction scheme for the precipitation reaction is depicted.

Upon exposure to an appropriate substrate (e.g. ELF 97, Molecular Probes), AP cleaves a phosphate group from the ELF reagent, which then becomes insoluble and, as a fluorescent label, precipitates at the site of enzyme activity. The main adsorption and emission wavelengths of the precipitate are 535nm and 545nm, respectively.

In contrast to the fluorescent ELF substrate, the material precipitated by the enzyme HRP is not fluorescent. HRP selectively deposits a highly localized dark stain of solid metal in the presence of a metal ion source such as e.g. DAB/Co by its peroxidase activity. An important prerequisite for this reaction is the presence of an appropriate activation agent such as hydrogen peroxide (H_2O_2). This dark stain is, as will be discussed in the experimental section, a good "reporter" for molecular binding events. However, the experimental procedure is very tedious and, besides that, the reagents are very toxic.

The different substrates and enzymes were tested in several experiments for both, their reflectivity, and their scattering behavior, using the CD-pickup imager.
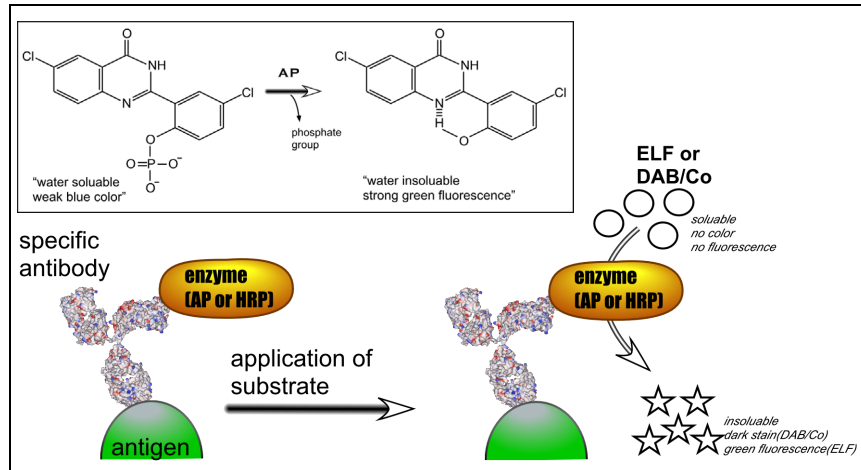
Figure 32: Schematic diagram for enzymatic precipitation of colored or fluorescent substance. AP = Alkaline phosphatase, HRP = Horseradish Peroxidase. The inset shows the cleavage of the phosphate group from the ELF97 compound.

3. Results & Discussion

All experiments performed in the course of this thesis and the results and insights gained from them will be presented in this chapter. The experiments were designed to contribute to the development of an inexpensive and highly flexible diagnostic biotest system. They will be presented in a logical sequence in the course of this work.

Section 3.1. introduces the newly constructed readout device for diagnostic assays, the CD-pickup imager. To prove its general functionality and to characterize the technical properties measurements of simplified assays are evaluated. Finally, a complete and relevant diagnostic assay is performed and analyzed with the CD-pickup imager. Subsequent sections focus on the development and improvement of novel fabrication methods for arrays of biomolecules such as DNA or proteins.

In Section 3.2. a novel method for the creation of alignment marks with a high aspect ratio on glass surfaces using proteins as resist and enzymes as "developer" is demonstrated. Substrates necessary for the precise positioning of molecules on the surface using an alignment apparatus are fabricated in this way. In Section 3.3. the setup and use of the alignment apparatus is explained and the fabrication of a dot-line array of sample molecules is demonstrated.

Finally, in Section 3.4. and Section 3.5. two completely new methods for the simplification and acceleration of the production process of DNA-arrays are presented and experimental findings are discussed.

3.1. The CD Pickup imager: Reader for bioassays

Immunoassays are among of the basic assays [Diamandis, 1996] used in research as well as in clinical diagnoses and drug screening to measure clinically relevant parameters such as the concentration of inflammation, infection or cancer markers, antibodies or other disease related molecules. For highly parallel solid-phase binding assays such as sandwich immunoassays, DNA expression analysis or protein chips, fluorescence constitutes the signal-generating means of choice [Irving, 2000; de Wildt, 2000]. To replace the established but expensive signal tags and detection systems used for today's array-based assays, inexpensive silver-staining and standard compact disc (CD) reader technology was suggested (see Section 2.4.). The catalyzed silver (Ag(I)) reduction, well-known from thin-film staining for electron microscopy, has already been successfully used for DNA binding assays in combination with a computer flatbed scanner [Taton, 2000] or a CCD camera readout [Reichert, 2000; Fritzsche, 2001].

In the course of this work, a CD-pickup imager was assembled that is capable of qualitatively and quantitatively detecting minute amounts of colloidal silver or gold grains on a thin transparent support such as a polycarbonate disk or a glass slide. Biomolecules patterned onto the surface by μCP and detected by colloidal-gold antibody conjugates (Section 2.4.3.) with subsequent autometallographic enhancement (Section 2.4.4.) were used to test the CD-pickups capability.

Initially, in the sections which follow, the results from measuring single metallic or non-metallic particles originating from positive binding of a biochemical test will be presented, completed by the setup for the measurement of simple binding assays.

Furthermore, it will be shown, that the CD pickup reader was successfully employed to measure the concentration of a clinically relevant antigen in a sandwich-type immunoassay format (see Section 2.4.1.).

3.1.1. Single particle measurements

Usually, a positive binding event in biochemical tests is visualized by means of labeling to produce a measurable signal for the read-out device. For the CD-pickup imager, the ideal signal-generating element is a high quality mirror with a minimum size of one square micrometer that reflects 100% of the laser light back onto the detector. In the ideal case, one positive binding event creates one signal-generating element. Autometallographic precipitation of metal around colloidal gold catalysts [Hacker, 1994; Hacker, 1996] is suggested as an appropriate signal element.

In the experiments performed for this work, a detection scheme, labeling positive biotests with colloidal gold particles with diameters of 1 nm, 5 nm, or 40 nm, respectively was used. These gold particles catalyzed the precipitation of elementary silver or gold around the colloidal particles. For the final size of the silver or gold grains it was observed that the size of the catalyst gold particle did not matter. The size of the grains was measured by AFM. After short metal enhancement (<10 min.) a narrow size distribution between 50 and 250 nm of particles was observed (Figure 33 A, B). Longer amplification resulted in "high background" and large clusters of grains.
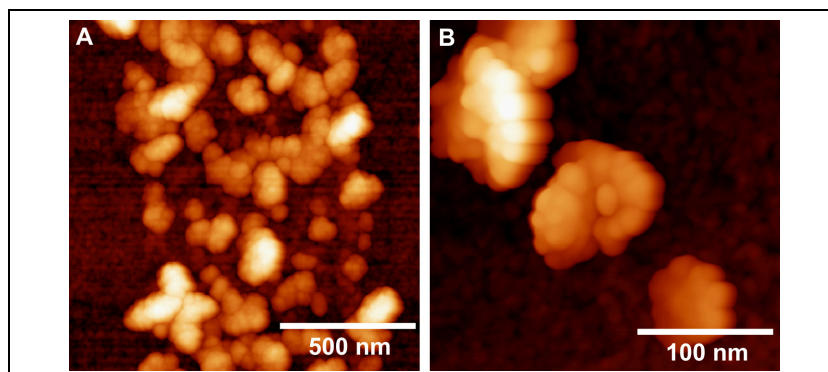
Figure 33: Atomic force microscope image of silver grains formed around 1 nm colloidal gold particles. (A) A line of contact-printed proteins that was detected with colloidal gold particle-labeled antibodies, which were subsequently silver enhanced. (B) Magnification of single binding events.

The average grain diameter that was achieved after prolonged enhancement time (>15 min.) was *505 ± 140 nm* under constant exchange of the enhancement solution. Without exchanging, the particles grew bigger to an average size of *795 ± 200 nm* (see Table 3.1.). Noteworthy, grains grown under constant exchange of the solution had a much smoother surface.

A possible reason for the larger size of the particles grown without exchange of enhancement solution could be that the development of the redox potential is slowed down. This in turn, would lead to a slower growth rate of the particles. This explanation is corroborated by the observed smother surface of the particles developed in exchanged enhancement solution. With a lower growth rate the freshly reduced gold atoms can more effectively adjust themselves into the lattice of the already existing particle, thereby creating an smooth and ordered surface.

Furthermore, it was tested to determine whether the presence of light had an influence on the grain size or its shape but here no significant impact was observed.

The smallest particles that were detected and distinguished from background noise with the CD-pickup had a diameter of roughly 300 nm (data not shown here). For single grains large enough to be detected by the pickup imager, the acquired signal output voltage was in a range between 0 and 2500 mV. The full dynamic range of the output voltage of the pickup imager was 4000mV.

exchange	light	average diameter (nm)	shape of grains
yes	yes	460 ± 109	smooth
no	yes	851 ± 192	rough
yes	no	551 ± 177	smooth
no	no	722 ± 270	rough

Table 3.1. Average grain size after silver enhancement under the influence of light exposure and solvent exchange.

An interesting feature of silver or gold grains could be observed in some of the measurements of enhanced test surfaces scanned with the pickup imager. Below a size of approximately 500 nm[16] the measured signal from the pickup became negative (black dots or holes in Figure 34 A, C), that is, less than the signal obtained from the plain glass surface[17]. These findings seem to indicate that there is a regime where the particles absorb or at least do not reflect incident light. In the line profile of Figure 34 B (arrows) a reduction of ~100 mV was observed well above background. This observation might help to improve the signal quality by shaping the particles in such a way that the reflected signal is maximized.
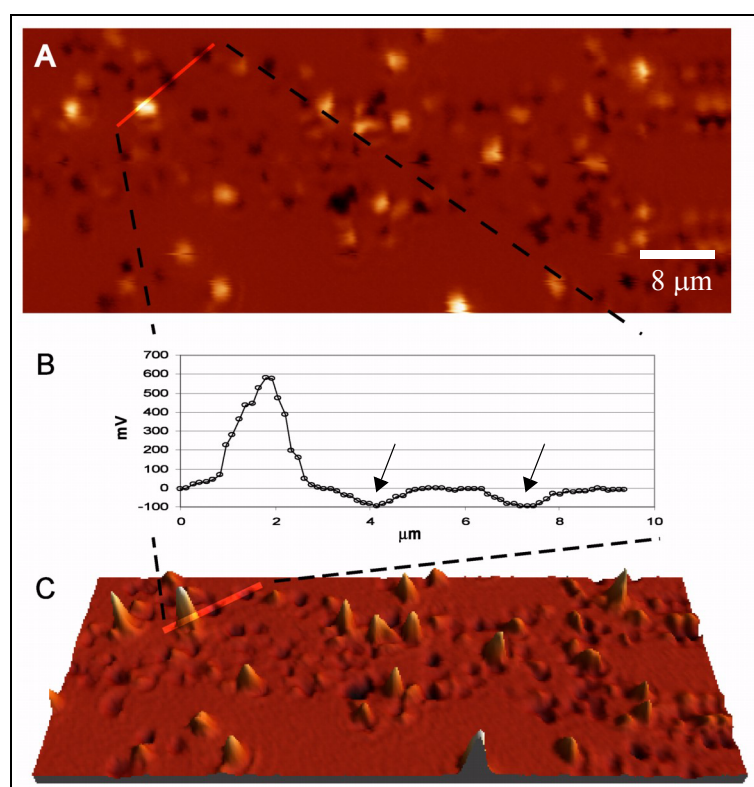
Figure 34: CD-pickup data showing the reflection of single enhanced metal particles. (A) Original CD-pickup image; (B) Line profile showing the signal from 3 particles; (C) 3D representation

In order to interpret this observation on the recorded images correctly it is necessary to understand the interaction of small particles with a laser beam. The dependence of the reflected (back scattered) signal intensity on the size of the gold particles can be estimated from a simulation based on the Mie theory (see Section 2.2.2.2.).

---

16) This value was determined by measuring microscopic images of gold or silver enhanced biotest samples. The images were acquired with the darkfield microscope using an 100x objective.

17) One has to remember that for the pickup to keep the focal point on the target surface, a reflectivity of a few percent (>~4%) is necessary.

The simulation was done for gold particles with diameters between 25 nm and 1.3 μm (Figure 35). The complex refractive index of gold was set to 0.4 + 7.36i. The numerical aperture of the CD-pickup optics was estimated to be 0.45 and the wavelength of the incident laser light was set to 780 nm. The refractive index of the surrounding medium was set to 1. By virtually scanning the particle through the laser focus, that is, changing the offset value in the software from -1.5 μm to +1.5 μm, the scanning movement of the pickup and thus the peak broadening was simulated (Figure 35 A, C).

Larger particles (>300 nm) showed an almost linear increase of the back-scattered intensity (B). Nevertheless, for particle sizes between 100 and 300 nm an interesting behavior was observed. At around 250 nm a dip in the intensity curve of almost 50% occurred (Figure 35 C, D). This behavior might be explained by an increased forward scattering process of particles with a diameter in this range. Nonetheless, this effect has to be investigated in much greater detail to be able to draw conclusions from the simulation data. In principle, this behavior could be responsible for the observed negative reflective values measured for small particles with the pickup imager.
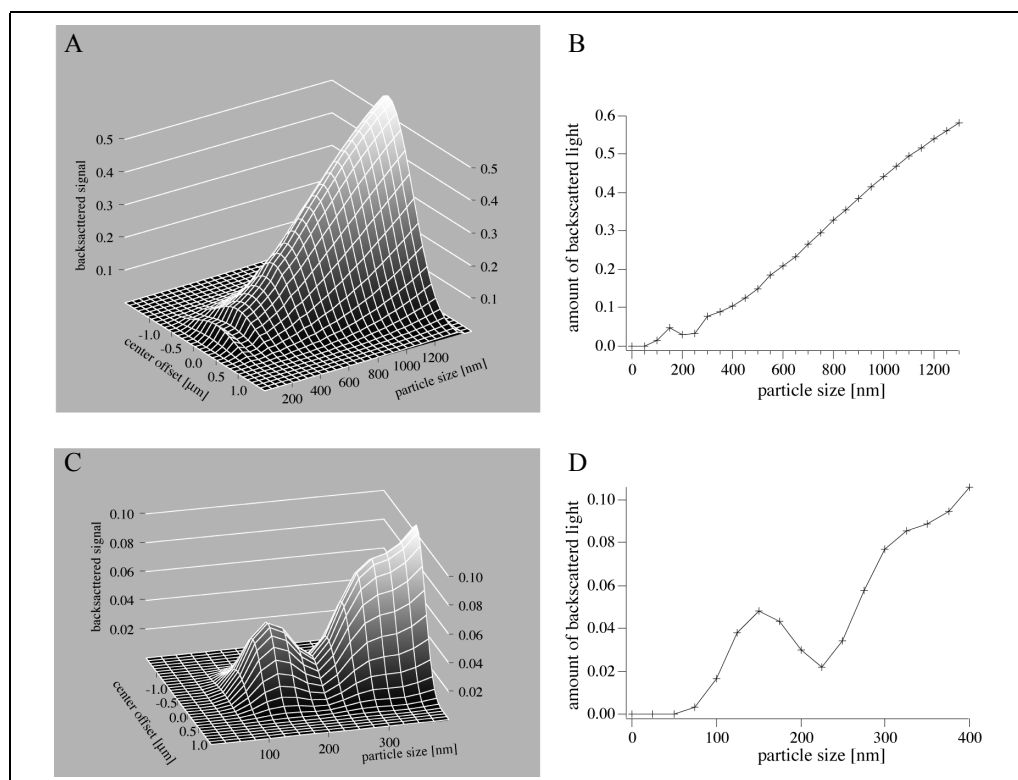
Figure 35: Simulation of back scattered light from gold particles of different diameter. Particles were moved through the focus perpendicular to the direction of the laser beam. (A) Surface plot of the scattered intensity vs. particle size and the position offset of the particle with respect to the focus. (B) Amount of back scattered light with the particle localized in the center of the incident laser beam. (C, D) Magnified section of the particle range from 0 to 400 nm diameter.

The results obtained so far, are primarily valid for a low concentration of enhanced particles. However, when the density of the precursor gold particles on the surface becomes higher, that is, many

gold antibody conjugates per area are bound, the final enhanced structures start to merge. At high concentrations no separate gold beads or particles evolve, but areas that are completely gold- or silver- plated appear (Figure 36). These areas show very good reflective properties and yield strong signals. In a regime where discrimination of single binding events is no longer possible it becomes necessary to employ a different strategy for measuring binding events and in the end analyte concentrations. However, in the course of this thesis measurements were only performed for low concentrations and no measurement algorithm for high concentrations of analytes was evaluated.
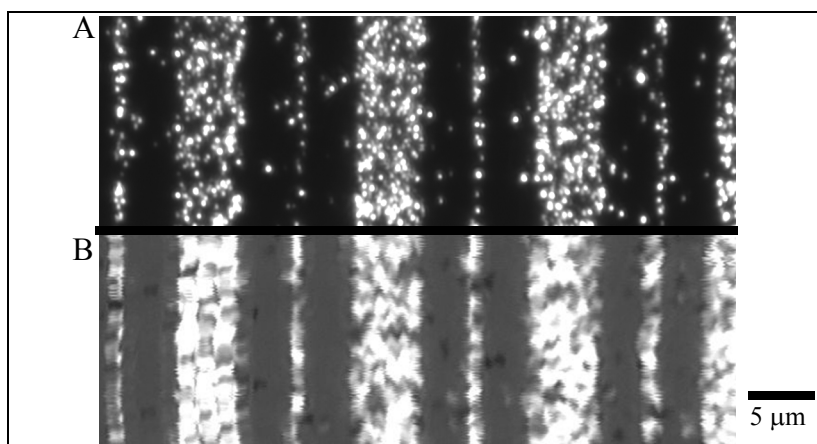
Figure 36: Darkfield micrograph of stripes of enhanced gold particles. (A) The particles are densely packed such that it is difficult to separate single particles. (B) Similar sample of enhanced gold particles imaged with the CD-pickup imager. Because of resolution limitations and due to mechanical instabilities no single particles are visible.

Autometallographic enhancement of bound gold particles proved to be very successful in labeling binding events for CD-pickup imager detection. Still some alternatives for creating solid precipitates as signal-generating elements at positive bio-test sites have been tested. As before, the tests were performed using contact printed bBSA(1mg/mL) that is bound with anti-biotin conjugated reporter enzymes and subsequently reacted with the enhancement solution for labeling. The following enhancement systems were compared:

(A) Precipitation of fluorescent material (ELF) by alkaline phosphatase (Section 2.4.5.);

(B) Precipitation of colored substrate (DAB/Co) by reduction with peroxidase (HRP) (Section 2.4.5.);

(C) Silver enhancement by autometallography (Section 2.4.4.);

(D) Gold-enhancement (Section 2.4.4.).

System A proved inefficient due to the low signals recorded with the pickup imager. Even though system B showed excellent signals it was abandoned for its tedious handling protocol and for its high toxicity of the components. Both, method C as well as D worked properly yielding good signals. Method C was chosen for its inexpensive compounds involved. Table 3.2. summarizes the measured

average signals for the different substrates. Clearly, the two metal enhancement procedures for reporting binding events resulted in the highest signal levels.

	system	max. pickup-signal [mV]
A	ELF+ alkaline phosphatase	880±110
B	DAB/Co + horseradish peroxidase	1054 ±240
C	silver enhancement	1312±130
D	gold enhancement	1410±120

Table 3.2. Measured signals for metal-enhancements and enzymatically precipitated substrates.

3.1.2. Qualitative measurements

Antibodies are the choice for the sensitive detection of biological analytes. To combine catalytic silver enhancement for signal generation with the sensitivity of antibodies for binding specific antigens, colloidal gold-conjugated antibodies were employed (see Section 2.4.3.).

An important characteristic of a detection method is its signal to noise ratio. The noise originates from a background signal that is determined by the specificity of the antibody to bind only to its antigen as well as the selectivity of the silver enhancement solution only to form precipitates around specifically bound gold particles. In summary, unspecific binding of antibodies and autoprecipitation of metal without binding event compromise the detection method.

It is well known for autometallographic enhancement solutions that they tend to react very sensitively on the presence of metal atoms like for example platinum or other trace impurities on the substrate surface and form unintended precipitates and thus create false positive signals. This effect has been observed e.g. when using PDMS stamps for contact-printing that were not fully cured. After printing a small amount of PDMS rested on the substrate surface. After autometallographic enhancement, a strong sliver precipitate was found even in the absence of gold particles on the surface. This nucleation of solid precipitate can be explained by the fact that the residual PDMS contains traces of the noble metal platinum, which serves as catalyst during polymerization of the stamps. This platinum atoms are then responsible for catalyzing the nucleation of solid silver particles. To avoid this interference it was important that the elastomer was either fully cured, or UV-curable elastomer that contains no platinum catalyst was used.

A variety of commercially available metal enhancement kits were tested with respect to the speed of development and the tendency of forming unspecific background. From this evaluation the two kits performing best were selected and chosen for further use with the pickup imager. A time-lapse study

of the development of silver particles using the silver enhancement kit from Sigma-Aldrich (USA) was performed. The reflectivity signal reached saturation after approximately 15 min. (Figure 37). The background[18] in this experiment was below 25% of the maximum signal and thus sufficiently low to distinguish positive binding events from background. The gold enhancement kit from Nano-probes (USA) turned out to produce the lowest background values (below 10%, data not shown) together with acceptable enhancement times (~12 min.). Nevertheless, for most experiments performed in this work the Ag-enhancement kit from Sigma was selected out of budget reasons.
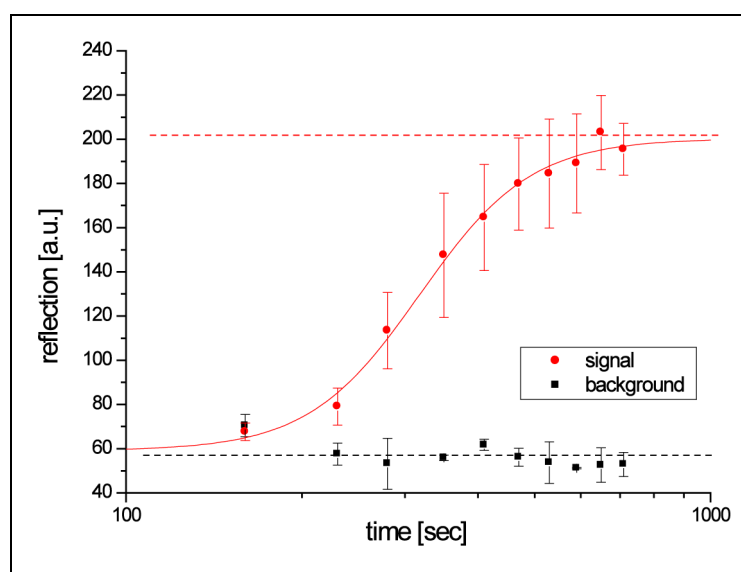
Figure 37: Time course of reflectivity signal generated by silver precipitation. Data was taken from 5 sample areas on the surface and fitted with a saturation curve. The background was measured on the non patterned areas.

A microcontact-printed pattern of mono-layered antigens arranged in a field of 3 by 3 squares was blocked with BSA to prevent unspecific interactions. The specific detection of the antigens was performed using colloidal gold-labeled antibodies. The pattern was observed with conventional dark-field microscopy (Figure 38 A). Since only the square features presented antigens, the silver grains found outside of them could be attributed to unspecific background induced by autoprecipitation of silver or gold. And indeed, electron microscope images (Figure 38 B) reveal that no bound gold particle was found outside the squares of the patterns. Hence, the unspecific background solely originates from auto-precipitation of silver respectively gold from the enhancement solution. Figure 38 (C) and (D) show the same surface area as (A) recorded with the pickup imager. In (D) the local signal intensity was plotted in the z direction creating a pseudo 3D representation of the reflection signal. Apart from a higher resolution of the light microscopy image by approx. a factor 2 to 4 (see

---

18) The background can be observed nicely if using μCP patterned substrates for enhancement tests. Areas between the stamped patterns show directly the local background.

Section 2.2.2.), there is no noticeable qualitative difference between the two images. All principal features appear also in the image acquired with the CD-pickup imager. Considering the cost of such a microscope of about 10000 Euro compared to 10 Euro for the CD-pickup, which is a factor of 1000, the CD-Pickup scanning microscope clearly outperforms the conventional microscope.
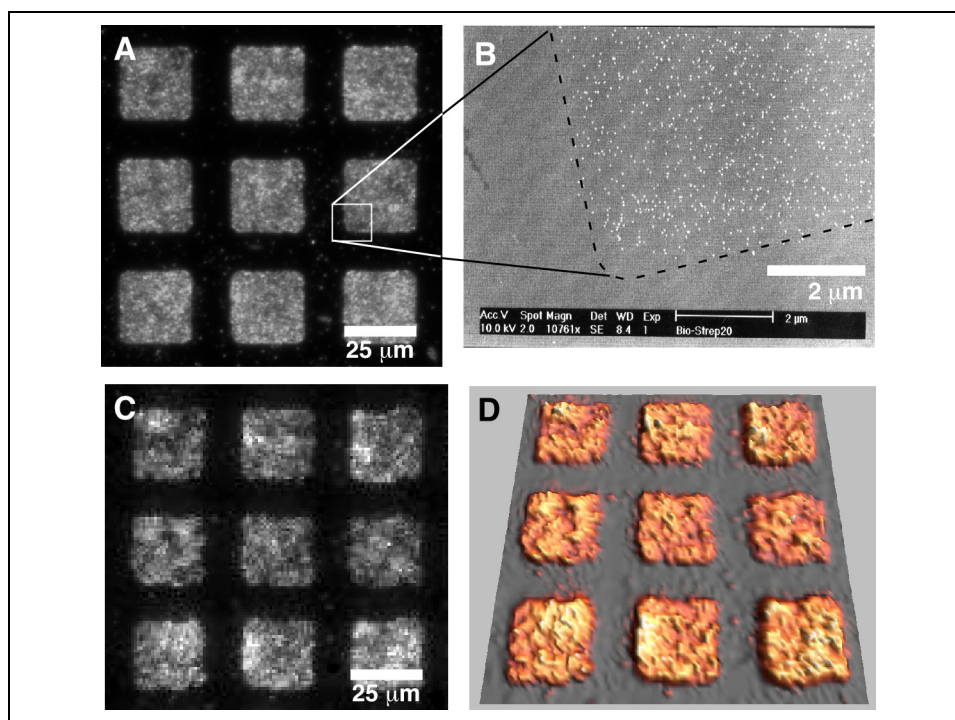
Figure 38: Bioactive recognition pads after gold enhancement. (A) Darkfield microscopic image (resolution ~0,3 μm). (B) Scanning electron microscope image of gold beads in the immunoassay before its amplification by gold enhancement. (C) CD-pickup image of the very same microcontact-printed array of recognition pads after gold enhancement. Resolution approx. 1μm (D) 3D-representation of pickup data from (C).

3.1.3. Quantitative biotest measurements

To apply the CD-pickup as a readout device for biomedical or biochemical assays it should be able to measure and quantify the concentration of the test marker in a sample. This should be possible by correlating the bulk concentration of analytes with the surface density of bound molecules as described in Section 2.4.1.

For reasons of simplicity, the biochemical assays used to characterize the concentration measurements consisted of a single target molecule (biotinylated BSA, bBSA) that was contact-printed to the surface, and a detection antibody (anti-biotin AB), that was directly linked to the colloidal gold particle (Section 2.4.1., Figure 27 B). The amount of bBSA stamped to the surface was varied by premixing and diluting it with different amounts of unlabeled (non-biotinylated BSA). Thus, surface patterns with different densities of binding sites from 0.01% to 10% were created. The idea of this assay was to link the concentration of bound particles directly to the amount of bBSA patterned on

the surface. The readout-signal of the CD-Pickup imager can then immediately be related to the surface concentration of bBSA molecules. The quantitative measures of bound molecules were obtained using three different methods. All had their advantages and disadvantages:

First, by counting individual grains a direct correlation to the surface concentration of adsorbed molecules can be found. This method is only valid for highly diluted samples where single grains can be separated. Knowing the average density of binding partners on the surface the concentration of the analyte can be determined by counting a large population of single grains on a given surface area. The result will then be a concentration of grains (positive biotests) per unit surface area.

Second, for surface concentrations that do not allow to separate individual grains or binding events, the fractional surface coverage is determined. The pickup imager scans a given surface and calculates the percentage of the area occupied by the grains over the total test area. To separate clustered grains from background, the images acquired by the pickup imager are processed with an image analysis software (SimplePCI, Hamamatsu) that helps separating objects by setting a signal threshold value. Objects are classified by size, shape and roundness to reduce detection of artefact. This procedure yielded a concentration value in terms of covered surface per unit surface area. When applying different concentrations of bBSA onto different substrates and scanning each with the pickup imager a dose-response curve (Figure 39) can be calculated.
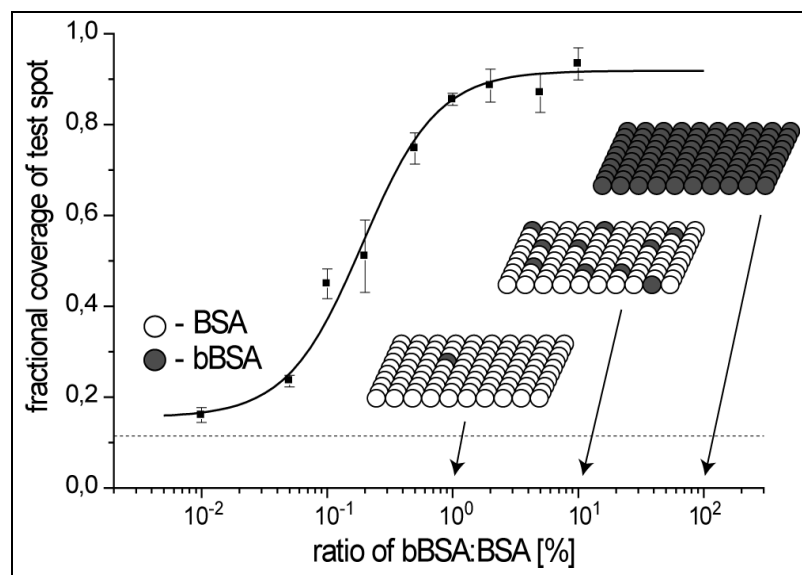
Figure 39: The graph shows a dose-response curve obtained by plotting the fractional surface coverage vs. ratio of biotin BSA to BSA. A curve of the type of Eq. 26 was fitted to the data from six different experiments. The insets depict the distribution of molecules on the surface.

Third, for high concentrations, where discrimination of single grains and patches is impossible, the intensity of the reflectivity signal itself that is recorded in units of millivolts by the photo diode in the pickup should be a measure for the concentration of bound molecules. It is expected to receive a sig-

moid curve when plotting against the applied concentration. This binding curve should in principle be equivalent to those obtained by the two other methods. However, in the experiments performed, it was not possible to obtain a clear dependence between the reflectivity signal and the concentration over a broad range of concentrations, and hence the third method was excluded from further investigation.

From these experiments it can be concluded that measuring the fractional occupation of an metal enhanced surface is the best method for determining the surface concentration of bound analytes in an quantifying immunoassay.

Most of the relevant biomedical tests are conducted as so-called sandwich immuno-assays (e.g. ELISA), where the measured analyte is sandwiched between two detection molecules. To prove the applicability of the pickup imager system to measure real world immunoassays, a conventional ELISA for C-reactive protein (CRP) was adapted for this purpose (Section 2.4.1., Figure 27 A). The capture antibodies (anti-CRP Clone 5) were contact-printed onto clean glass substrates. The free surface areas were passivated using unspecific adsorption of BSA. Then, different concentrations of the sample analyte (CRP) were applied. Subsequently, in a secondary detection step, the captured CRP-molecules were detected with biotin labeled antibodies (anti-CRP Clone 7), of which the concentration was kept constant for all substrates. In the last step the biotin label of the detection antibody was detected with an anti-biotin antibody conjugated to a colloidal gold particle that was finally amplified and visualized by silver or gold enhancement. The resulting reflective pattern of the precipitated metal "film" was imaged using a light microscope as well as the pickup imager. The fractional occupation of the metal enhanced areas was analyzed for both. The different applied concentrations of antigen (0,1-5 µg/mL) clearly showed a good correlation with the signal recorded by the pickup imager (Figure 40). This demonstrates that the pickup imager is capable of measuring concentrations over at least three orders of magnitude for CRP.
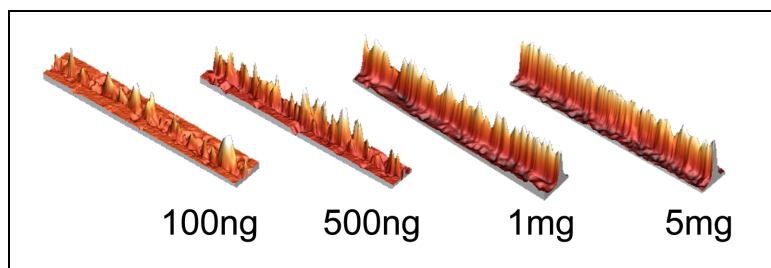
Figure 40: Concentration-dependent signals recorded using the pick-up imager. Reflectivity is translated into a topographic map after applying different concentrations of CRP antigen and subsequent gold enhancement (100ng/mL, 500ng/mL, 1µg/mL, 5µg/mL).

When plotted against the applied antigen concentration the surface coverage showed a sigmoid behavior (Figure 41, solid line, round dots). This result compares well with a binding (dose-response) curve measured in a conventional standard ELISA experiment (Figure 41, dashed line, square dots)[19]. The sensitivity of binding assays is usually determined by measuring the range of the linear segment of the binding curve. With respect to this the CD-pickup-ELISA offers a sensitivity over almost 5 orders of magnitude. This is truly a remarkable value, compared to the two orders of magnitude of sensitivity achieved with conventional ELISA assays.
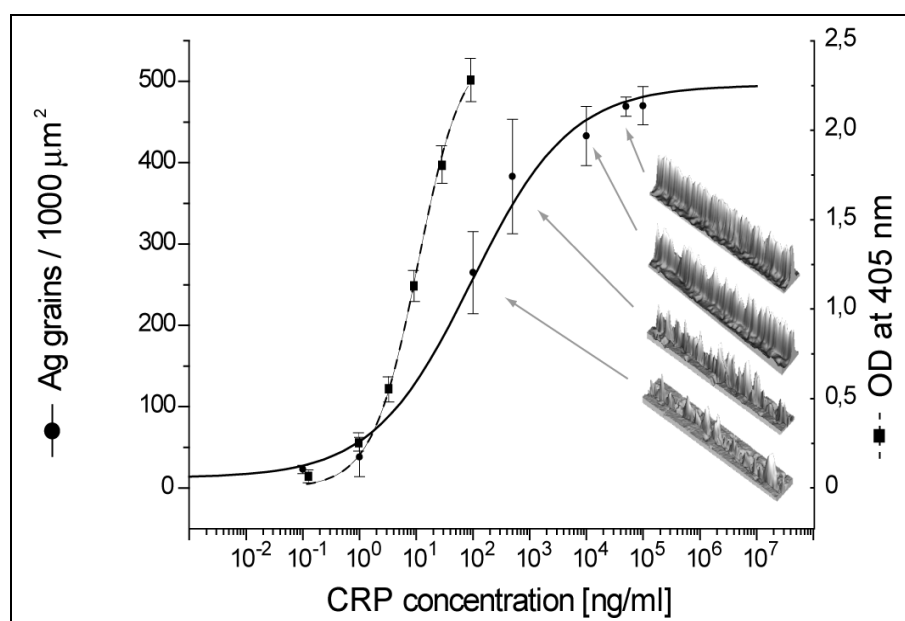
Figure 41: CRP-ELISA measured with the pickup imager (dots). Concentrations ranging from 100pg/mL to 100µg/mL CRP were applied to the immunoassay and amplified using silver enhancement. The number of counted silver grains per test area vs. the employed antigen concentration reveals a classical binding curve (fitted lines). Square data points and the corresponding fit (dashed line) represent a standard CRP-ELISA curve (0,1 ng/mL – 100 ng/mL) determined with a conventional ELISA experiment (taken from Hy-Test, CRP-data sheet).

Further experiments were conducted exploring the possibility of shrinking the size of printed capture antibody spots, such that positive binding to an antigen spot would result in only one single metal grain. The hypothesis would then be that simply counting grains on a test surface is sufficient to estimate the applied concentration of antigen. A straightforward method for generating capture spots in the low micrometer range was to use the indentions ("pits") found on a common compact disc (CD) as a master for molding an elastomeric stamp. This stamp was then used to microcontact print the capture antibodies. Performing the same procedures used before, a dot pattern with single or almost single grains was created, which then in turn was imaged by light microscopy and with the pickup

---

19) The data for the conventional ELISA experiment was obtained from the data-sheet of the CRP-antigen supplied by Kalon Biological Ltd., USA.

imager (Figure 42 A, B). Unfortunately, so far it was not possible to relate the applied concentration to the number of developed spots on the test surface. Here further experiments have to be designed to show a clear dependence between the counted grains and the concentration of applied antigens.
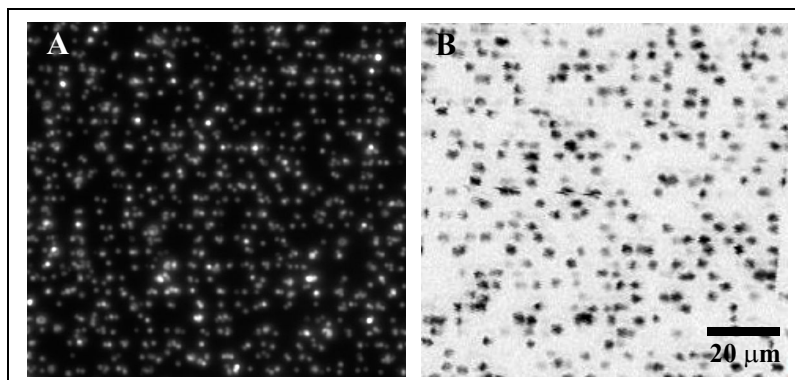
Figure 42: Microscope image (A) and pickup image (B) of microcontact printed CD pit structure of biotinylated BSA, which was subsequently Au enhanced.

3.1.4. Discussion

In this section it has been demonstrated that the developed CD-pickup imager could be used to quantitatively measure bio-molecular binding events on the single molecule level. The results showed at least comparable, if not higher, precision, dynamic range, and accuracy as those obtained with much more expensive instruments, such as e.g. a conventional ELISA reader, a Luminex system, or a confocal laser scanner.

The lowest concentration that was detected with the pickup imager and discriminated from background was *0,9 pM* for the CRP antigen having a molecular weight of 114 kD.

Since biomolecules such as antibodies or DNA can be placed as individual binding areas onto solid supports with high lateral control and on the micrometer scale, using µCP and an alignment tool such as the one presented in Section 3.3., large numbers of separate immunoassay "spots" can be generated. By using ligand concentrations adjusted to yield less than one detected binding event per individual spot, counting of silver grains would in principle allow quantification of the number of binding events. This regime reduces detection to a "binary decision" - either a spot carries a silver grain or not. The number of "positive" spots measured in a field of many (>hundreds) identical spots then directly correlates to the concentration of ligand. A possible error that is introduced when more than one molecule binds per spot can be described by a Poisson distribution and can be compensated for mathematically.

Moreover, it was shown that microcontact printing and silver enhancement combined with a CD pickup readout system provide the necessary precision and accuracy for sensitively detecting molec-

ular binding events. The CD-pickup is already optimized for measuring optical properties in a binary way to yield "yes-or-no" signals of the "pits" encoding the information of the audio CD format. Consequently, this device is well suited to be developed into an apparatus for true binary concentration measurement.

Even an adaptation to the spiral scanning track of the conventional compact disc format seems feasible by printing millions of individual reaction areas on polycarbonate discs [La Clair, 2003]. Further, by printing "spots" with many different receptor substances onto the CD track, multiplex-binding experiments can be envisaged. As the number of binary information units available on a single CD exceeds six billions, the implementation of multiplex tests seems to be limited only by the logistics of receptor application and fluidic handling. In the light of the exploding demand for the parallel analysis of multiple binding partners (currently mainly achieved on microarrays using fluorescence readout), this "binary biochemistry" detection method could add a novel approach to the microarray technology available today.

3.2. Enzyme assisted inverse µCP (*EAI-µCP*)

Microcontact printing has become a well-established method for patterning surfaces with molecular monolayers of a diverse origin. Especially the printing of alkane-thiol monolayers onto noble metal surfaces such as gold or silver and subsequent etching of the surface, proved to be a very successful technique for structuring inorganic surfaces (Figure 43 A).[20]

However, a major problem in soft lithography arises when trying to pattern surfaces with structures that bear an unfavorable aspect ratio (Section 2.1.1.). Here the elastomeric material, which is used as stamp, tends to collapse and hence destroys the shape of the structures. In order to circumvent this problem, a novel process was developed. The idea is to convert an unfavorable structure design by inverting high aspect ratio structures into a favorable structure definition with larger supporting structures such that the stamp does not collapse anymore during the surface contact. For this purpose, it becomes necessary to also invert the patterning, respectively the etch process, to finally obtain the correct pattern again. This pathway has been recently investigated by Delamarche et al. [Delamarche, 2002]. To invert the structure definition they used two sorts of thiols. The first employed alkylthiol of short length, incapable of forming an etch resistant monolayers, was stamped onto the gold surface. It served as a mask for a second thiol molecule, a long chain alkylthiol. These thiols are capable of forming tight monolayers resulting in good protection against etchants. The etch resistant monolayer assembled around the masking molecules of the first thiol. Subsequent etching of the underlaying gold surface then revealed the inverted image of the previously stamped structures, which are now structures of high aspect ratio (Figure 43B).

Thiols however, especially the short molecules, have a high diffusion rate on the surface which can lead to "washed out" structures. Given the nature of the stamping process it is not possible to create structures with extreme aspect ratio. Large flat areas pose problems in transferring a uniform thiol monolayer without defects. This can be attributed to an insufficient amount of molecules present on the stamp surface upon contact with the surface [Larsen, 1997].

In this work, a simple and versatile method is presented to allow for creating extreme features, such as for example single wires, alignment crosses or a two dimensional metallic meshwork with big voids. The shortcomings of the inverse microcontact printing reported by Delamarche et al. were overcome by printing proteins as substitute for the short thiol molecules. Proteins have the big advantage, that they do not diffuse on the surface once they are stamped. Hence, patterned structures are stable and can serve as high-definition mask for subsequent monolayer formation of long chain

---

20)Besides thiols, many biological molecules such as proteins or antibodies can be printed using soft-lithographic techniques. See Section 2.3.2.

alkane thiols. The crucial step in this new process now is to remove the proteins from the surface to render the surface accessible for the etchant (proteins hinder etching of the gold to some extent). The removal of the proteins from the surface was realized by digesting the protein layer with a proteolytic enzyme. A protease breaks the backbone of the polypeptide chain and releases single amino acids or protein fragments into the medium leaving back a more or less blank, uncovered surface that is ready to be etched (Figure 43 C).
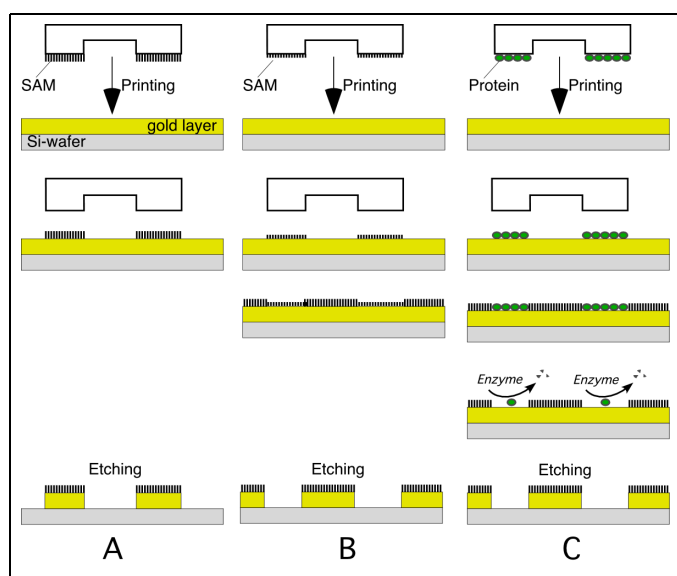
Figure 43: Diagram of (A) µCP of alkane thiols and subsequent etching, (B) positive µCP and (C) Enzyme Assisted Inverse µCP (EAI-µCP).

During the evaluation process of EAI-µCP several different protein mixtures have been tested. All the proteins that are commonly used for blocking surface interactions showed a residual etch protection against the KCN etch bath. Even after prolonged protease digestion the surface still did not behave like a bare surface. Common to all blocking proteins was their globular structure, which might hinder full digestion by the enzymes. Hence, in a further experiment gelatin, pre-digested (pre incubated with enzyme), and sonicated gelatin was proved successful as ink. Gelatin consists of a loosely connected meshwork of long polypeptide chains. This meshwork could easily be digested by the proteases. The structures that were fabricated with this novel approach, showed good patterned features and also highest aspect ratios, e.g. free standing wires, were obtained without loosing the high resolution.

3.2.1. Experiments & Results

The experiments performed to proof the principle of EAI-µCP were done as described in Section 4.3. In brief, first a PDMS stamp was inked with the block mixture of proteins[21]. Then the pattern of proteins was printed onto a clean gold surface. The uncovered areas on the gold surface were then cov-

---

21) The blocking mixture consists of BSA and casein molecules, or of gelatin.

ered with an monolayer of eicosane thiol (ECT) by dipping the whole surface in the thiol solution. Subsequently the such prepared gold surface was incubated with an enzyme digestion mixture for a few hours in order to digest and remove the proteins covering parts of the surface. Finally, the gold surface was etched in a KCN bath, thereby removing the gold at places where the stamp process previously had deposited masking proteins (Figure 43 C).

From all protein containing blocking agents tested, fish gelatin turned out to be the most effective blocking and template agent for enzyme-assisted etching. In exchange with the blocking mixture a 5% solution of fish gelatin in ddH$_2$O was applied to the stamp surface for 45 min. Then the same procedure described in 4.3. was performed including thiol coating, protease digestion and subsequent gold etching. It was found that gelatin enhances the discrimination between covered and uncovered areas in the etch process and allows for shorter etch times.

In order to characterize the properties of the protein layer on top of the gold surface before and after protease treatment, samples were imaged by atomic force microscopy in air and tapping mode.

Figure 44 shows an AFM image of the gold surface after microcontact printing protein. The boundary is clearly visible. Examining the profile across the edge reveals a protein layer thickness of roughly 3nm.
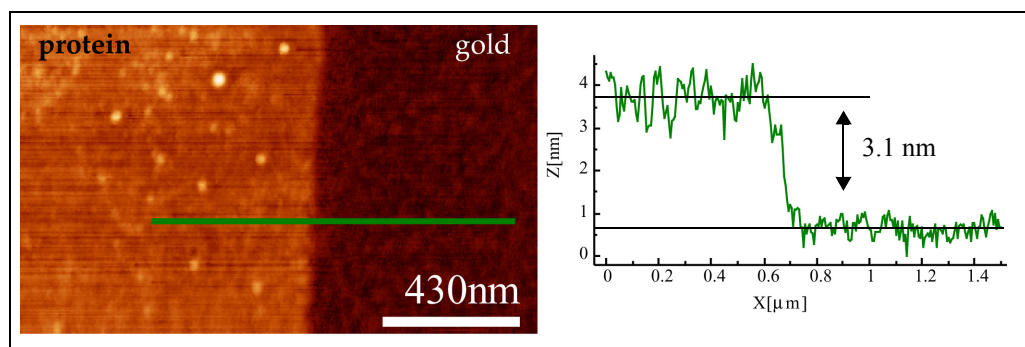
Figure 44: AFM image of protein-gold boundary: On the left side the surface is covered by a protein layer, on the right side the pure gold surface is visible. The profile shows a sharp boundary and reveals a layer thickness for the protein layer of ~3 nm.

After applying the thiol solution (ECT) to the surface, the boundary is still prominent. However, areas covered with a thiol layer (right side) show increased surface roughness. The surface roughness of the proteineous area, on the other hand, did not change much. The decrease in the step height from 3nm to 2nm indicates that a 1 nm thick thiol monolayer assembled on the free gold areas. Furthermore, no major defects in the protein layer are visible (Figure 45).
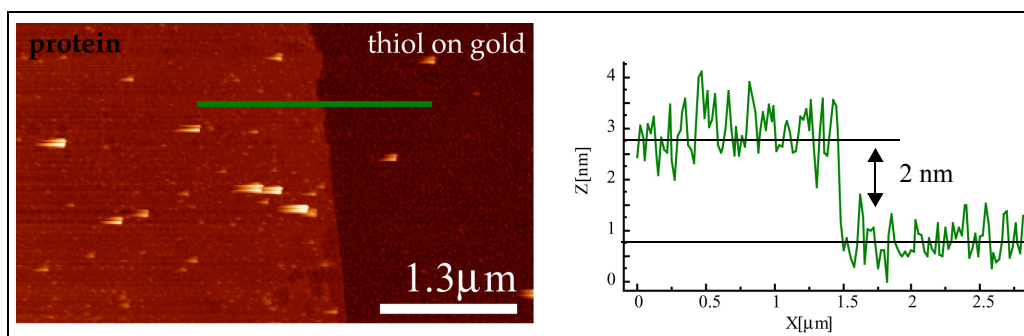
Figure 45: AFM image of protein-thiol boundary: On the left side the surface is covered by the protein layer, on the right side with a monolayer of alkane thiols adsorbed on gold. The profile shows an increased surface roughness were thiols where adsorbed. The height difference drops to 2nm because of the additional thiol layer (thickness ~1nm) on the gold surface.

After digesting the protein layer with *Pronase E* for 4 hours at room temperature, the AFM images show no intact protein layer anymore (Figure 46). Only fractions of the protecting layer are visible. The profile across the rim of the structure indicates the appearance of wholes in the protein layer, which makes the underlaying gold surface susceptible to etching. The large wobbles in the profile might be attributed to debris or remainders of enzymes from the digestion process. However, the etch protecting thiol monolayer on the other side is not effected by the protease treatment, as this part is still resistant to KCN etching.
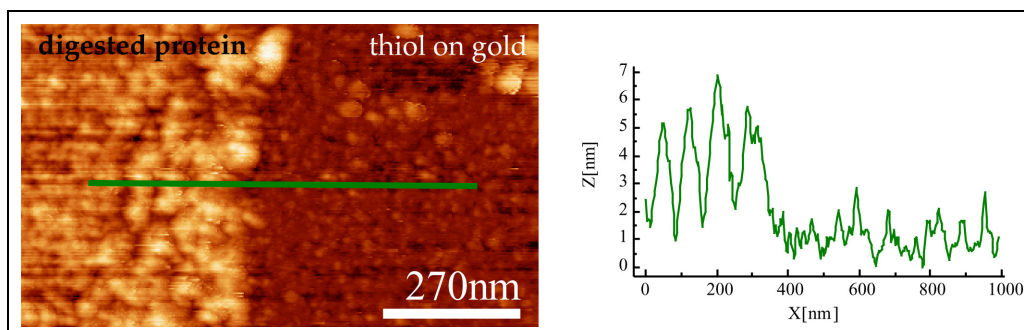
Figure 46: AFM image and profile of the surface after proteinase digestion. The protein layer did not vanish fully, but a fragmentation is clearly visible. The profile indicates a less dense protein layer.

Finally, a fully etched structure was imaged by AFM (Figure 47). The profile nicely reveals the steep drop at the edge of the gold structure of 15-20 nm. The remaining gold structure shows no holes or defects at all, which confirms that the protein layer can be reliably removed by enzymatic digestion leaving the SAM as etch resistant on the gold fully intact.
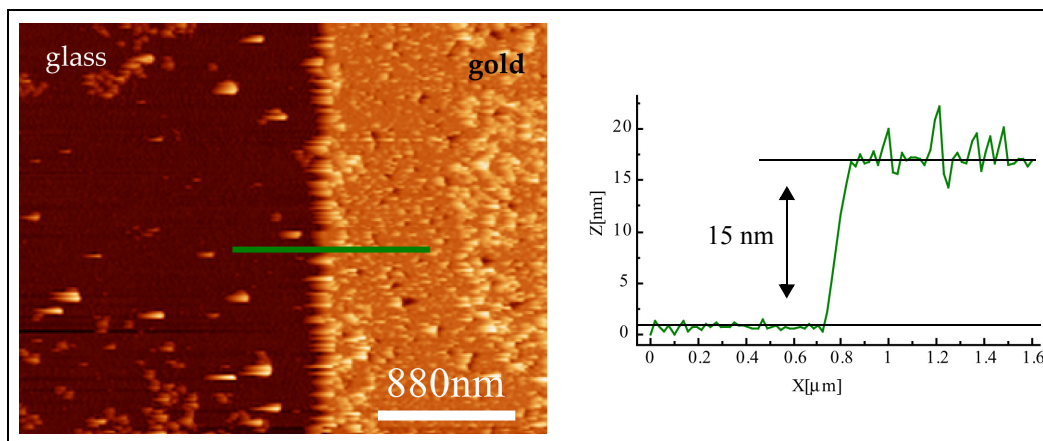
Figure 47: AFM image and profiles of surface after etching the probe with KCN. The profile nicely shows the step drop at the rim of the etched gold structure. The thickness of the gold layer was ~ 15 nm.

To test the universal applicability of EAI-μCP, a variety of patterns with structures of different aspect ratios was printed onto gold covered glass slides. After enzyme digestion and etching, images were acquired using a darkfield high magnification microscope (Figure 48). Amongst the fabricated structures were alignment marks (a), line patterns with varying pitch and line size (b), grids of different sizes (c), and freestanding wires (d). Noteworthy, these freestanding lines were only achievable using EAI-μCP. Even the method used by Delamarche et al. failed creating such structures due to the insufficient amount of thiols stored on the stamp to cover the large free area.
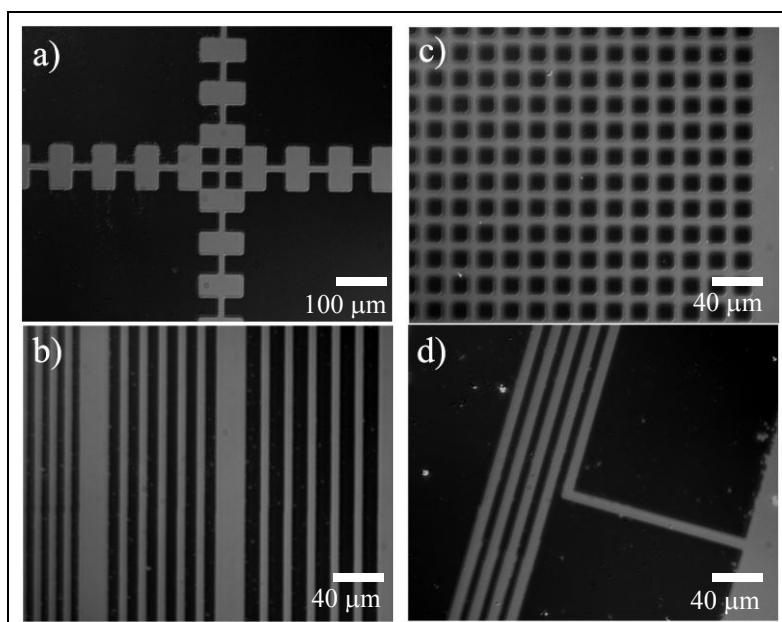
Figure 48: The micrographs show some examples for generated structures. (a) alignment cross; (b) line pattern; (c) grid; (d) free standing wires.

3.2.2. Discussion

EAI-μCP will be a very useful addition to the toolbox of soft-lithographic techniques. It is now feasible to pattern surfaces with high aspect ratio gold or other noble metal-structures. Without having to fear the loss of features through the collapse of fragile PDMS, structures such as e.g. freestanding "wires" or single alignment crosses can be created. In the next chapter this novel technique is applied to pattern glass surfaces with alignment structures necessary for the fabrication of molecule arrays. In conclusion it can be said that EAI-μCP is, although not extremely fast or straightforward, very useful for applications where patterns of widely separated features have to be fabricated.

3.3. The stamp aligner and its use for array printing

Arrays of molecules consisting of hundreds or even thousands of features have become increasingly important in the modern world of research and diagnostic assays. In research laboratories, piezo-or pin-based dispensing systems for printing arrays with molecule spot sizes larger than 100 μm are routinely used. However, up till now, no mass fabrication technology has been introduced to decrease the spot size and increase the spot density on a given surface.

μCP already proved to be an extremely useful method for patterning a flat surface with biological molecules in the micrometer dimensions. So far, only one or a few sorts of molecules were stamped at a time, and building an array of microcontact-printed molecules was not feasible for alignment of the stamps is difficult and tedious.

When dealing with structures in the micrometer range or below, the need for a precise positioning system becomes apparent. Mask aligners, which are used predominantly in the semiconductor industry for aligning photolithographic masks on top of substrates (wafers) in the sub micrometer range, could be a solution for this problem [Burgin, 2000; Michel, 2001; Folch, 1998; James, 2000]. However, mask aligners are expensive, are not built for handling elastic substrates, and do not allow observing fluorophore-labeled features on a patterned surface. For a cheap on-site production of molecule arrays with a small number (<100) of different molecules an alternative had to be found.

By using precise stepping motors mounted on top of an inverted microscope it was possible to setup a simple alignment tool for the fabrication of arrays for laboratory use. Adding tilt and rotation capabilities for the sample stage gave the full range of motional freedom for convenient alignment of elastomeric stamps to surface structures (see Section 4.4.2.). This self-built alignment tool was then used in subsequent experiments to create arrays of biomolecules required for the different diagnostic assay applications.

3.3.1. Alignment marks

An important prerequisite for aligning stamps on a surface are alignment marks. These alignment marks consist of geometrical features patterned on the target surface that can be matched by similar features on the stamps surface. For the experiments with the stamp aligner, a design consisting of 3 different crosses as described in Section 4.1.1.1. was chosen. In principle, these alignment marks, together with the use of precise stepping motors, allow to achieve an alignment accuracy of roughly 1 μm.

When using PDMS stamps with integrated alignment marks on their surface it is necessary to take into account that PDMS shrinks slightly after curing the polymer. The rate of shrinkage can amount

to 1-2% difference [Rogers, 2001] in structure size between the original structure definition on the master mold and the final PDMS stamp. The exact shrinkage rate depends strongly on the thickness of the elastomer, on the composition of the elastomeric material, and on the curing temperature. For structures with sizes from 10 to 100 micrometers this shrinkage can already amount to deviations of 0.5 to 1 micrometer. Even more profound is the concern about the so called runout failure, that is the sum of all deviations over larger (centimeter) areas.

This shrinkage leads to a miss-alignment if using the same feature dimensions on the target surface and on the stamp master. One way to circumvent this problem, is to determine the shrinkage rate and increase the structure sizes in the master for stamp molding by exact this factor. However, the shrinkage rate of PDMS depends on thickness and material composition and thus might vary from batch to batch.

Several reports in literature [Burgin, 2000; Michel, 2001] have suggested a cure to that problem, e.g. using multi-material layered rigid stamps. As an alternative to the published solutions and when only relative, rather than absolute, accuracy is needed, the creation of alignment marks on the target surface by using EAI-µCP is suggested in this work.

It has been shown in Section 3.2. that EAI-µCP is capable of creating high aspect ratio gold patterns on surfaces using elastomeric stamps. To avoid the different sizes of alignment marks, due to shrinking of PDMS, the stamps that were used for the EAI-µCP process were taken from the same batch as the stamps used for the final pattern printing. Thus, the shrinkage was the same for both structures, the alignment marks and the marks on the stamp surface, and aligning them posed no problems. Glass surfaces that present the such created alignment marks were then used in subsequent experiments to align stamps containing dot patterns to them. It has to be mentioned, that EAI-µCP was in fact originally developed for exactly the purpose of creating alignment marks on glass surfaces.

3.3.2. Overlay printing of a protein array

To prove the functionality of the built stamp aligner a set of four different stamps has been designed (Section 4.1.1.1.), such that they together constitute a linear array of dots. The stamp aligner is used to align the set of stamps and overlay microcontact print an array of 50µm sized molecule dots (Figure 49 A). The precision of positioning a single stamp affects the over-all conformity of the entire array to a high degree and thus, each alignment step has to be performed carefully.

A convenient way to confirm the quality of the aligned stamping, is to use fluorescently labeled proteins for inking the stamps, each with its own "color". After three (Figure 49 B) and four (Figure 49 C) consecutive aligned printing steps, fluorescence microscopy revealed the accuracy of the work

and proved the alignment apparatus useful for generating precise arrays. The whole alignment procedure takes roughly 15 minutes for an array consisting of four different sorts of molecules. This seems to be rather long, but by pre-programmed positioning of the stamps and by using pre-aligned stamps and substrates this procedure could be converted into a rapid array production technique comparable to that used for microarray fabrication by aligning lithographic masks [Fodor, 1991].
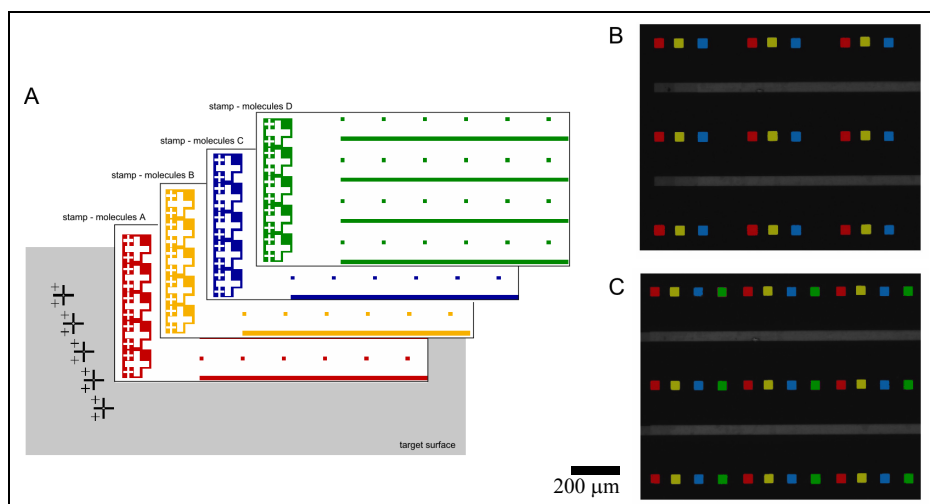
Figure 49: (A) Schematic drawing of aligned stamping process of four different sorts of molecules. The fluorescent micrographs show the stamped protein dots. Dots from different stamps are coded in false colors. (B) Target surface after three stamping steps; (C) Surface after positioning the fourth stamp.

3.3.3. Measuring printing and alignment precision

By performing several overlay printing experiments, the overall positioning precision could be determined. The accuracy of alignment is defined as the deviation of the actual position of the pattern from the nominal position. The stamps used for these experiments exposed features of 50 μm. After the acquisition of fluorescent micrographs of arrays constituted by repetitive alignment of four individual stamps (Figure 50 A), the individual positions of the printed dots were analyzed. The average deviation from the ideal position resulted in a positioning accuracy for the stamps of approximately *4 ± 2 μm*. Additionally the positions of the alignment marks that were co-stamped to the surface were analyzed. These deviations resulted in an accuracy for positioning of *3 ± 2 μm* (Figure 50B).

The step size of the stepping motors used in this setup is *100nm* and the accuracy of moving to a predefined position (repositioning) is less than *1μm*. Given this, one should expect better results for the alignment accuracy, however, a few mechanical instabilities in the setup impaired the practical precision. By increasing the mechanical rigidity the setup could be improved to perform alignment experiments with higher precision. Nevertheless, for the purpose of the present study of overlay aligning elastomeric stamps on target substrates, this setup was sufficient.
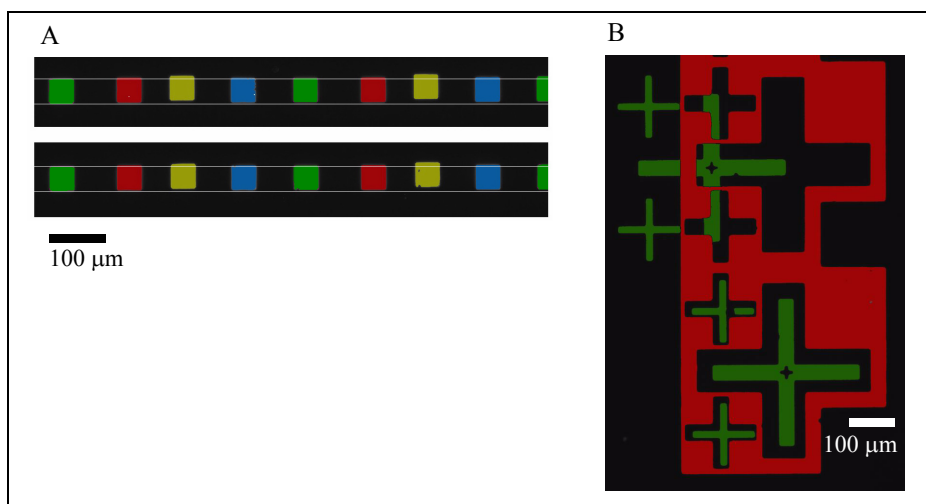
Figure 50: The deviation of dot patterns from the ideal line array was measured by determining the deviation of the single dots from the ideal position (A). Alignment marks: The red structures were aligned with respect to the green ones already present on the target surface (B). The average deviation could be determined by measuring the offset from the ideal position.

3.3.4. Discussion

It has been shown that it is possible to build a stamp aligner using simple devices such as three stepping motors for the three spatial directions and an inverted microscope for the optical control. The accuracy of alignment that could be reached with the present apparatus was limited to 3-4 µm due to instabilities in the mechanical design. After all, for the application of printing arrays of biological molecules with spot sizes in the lower micrometer range (>25 µm), this apparatus was fully sufficient. But printing of arrays is not the only application that can be envisioned for this apparatus. The precise alignment of molecule structures might also be useful for other fields such as patterning cell guiding molecules on surfaces or preparing multifunctional bioactive surfaces with regions of different molecules for e.g. screening purposes.

3.4. Microcontact printing of DNA

Emerging microarray technology allows the expression of thousands of genes to be studied simultaneously. This has become possible by attaching DNA molecules (probes) to the surface of a microscope slide arranged in an array format. These arrays are applied broadly, [Southern, 1999; Schena, 1998; Watson, 1998] in particular in gene-expression profiling [Schulze, 2001; Harrington, 2000; Schena, 1995; Lockhart, 1996], single nucleotide polymorphism (SNP) detection [Hacia, 1996] and sequencing [Drmanac, 2001].

A common way to fabricate DNA arrays [Schena, 2000] is to spot fluids containing the desired DNA fragment onto a microscope slide using metal pins [Shalon, 1996] or microactuated nozzles [Schober, 1993]. A technologically more demanding way has been demonstrated by in situ synthesis of oligonucleotides (up to 25 bases) using light-activated chemistry combined with photolithographic techniques [Fodor, 1991; Lipshutz, 1999]. A major drawback of both production techniques is the inherent sequential nature of the process. Either one spot of oligo-nucleotides is deposited after another, or one base is coupled to the previous one with the consequence that each array is written de novo as an original. Thus, the speed of fabricating an entire DNA array is quite low (on the order of 30 minutes per array containing 10,000 features).

Analogously to conventional book printing, the standard techniques of DNA array production, as described above, correspond to each letter being written individually, one after another. Hence, the idea to adapt concepts from the printing industry is obvious and calls for a "color printing drum" of DNA. A page of a book is printed in one step, so why should this not work for a complete array?

Microcontact printing (μCP) has been demonstrated as a technique for the parallel delivery of proteins as surface patterns onto a target substrate [Bernard, 1998; Bernard, 2000]. A stamp made of an elastomeric material such as polydimethylsiloxane (PDMS) can be topographically structured by casting the pre-polymer against a 3D master [Xia, 1998; Kumar, 1994]. The stamp is inked with the molecules of interest, forming a more or less complete monolayer, rinsed with buffer, blown dry under a stream of nitrogen, and then printed onto the substrate surface.

In this chapter it will be demonstrated that these concepts also apply to printing of DNA. Similar to printing proteins, μCP of DNA calls for carefully tailored surface properties of the PDMS stamps. The surfaces have to be attractive enough to bind DNA molecules reversibly from solution. However, the binding forces must not be too strong to hinder the release of the DNA when the stamp is removed from the target surface. Proteins, which are charged depending on their isoelectric point and on the pH in the surrounding medium (amphoteric), adsorb to uncharged surfaces such as PDMS mainly through hydrophobic interactions, which act over a very short sub-nanometer distance

[Kumar, 1994; Norde, 1986; Eckert, 1997], and form monolayers. This layer formation is in principal governed by a self-limiting deposition process, in which the growing number of adsorbed proteins renders the surface hydrophillic and thus inhibits further adsorption of additional protein (see Section 2.1.5. for the theoretical description of protein adsorption at the solid liquid interface).

DNA on the other hand, owing to its phosphate backbone, is a highly negatively charged polymer or poly-electrolyte. Hence, electrostatic interactions play the major role for adsorption and transfer properties. Electrostatic forces, with their extended reach of a few nanometers, could allow a multi-layered adsorption of DNA molecules to a point where the total charge compensates that of the surface (for a theoretical discussion of the adsorption of DNA to charged surfaces see Section 2.1.6.). The impact of the surface charge has already been reported for adsorption kinetics of DNA fragments from solution to rigid substrates [Chan, 1997; Fang, 1998]. Thus, it becomes obvious that careful control of the surface properties, that is, especially the charge density, was of great importance for the experiments performed.

3.4.1. Experiments and Results

In microcontact printing, the transfer of DNA from the stamp to the substrate surface takes place during a brief (a few seconds) contact between the two surfaces (Figure 51). Fluorophore labels were used to follow the fate of DNA molecules after being adsorbed to the stamp and to visualize the printed and patterned DNA layer on a glass substrate.
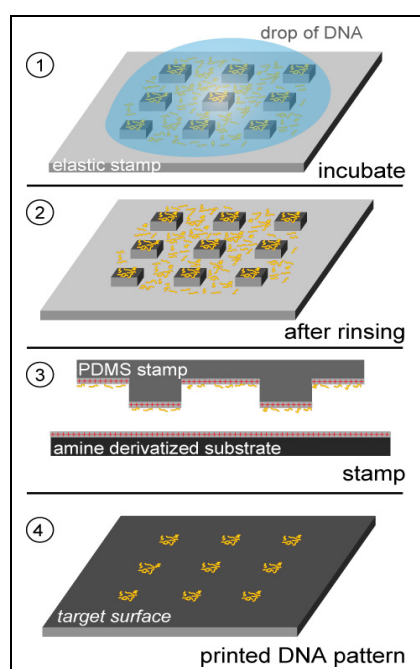
Figure 51: Microcontact printing of DNA molecules. Scheme of DNA microcontact printing. The surface of the elastomeric material (polydimethyl-siloxane - PDMS) was modified such that it exposes positive charges on its surface. The stamp was incubated with target DNA molecules in a solution of low pH. The stamp is then rinsed, blown dry, and printed to deliver the DNA to the target surface.

A precise and clear pattern was generated that lacks the typical inhomogeneities common to spotted arrays [Blossey, 2002]. Feature sizes down to 1 μm were achieved easily (Figure 52 A and B). To

ensure tight binding of DNA on the stamp during rinsing, the adsorption and rinsing buffers must have a pH between 5 and 9. If the pH rises above the pKa of the surface amines at 9.2, the positively charged amine groups become deprotonated and hence neutral, allowing the negatively charged DNA molecule to detach from the stamp surface. To further corroborate the high uniformity of the printed films, atomic force microscopic (AFM) images were taken (Figure 52 C and D). They revealed a homogeneous layer of the DNA at the surface. The edge definition of the surface pattern is very clean, and no excess of DNA was found at the rims of the structures.
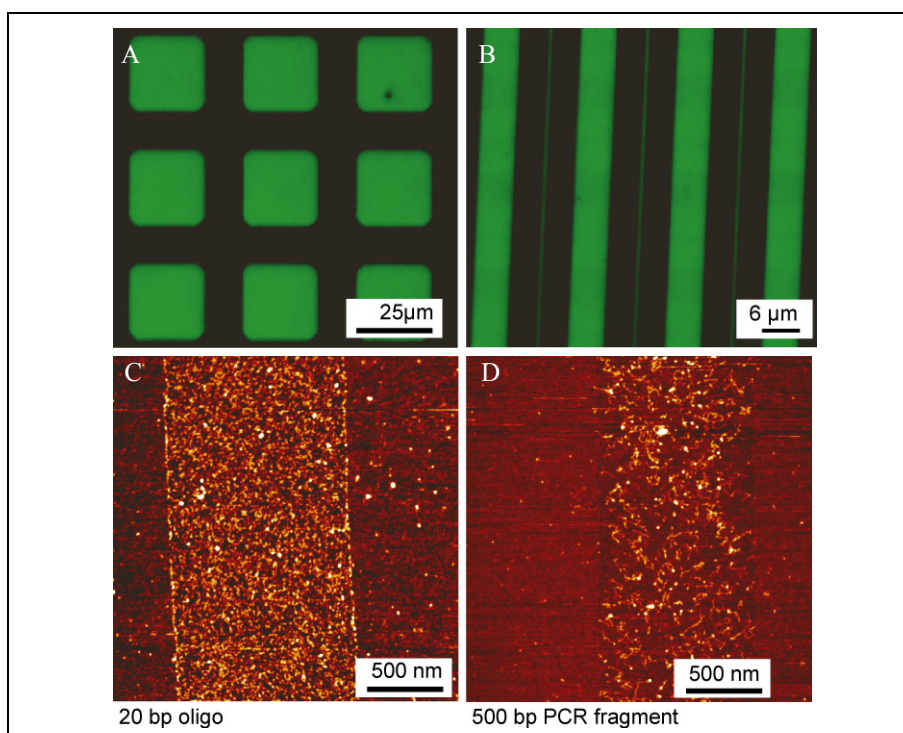
Figure 52: (A, B) Fluorescence images of patterned, FITC-labeled, oligo-nucle-otides on a glass surface after printing. The pattern size is limited only by the ability to manufacture molds with the desired feature size. Atomic force microscopy images revealing the printed DNA molecules deposited as patterns on mica sub-strates. AFM images (tapping mode in air) of stamped 1 μm lines of 20 bp oligonu-cleotides (C) and 500 bp PCR fragments (D).

The density of DNA on the target surface after stamping was quantified by fluorescence measure-ments of labeled oligonucleotides. Each DNA molecule contained one fluorophore. A reference curve was made by spotting defined amounts of labeled 20 base pair (bp) DNA oligonucleotides onto positively charged amine glass slides (Figure 53). This curve follows a typical saturation behav-ior, with saturation reached at *0.9·10⁴ (±0.1·10⁴)* molecules/μm². Increasing the concentration of molecules in solution from this point on did not increase the measured intensity any further. Calcu-lating the "maximum density" of a tightly packed surface of molecules spanning *19 nm²*, assuming a length of *8.2 nm* and a width of *2.3 nm* for 20 bp oligos, resulted in approximately *5·10⁴ molecules/ μm²* and agrees well with the experimental value. The deviation of experimental vs. calculated val-

ues may be explained by an incorrect approximation of the molecule geometry and dimension as well as by neglecting repulsive forces between molecules of the same charge; Especially the formation of an electrostatic double layer exerting repulsive forces on the incoming molecules can have significant impact on the surface density of molecules up to total suppression of adsorption, depending on buffer pH and ion strength (see Section 2.1.6.). In addition, the experimental value may also be subject to fluorescence quenching.
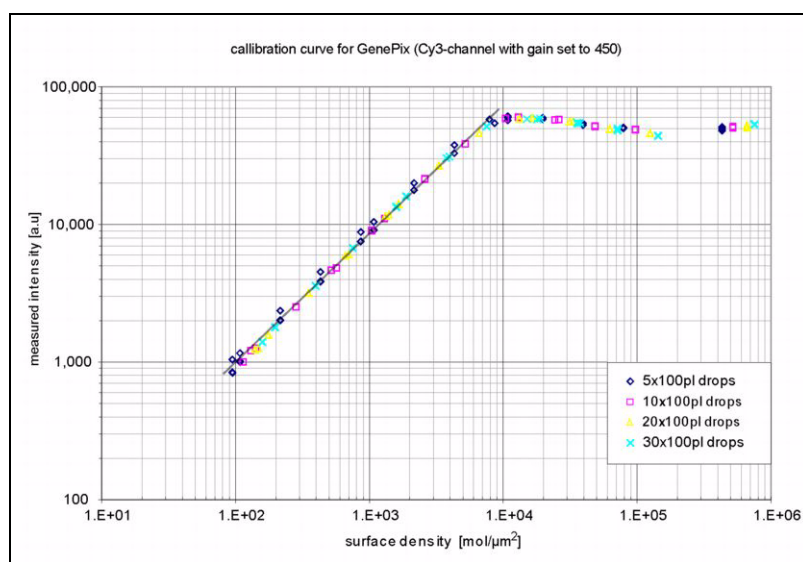
Figure 53: Measured fluorescent intensity vs. surface density of molecules for calibrating the measurements of the confocal fluorescent scanner.

The influence of the buffer composition on the adsorption of DNA to the PDMS stamp was examined. DNA molecules from a solution of 1 pmol/mL DNA, diluted in deionized water (DI), were adsorb to an elastomeric stamp under various conditions and subsequently printed onto the target surface. After rinsing, but before printing, the measured fluorescence indicated the formation of a dense layer on the stamp surface with an effective surface coverage of *8000 ± 500 molecules/μm^2*. On the first print, a surface density of about *4000 ± 500 molecules/μm^2* was measured. Thus, the molecule density on the target surface amounts to only *50%* of the initial density on the stamp. Different adsorption buffers decreased the initial surface coverage dramatically (*30%* of the maximum value for MES pH 7.0 buffer, 10% for PBS pH 7.2 buffer), and using carbonate buffer at pH 9.6 fully inhibits adsorption of DNA on the stamp (< 1%) and its subsequent transfer (Figure 54). A high salt concentration as well as the presence of divalent ions such as Mg^{2+} in the PBS buffer did not change the coverage significantly (less than 13% of the maximum value). From these findings, it can be concluded that indeed the pH of the buffer is the key factor in adsorbing DNA to charged surfaces as has already been predicted by the calculations in Section 2.1.6.
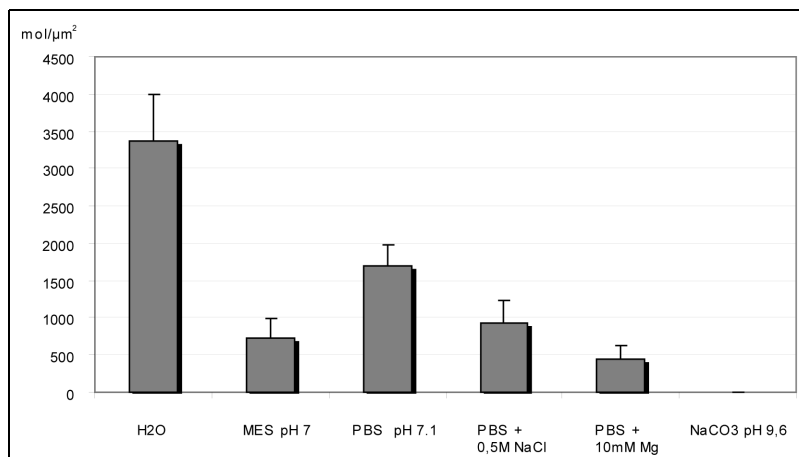
Figure 54: The surface density of DNA after printing depends strongly on the adsorption buffer. Stamps were incubated with DNA diluted in buffers of different pH and salt concentration.

Subsequent to the observed partial transfer of the DNA molecules, the possibility of inking a stamp once and printing it several times was analyzed. The evaluation of the fluorescence of multiply stamped 20 bp oligonucleotide patterns showed an exponentially decaying behavior (Figure 55 A). Fitting a function of exponential decay (solid line in Figure 55) yielded a value close to 0.5 for the exponential basis, indicating a ~50% chance for each molecule to be transferred. This transfer probability remained constant over several (at least five) stamping steps. Dashed lines represent the theoretical values for 25%, and 75% transfer probability.

A significantly different transfer behavior was found for repeated stamping of longer molecules (500 or 1600 bp DNA). Here, the transferred amount of molecules was significantly higher than 50% for the first printing step, whereas the subsequent prints showed a dramatic drop in transfer rate (Figure 55 B and C). Again, each molecule contains one incorporated fluorophore. Changing the concentration of the molecules in solution over three orders of magnitude (squares, circles and triangles in Figure 55) did not influence the aforementioned behaviors. The transfer process is apparently governed by either of two considerably different regimes, depending on molecular size: Short DNA molecules appear to lie on the stamp surface without intersecting one another. In this case, stamping will transfer each molecule with a certain probability that solely depends on the net charge of the molecule. In contrast, the longer molecules adsorb onto the stamp surface in such a way that they intersect each other and thus form a (multi-)layered and more or less entangled meshwork. The degree of entanglement may be related to the density of molecules in the incubation solution as well as to their size. During the stamping process, individual molecules are no longer transferred independently of each other: an entire layer of entangled molecules is transferred simultaneously. This "cooperative regime" seems to apply only to the first printing step (Figure 55 B, C), whereas in the following steps the transfer rate dropped to 25%.
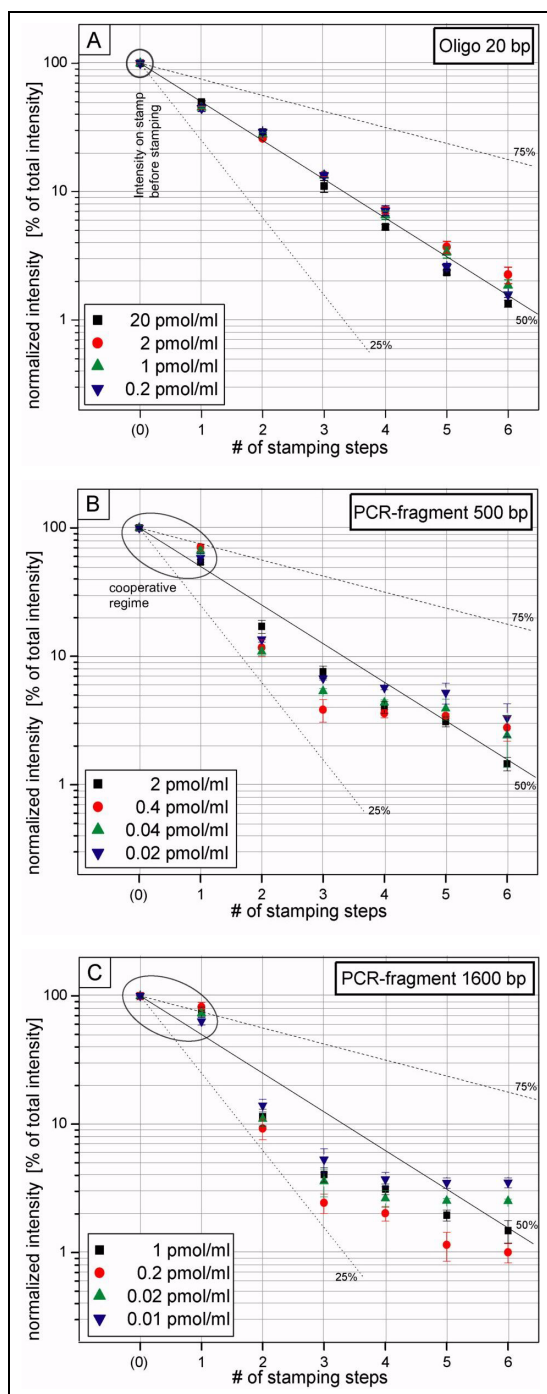
Figure 55: Transfer behavior of DNA for multiple successive stamping steps. Consecutive stamping without re-inking was performed using fluorescently labeled oligonucleotides of various lengths; (A) 20 bp, (B) 500 bp, and (C) 1600 bp. For each fragment length, four data sets with different initial molecule concentrations were recorded (symbols in plot). The amount of molecules transferred onto the target surface after every stamping step was quantified by measuring the fluorescence on the print. The intensity of each printing step was normalized to the initial intensity on the stamp and plotted on a logarithmic scale against the number of printing steps. Dashed lines are guidelines and mark the transfer rates of 25% and 75%, respectively.

This interpretation is corroborated by AFM images (data not shown) that show meshwork formation of the transferred long DNA fragments. It seems that after removal of the DNA meshwork, the remaining molecules have reached a density where they can act independently of each other. For the third and subsequent printing step an exponentially decreasing transfer behavior was again observed. This leads to the conclusion that for long DNA fragments the surface concentration has to be even lower than tested in order to circumvent the cooperative regime. For small molecules, it may have to be even higher to reach the regime of cooperative behavior. To pinpoint the transition between the

two encountered regimes of DNA transfer, a much wider range of variations of molecule lengths and their concentration in the incubation solution have to be employed.

Having demonstrated that DNA can be successfully printed in multiple copies, yielding uniform surfaces with excellent edge definitions, the transfer of various molecules in a single parallel printing step was demonstrated. Furthermore, the generated pattern allowed for specific differential hybridization of labeled DNA from a complex mixture. To achieve this, spatially localized inking was performed by means of micro-fluidic networks [Delamarche, 1997; Papra, 2001]. Sixteen parallel micro channels, each loaded with a different sample, were brought in contact with a topographically flat stamp in order to generate arrays of several different DNA molecules. A series of slides carrying the resulting line arrays of DNA probes were then hybridized with different combinations of complementary and non complementary DNA probes labeled with biotin. In order to visualize the hybridization, the biotin-labeled probes were treated with colloidal gold particles coated with an antibiotin antibody. Bound complexes were visualized using a gold enhancement kit. Four different target DNA sequences were employed (labeled A to D). Accordingly, probe molecules with the complementary sequences are labeled A' to D'. The enhanced line pattern (Figure 56) reflected the specificity of the probe molecules; low intensities correlated with base pair mismatch, e.g. A' binds to the target molecules B even though the sequence is not perfectly complementary (six mismatches overall). To avoid the detection of mismatched binding, a greater stringency of washing conditions could be employed.
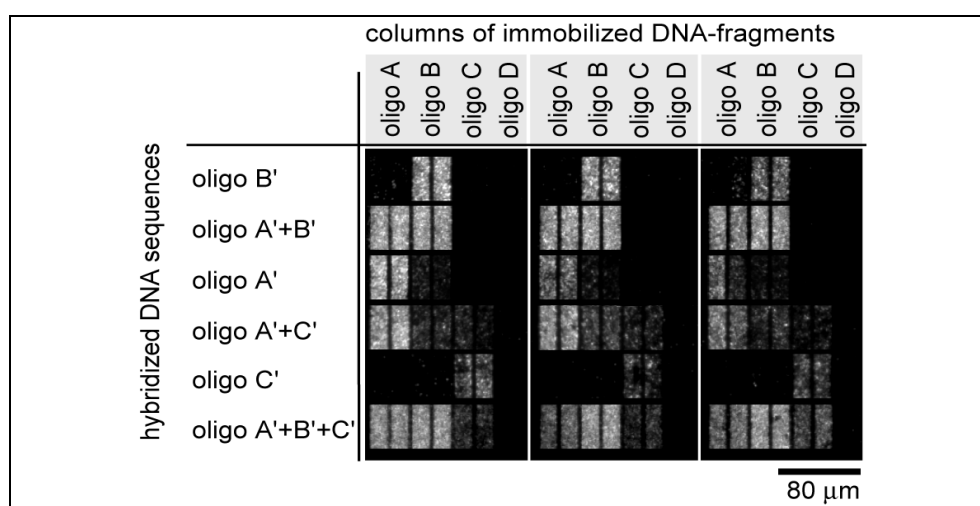
Figure 56: Parallel and simultaneous printing of various DNA molecules onto a target surface, visualized after hybridization using immunogold labeling and subsequent gold enhancement (autometallography). A 16-channel silicon microfluidic network (20-μm-wide channels with a 5-μm gap) has been used to ink a flat PDMS stamp with lines of different DNA molecules (A to D). After printing onto a glass substrate, spatially separated hybridization with probes specific to a sub-fraction of the arrayed molecules (A' to D') was performed. The resulting line pattern (repeated twice to show reproducibility) reflects the specificity of the probe molecules used.

In order to demonstrate the feasibility of microcontact printing of DNA further and to show its versatility, a conventionally spotted array of longer DNA probes (PCR products) on a PDMS stamp was used to print the entire array several times in parallel. Subsequent hybridization with fluorescent target DNA, prepared from a mixture of RNA sample material, produced results comparable to standard arrays (Figure 57, panel A to C: stamped; panel D: directly spotted). Three observations are noteworthy: First, the total amount of DNA adsorbed in one spot on the stamp surface - after drying the droplet - appears to be transferred layer by layer and in fractions to the target surface. Individual spots in panel A to C showed regions of higher and lower intensity, which add up to the initial intensity. This is in accordance with the hypothesis of layered stamping of DNA discussed above. Second, stamped and then hybridized microarrays appeared to be more sensitive to a low concentration of starting material of total RNA, which can be seen from the upper part of Figure 57. Compared to directly spotted microarrays, much lower concentrations of starting RNA were detected. DNA may be more accessible in stamped spots, thus allowing for a more efficient binding of DNA from hybridization solution. Third and most important, multiple stamping of entire arrays is possible and it was found that at least three replicas of the array were fully functional (Figure 57, compare panels A, B and C) and can be used independently and without loss of information in separate hybridization experiments.
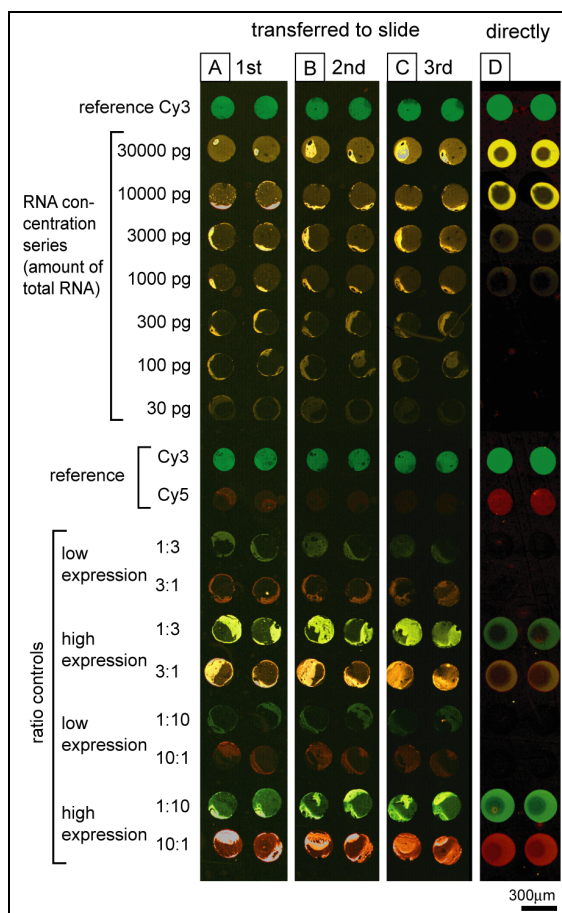
Figure 57: Parallel transfer of a complete DNA array and subsequent hybridization. Using a spotting device a DNA array has been generated on a PDMS stamp, and was subsequently microcontact-printed three times in succession onto glass substrates. Standard hybridization with fluorescent target DNA reveals the binding pattern (Panels A, B, C). As a control, a conventional microarray slide (amino silane glass) was directly spotted (Panel D). All slides were treated in accordance with common microarray protocols. The upper part of each slide represents a concentration series with different amounts of starting RNA material. The lower part is a ratio series, where relative intensities between the two channels Cy3 and Cy5 are compared. Direct labeled reference oligos with no match in the test material where spotted independently to control transfer properties. All the stamped and the directly spotted slides showed the expected values after scanning the slides with a confocal microarray scanner.

3.4.2. Discussion

In this chapter it was shown that microcontact printing can be expanded to the use of DNA array generation. Electrostatic interactions seem to play the key role in the transfer behavior of DNA. Two distinct regimes with different transfer properties were encountered and could be explained as a dependency on the length, or the total net charge per molecule and the density (surface concentration) of the molecules adsorbed on the stamp surface. For short DNA molecules with every stamping step 50% of the molecules present on the stamps' surface were transferred to the target surface. The major advantage of μCP of DNA is the capability of printing multiple arrays from a one time loaded stamp. This method could be developed to a potentially cost and time-saving process, particularly for gene-expression studies, where the ratio of bound to labeled molecules but not the total amount of material matters.

In the future, μCP of DNA – and analogously of other charged polymers or molecules – may help to simplify, accelerate and improve the fabrication of arrays. Gaining a full understanding of the transfer properties of DNA will enable researchers to adopt the technique of μCP for the production of precisely defined arrays with well-characterized molecule densities on a variety of substrates.

3.5. PCR-on-stamp

Microcontact printing (µCP) of biological molecules has been shown to be a versatile and fast technique to create surfaces with patterns of biological activity and usability [Bernard, 1998; Bernard, 2000]. Proteins, from peptides to antibodies and enzymes were microcontact printed for applications such as micro ELISAs (µELISA), enzymatically active surfaces and patterned substrates for cell attachment and guidance. Very recently, single- and double-stranded DNA has been shown to be a suitable ink for microcontact printing (Chapter 3.4.), [Lange, 2004]. However, so far the stamp was only acting as a simple transfer vehicle for the biomolecules to be placed onto the target surface. In 2001 Bernard et al. [Bernard, 2001a; Renault, 2002] developed a new technique called "affinity-contact printing" (αCP) to pattern surfaces in an "intelligent" way (Section 2.1.8.). They used receptor molecules fixed covalently to the elastomer surface to act as specific anchors for the target molecules. Now molecules could be localized to certain sites on the stamp by fishing them from an otherwise crude inking solution. This intelligent inking is followed by the transfer of the captured molecules by contact printing, thereby separating the captured from the capturing molecule in a mechanical fashion. In analogy to αCP for proteins the DNA variant, called PCR-on-stamp, was developed. PCR-on-stamp allows to microcontact print entire DNA arrays repetitively with a single stamp.

PCR-on-stamp could in the future help to easily fabricate surfaces structured with a multitude of different DNA probes. These surfaces could be used as either microarrays for e.g. gene expression studies or as multi purpose surfaces, where the DNA molecules serve as general linkers to guide other molecules to certain surface locations.

In 1984 Kerry Mullis [Mullis, 2003] developed a method to duplicate and amplify DNA molecules, called the "Polymerase Chain Reaction" (PCR) for which he received the Nobel Price in 1993. In the PCR process, enzymes are used to replicate single DNA strands by synthesizing the complementary strands along a template DNA strand. To initiate the process short sequences (primers) are bound to the template strand and elongated enzymatically by incorporating the appropriate free nucleotides present in the surrounding medium. After heating the two strands separate. By repeating several times the cycles of binding the primer, elongating the primer and melting the newly formed strand, an exponentially growing amount of identical copies of the original molecules is produced. Only recently, PCR was shown to work on DNA that is immobilized to a solid substrate [Adessi, 2000]. It has been reported that in this so called "solid phase PCR" the enzymes are fully functional in the close proximity of a surface.

The idea underlaying PCR-on-stamp is to combine the methods of µCP of DNA, αCP and PCR to create an intelligent, rechargeable stamp that facilitates a fast DNA microarray production.

The principle of PCR-on-stamp can be summarized as follows (Figure 58):

(A) A single stranded DNA molecule is immobilized on the surface of an elastomeric stamp;

(B) A suitable PCR solution that contains enzymes, primer oligonucleotides, and single nucleotides is used to enzymatically duplicate the attached strand;

(C) The ssDNA fragments of all spots on the stamp are duplicated in one single process step.

(D) The stamp is brought into contact with the target surface where the second strand can firmly bind to this surface.

(E) The two strands still paired are now separated by either mechanical force or by heating;

(F) The target surface carries now a copy DNA delivered by the stamp and the stamp, still exposing the template DNA, is ready for another round of the process.
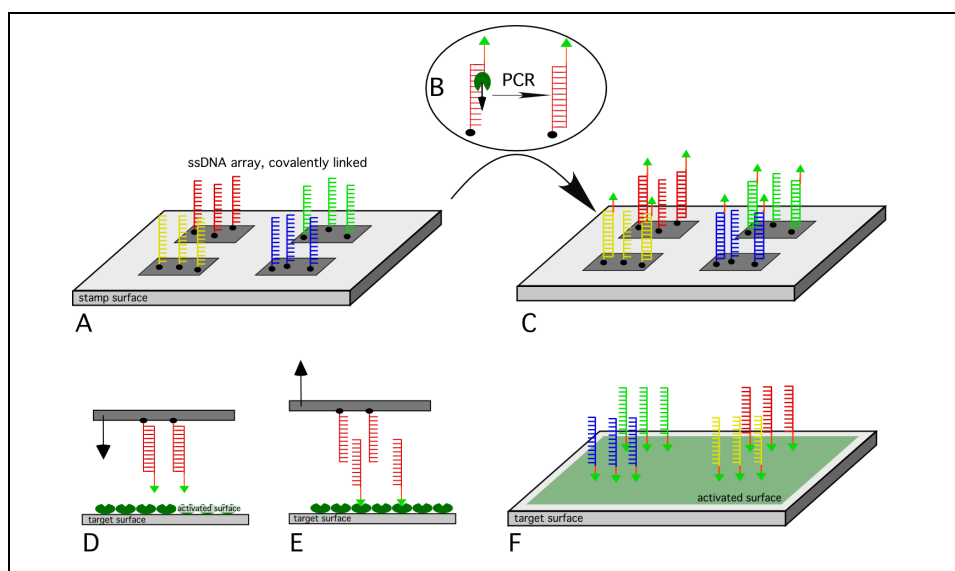
Figure 58: Schematic diagram of the PCR-on-stamp process. (A) Individual single stranded DNA fragments are immobilized in spots on the elastomer surface. (B) By enzymatic elongation (PCR) a second strand is synthesized elongating the primer oligonucleotide along the first single stranded DNA fragment which serves as template. (C) The ssDNA fragments of all spots are transcribed into dsDNA by PCR in a single bulk process step. (D) The stamp is brought into contact with the target surface, where either specific binding or unspecific binding of the synthesized molecules to the target surface can occur. (E) The double strands are separated by either mechanical force and / or by heating. (F) The original pattern of the stamp is replicated to the surface.

Important for the success of DNA strand separation and transfer is, that the attraction of the synthesized "copy" strand to the target surface is stronger than the bonds keeping the two DNA strands bound together. Only then the newly formed strands are transferred to the acceptor surface and the template strands are left firmly attached to the stamp surface. At this stage a new cycle of duplication and transfer can be initiated (A,B).

The process of PCR-on-stamp should in principle be repeatable for an infinite number of cycles. Taking a gradual loss of starting material from the stamp surface into account, it is valid to expect that only a finite number of replication steps are possible. Still, it can be envisioned that PCR-on-stamp has the potential of replacing today's standard fabrication process and finally leads to a much cheaper and faster DNA array production.

To prove the principal feasibility of PCR-on-stamp several experiments were conducted. First, the covalent attachment of the first strand to the elastomer surface was tested. Second, the conditions were determined under which a hybridized strand is transferred from the elastomer surface to the target surface with high yield. And third, PCR performance at the stamp surface had to be evaluated. The results of all three steps will be presented in the subsequent paragraphs.

The DNA test system, chosen for the experiments, consisted of a set of three mutually complementary fluorophore-labeled oligonucleotides. The first oligo (abbreviated SL-1) is used to investigate covalent binding of amine end-labeled oligos to the surface. The second oligo (SL+1) is used to test the hybridization and transfer behavior. A separate set of oligos was designed to test the PCR reaction on the stamp surface. MATT1 is immobilized to the stamp surface. PRIM1 is the primer used to initiate elongation and MATT2 is finally used to test if the newly formed and transferred strand is susceptible to hybridization after printing.

3.5.1. Modification of the stamp surface

An important prerequisite for the success of the experiments is the strong coupling of the DNA molecules to the elastomer surface. Therefore, a big effort was put into the modification of the elastomeric surface such that the DNA molecules are bound covalently but accessible to the stamp surface. Firm attachment of the first strand to the surface prevents a loss of molecules during the transfer or the replication step. Due to the polymeric nature of the stamp surface modification protocols have to be chosen carefully to insure a chemistry that is compatible with the PDMS material.

The covalent coupling of the template DNA was performed by amine silanization of the elastomer surface and then using cross-linker chemistry. These cross-linker molecules have different reactivity towards chemical groups such as e.g. amine-, thiol- or carboxy- groups. DNA molecules that present such groups at their end are bound to the elastomer surface.

In order to find the best coupling chemistry, various silanes such as amino- or mercapto-bearing chains were tested (see Section 2.3.1.1.). Due to their fast deactivation through contact with ambient oxygen, mercapto surfaces were soon ruled out for use in binding DNA. Various protocols for amino silanizations were tested and the resulting thicknesses of the silane layers were measured. The results

for most silanes were quite inconsistent and layer thicknesses showed extreme and not reproducible variations. The formation of a good and reproducible silane layer was only found when using APTMS and APTS diluted in an ethanol / water mixture (Section 4.1.5.1., Method B). For this protocol the increasing layer thickness measured by ellipsometry followed the expected saturation behavior (Figure 59). The maximum thickness of the grafted silane of *1.2 nm* was reached after 50 minutes and agrees well with the calculated thickness of *~1.1 nm* for a complete monolayer. The correct calibration of the instrument was confirmed by measuring reference layers such as the SiO_2 layer of a purchased wafer with known silicon oxide thickness of *2.3 nm* (datasheet and single measurement in Figure 59). All other silanization methods resulted in unpredictable silane thicknesses and were thus not used in subsequent experiments.
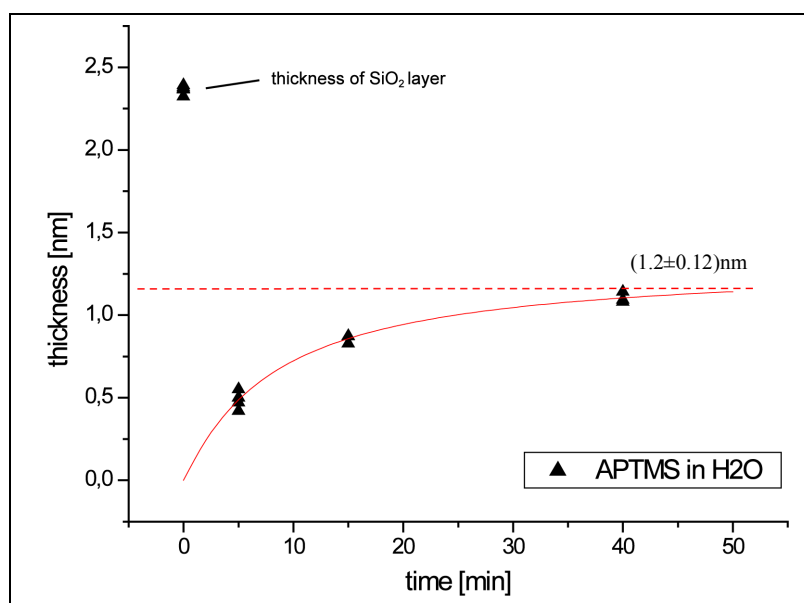
Figure 59: Increasing silane layer thickness up to one monolayer (approximately 1nm) measured by ellipsometry.

Table 3.3. summarizes the experimental findings for the different silanization protocols. The thickness of the silane layers formed on the transparent PDMS could not be measured. However, as it is believed that PDMS presents the same density of OH groups on its surface as a Si-wafer or a glass surface, the silanization chemistry should be comparable to that of silicon. The use of amino(propyl-tri-methoxy-silane) (APTMS) diluted in ethanol and water turned out to be the appropriate solution for a high quality functionalization of the PDMS surface.

Method	on glass	on PDMS
APTS at 80°C	inconsistent	inconsistent
APTS in EtOH/H2O (95:5)	ok; 1-2 nm	ok; thickness not measured
APTMS in EtOH/H2O (95:5)	ok; 1.3 nm	ok; thickness not measured
APTS in Toluene	ok; >2nm	PDMS is dissolved
APTMS in Toluene	ok; >2nm	PDMS is dissolved

Table 3.3. Comparison of different silanization methods with respect to the resulting layer thickness.

3.5.2. Crosslinker evaluation

The performance of the cross-linker molecules in terms of binding efficiency, bond strength and alteration of the chemical properties of the surface was a key aspect for the success of PCR-on-stamp. A variety of cross-linking molecules, which employ different chemical pathways to form covalent links between the surface and the molecule of interest were tested for their ability to immobilize a single stranded DNA fragment on the PDMS surface. In a set of experiments it was confirmed, that using an amine modified surface and homo-bifunctional[22] cross-linkers such as DSS, BS^3 and EGS yielded the best binding of the DNA molecules.

It should be mentioned again that the charge on the surface plays a crucial role for successful adsorption and binding of DNA molecules. It has been observed that using cross-linking molecules bearing negatively charged sulfonate (SO_3^-) groups for increased water solubility, hindered the efficient binding of DNA. Furthermore, it is believed that the presence of negative charge on the surface creates a strong electrostatic repulsion preventing negatively charged DNA fragments from diffusing and binding to the reactive groups on the surface. The experiments clearly showed: only a water insoluble cross-linker such as DSS allows DNA binding with high efficiency. DSS was thus chosen for further experiments, along with fluorescently labeled probe DNA.

The amount of DNA, bound by the crosslinker-activated surface after washing, was analyzed by measuring the fluorescence on the elastomer surface. The results for the different cross-linker molecules are summarize in Table 3.4., rating the ability to retain DNA molecules from bad(-) to very good(++). For comparison, the ability to bind uncharged proteins to an amino-modified surface is given as well.

---

22) Homo-bifunctional: the two chemical groups present at either end of the cross-linker molecules are reactive towards the same chemical groups such as e.g. amines (<-> hetero-bifunctional).

Crosslinker	reactive towards	cross-links proteins	cross-links DNA (NH$_2$,SH modified)
BS^3	NH$_2$ - NH$_2$	++	-
DSS	NH$_2$ - NH$_2$	++	++
sulfo EGS	NH$_2$ - NH$_2$	++	-
sulfo SMCC	NH$_2$ - SH	only if SH groups are present	-
sulfo SMPB	NH$_2$ - SH	only if SH groups are present	-
GMBS	NH$_2$ - SH	only if SH groups are present	-

Table 3.4. Comparison of different cross-linker molecules for attaching proteins and DNA to the PDMS elastomer surfaces.

3.5.3. Proof-of-principle experiments

In order to prove the concept of PCR-on-stamp a set of experiments was designed to show the behavior of the DNA molecules at the intermediate steps of the suggested cycle.

First it was necessary to prove that DNA is truly and stable bound to the stamp. Therefore, labeled oligonucleotides (oligo "SL-1", FITC labeled) were bound to the stamp surface using the cross-linking protocol. Then the stamp was brought in contact with an aminated glass surface. After printing, the amount of transferred material was measured using a fluorescence microscope. Even increasing the exposure time to 10 sec. revealed no transferred fluorescence on the target surface. This leads to the conclusion, that binding of the cross-linker molecule is strong enough to withstand the pulling forces present during stamping.

To test the stability of the surface-bond DNA under hybridization conditions, that is, especially heating the stamp to 70°C, a second oligonucleotide (oligo "SL+1", TRITC labeled) was hybridized and the fluorescent intensities of the first and second strand were measured individually (Figure 60 A, B). A loss of 10% of immobilized template strands was observed after heating the stamp to hybridize the "copy" strand to it (Figure 60, Bars 2). This loss might be caused by the partial unbinding of silane groups from the elastomer surface. Bleaching of the fluorophores of the template strand during the incubation period could also be responsible for the loss in signal. However, this loss is small and not compromising for the preliminary tests. The stamp, now carrying double stranded DNA fragments was then contact-printed to an amine target surface and the fluorescence was again measured on both surfaces.

After printing a further loss of template DNA became apparent. This amount of template DNA was found to be transferred, despite its covalent attachment, onto the target surface (Figure 60 A, Bar 4). The loss might be explained by the stronger attraction of the two strands to the target surface due to twice the charge now present and dragging on the covalent bond of the template strand. However, the "copy" DNA strand was completely transferred to the target surface as intended (Figure 60 B, Bar 3 and 4). In conclusion, the hybridized "copy" DNA was microcontact printed, leaving a significant fraction of template strand behind, still attached to the stamp surface. It should be noted that these preliminary data were subject to significant inhomogeneities. These inhomogeneities made it difficult to apply a correct normalization of the measured values, which in turn explains why the intensity values of the transferred and retained molecules do not always add to 100% (e.g. bar 3 and 4 in Figure 60 B).
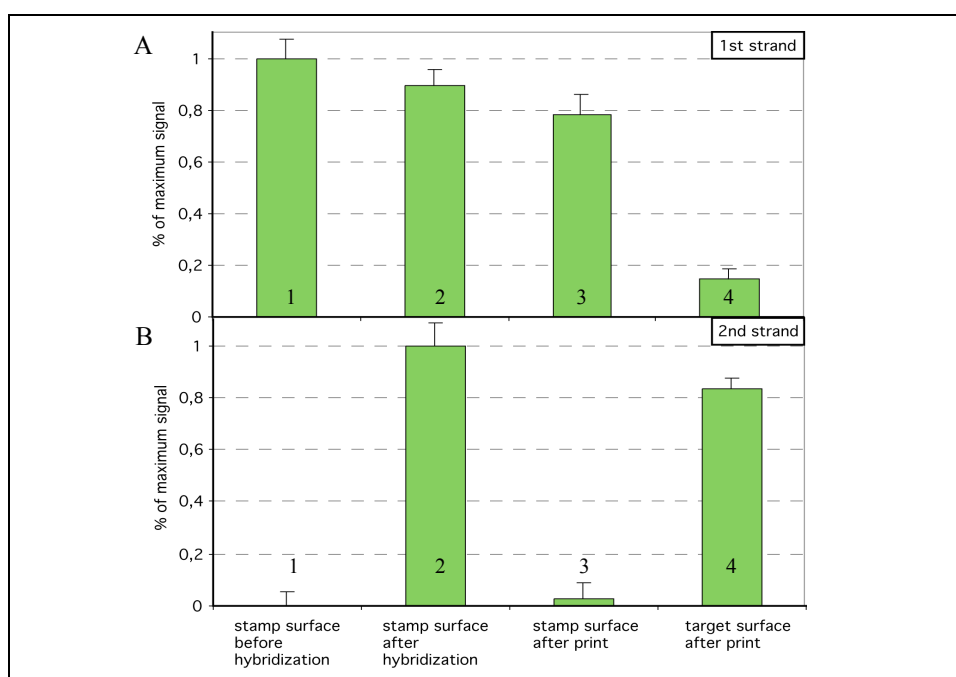
Figure 60: Barcharts representing the measured fluorescent intensities present on the stamp, respectively the target surface before (1) and after (2) hybridization and after printing once (3). Intensities in the respective panels (A - FITC / template strand; B - TRITC /"copy"-strand) are normalize to the maximum intensity measured. Fluorescent background was subtracted from the values beforehand.

It was found out that the presence of a thin film of fluid is crucial for the successful separation of the two strands during printing. The application of buffer solution to the contact printing process as it was used for the described experiments improved the transfer rate significantly. It seemed that the aqueous environment aided to unbind the two strands and to adsorb the second ("copy") strand to the target surface. Hence, rehydrating the stamp surface by applying a drop of buffer before contact-printing was included in the preliminary recipe for the transfer of DNA molecules. To even further

improve the printing procedure in future experiments, a printing tool for microcontact printing while surface and stamps are immersed in buffer could be developed.

Another crucial factor for the quality of the result was the appropriate temperature of the substrate and the surrounding medium. To achieve a constant temperature, the transfer by contact printing was performed on top of a thermocycler set to 70 °C. This temperature obviously facilitated unbinding of the dsDNA molecules and thus molecules could be separated readily. It can be summarized that humidity as well as temperature seemed to greatly increase the ability of the "copy" DNA to separate from the tightly bound strands. Concluding from this it seemed to be very important to carefully control the temperature and humidity to achieve a maximum transfer.

In order to demonstrate the rechargeability of the stamp after its first round of hybridizing and printing, the de-loaded stamp was hybridized to copy DNA again. Fluorescence served again to follow the fate of the DNA molecules.

Figure 61 B shows the amounts of fluorescence of the transferred DNA molecules measured during two cycles of the stamping and loading process. Figure 61 A shows the corresponding fluorescent image of the sample or the substrate surface, respectively. The first three bars indicate that the intensity of the fluorescence transferred to the surface (bar 2) is almost equal to that present on the stamp surface before printing (bar 1). Hence, nearly all material was transferred from the stamp to the surface and only a small amount remained on the stamp surface (bar 3). The next three bars show that reloading of the stamp by hybridization was possible, however, not to the same extent as for the first cycle (bar 4). Nevertheless, transfer was again about 100% (bar 5). Interestingly, the stamp surface showed a higher amount of residual material on the stamps' surface (bar 6) than in the first cycle. Residual fluorescence intensity on a stamp surface can be the result of either molecules that were not separated from the 1st strand, or molecules that adsorbed unspecifically to the stamp surface during hybridization and are not transferred by μCP. The molecules not separated during the second printing step then add to the already existing fluorescence. Measuring the residual fluorescence after further printing steps would probably show that the specific loading capacity of the stamp surface degrades. However, in this work stamps were only reloaded once, thus long-term behavior of the residual intensity can not be discussed here.
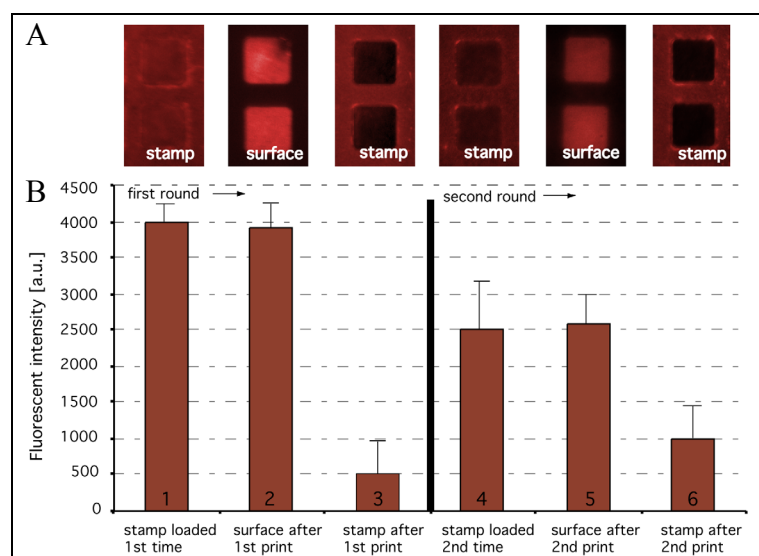
Figure 61: (A) The inset images illustrate the fluorescence on the stamp- or target-surface.(B) Comparison of material transferred and retained on the stamp surface.

The amount of the fluorescence originating from template strand DNA was followed separately. Apart from a high background fluorescence measured in the FITC channel, only small amounts of fluorescence was found on the target surface after printing (Bars 2, 5 in Figure 62), indicating that the template strand DNA was bound strongly to the elastomer. During all steps of the two cycles (bars 1, 3, 4, 6 in Figure 62) the amount of template DNA found on the stamp surface stayed high. Nevertheless, after the second printing step a little more than 50% of the original value above background for the fluorescence on the stamp was left. This loss can be attributed to either a loss of molecules during transfer and hybridization or to bleaching of the fluorophores.
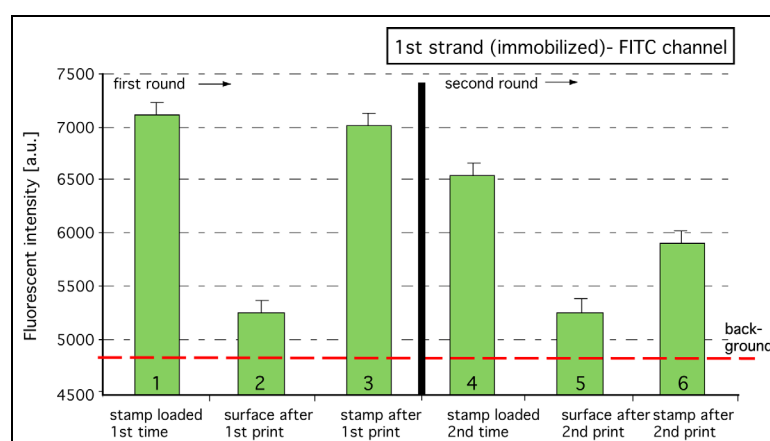
Figure 62: Chart illustrating the behavior of the immobilized first DNA strand during the printing and reloading process.

The transfer behavior observed in this experiment differs slightly compared to the experiments performed before, where the stamps were not reloaded. This stresses the fact that more experiments are necessary to find the perfect experimental conditions for a 100% transfer of the "copy" strand and

0% transfer of the template strand. Radioactive labels not prone to bleaching might be helpful for future experiments to investigate these transfer regimes.

The next step within this set of experiments was to use PCR to reload the stamp after printing once and then to print again. The feasibility of reloading the stamp by PCR could be experimentally confirmed. Furthermore, findings by other groups [Adessi, 2000] suggest that PCR performed on solid surfaces poses no problem. However, during this work, the transfer of the newly synthesized "copy" strand DNA was not achieved and remains to be investigated. Considering all the experience gained from printing hybridized "copy" strand DNA, it should be possible to perform solid phase PCR on an elastomer surface and transfer the synthesized molecules to the target surface with little effort. This means that a final proof-of-principle of PCR-on-stamp will be only a matter of time and is subject of ongoing work.

3.5.4. Discussion

PCR-on-stamp uses elastomeric stamps as rechargeable matrices for the replication of pre-patterned molecule ensembles. It opens up a variety of new applications. With this method biochip production can truly be industrialized to the level of book printing. All important parts of a principal proof of this concept have been presented in this work. It is now a matter of engineering to adjust all parameters such that a consistent and reliable transfer and recharging of the molecules is guaranteed.

4. *Materials & Methods*

This chapter presents detailed descriptions of the experimental methods and materials as well as chemicals used for the experiments described in Chapter 3. Before the explicit description of the experimental methods and procedures used in each section an overview of generally applicable procedures is given.

4.1. General methods

4.1.1. Softlithography

Three dimensional surface structuring in micrometer dimensions is a well established process in the semiconductor industry. Usually electron beam written chromium masks are used to shine UV light onto a photosensitive resist that was spun onto a silicon wafer. After illumination the resist is developed. Depending on the resist thickness a well defined three dimensional pattern is created that can then serve as a master for elastomer molding or is in a subsequent etching process transferred into the silicon wafer.

4.1.1.1. Photolithographic mask design

The photolithographic masks used in this work were designed using the CleWin Software from WieWeb (Netherlands). Design files were sent to DeltaMasks (Netherlands) where they were translated into 5 inch chromium masks. A conventional mask aligner (Karl Suss MA6) was used to do the photolithography.

For most µCP experiments a standard stamp (abbreviated "GRO") containing features of various sizes and shapes, depicted in Figure 63, was designed. The smallest features were designed to be just big enough to be reproduced using common photoresist (maP 215, Microresits GmbH, Germany). They had lateral dimensions of 2 by 2 µm. The largest features (squares) were 100 by 100 µm.

For all experiments for which a precise alignment was necessary, a special alignment mark was designed. These alignment marks, positioned at least at three different positions across the stamp and target surface, allowed to correct the position of the stamp with respect to target surface marks. Figure 64 A and B shows the definition pattern of the alignment features for the target surface (A) and for the stamp surface (B). Each alignment feature comprises three individual alignment crosses of varying size. Each narrow cross in (B) has a thickness of 1/3 of the wide cross in (A). This special

design is often used in the semiconductor industry and facilitates the precise alignment of photolitho-graphic masks on the wafer surface in the micrometer range.
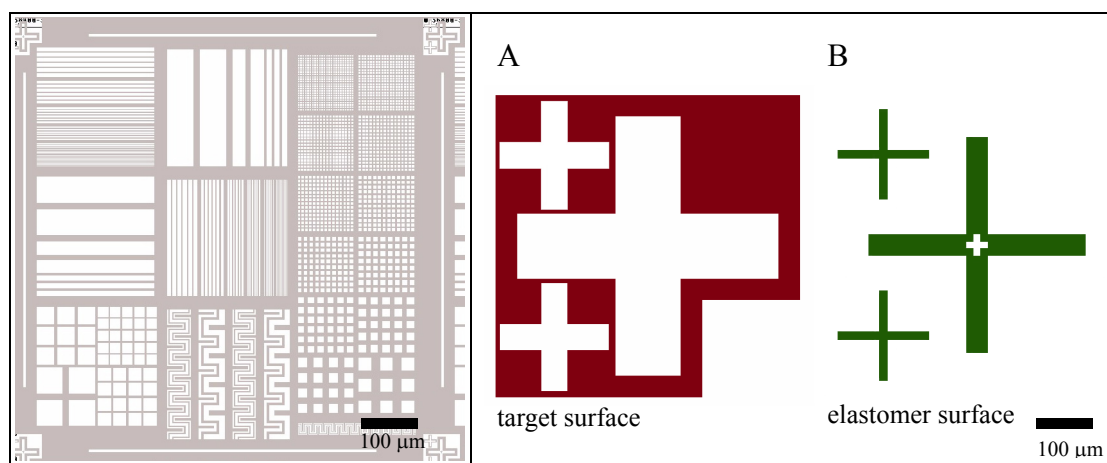
Figure 63: Design pattern "GRO-stamp" offering a host of different shapes and sizes of features.

Figure 64: Definition of the alignment features for target surface (A) and stamp surface (B).

The design of the micro-fluidic network was carefully chosen, such that the collapse of the structure is prevented, and second, easy filling of the inlets is possible (Figure 65). The depicted µFN was designed to be molded into PDMS. After piercing the inlet and outlet ports and application to a target surface, 10 different molecule solutions could be directed over the surface. The alignment marks found in the middle, support precise positioning of the network on the target surface.
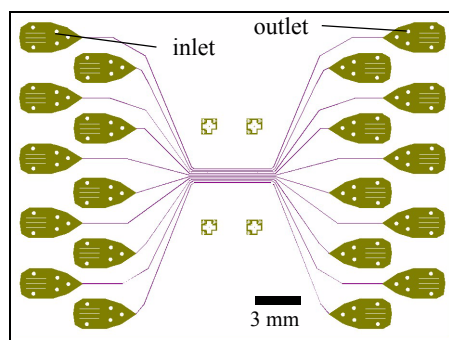
Figure 65: Design pattern for µFN, colored areas are recessed once transferred to the elastomer.

4.1.2. Photolithography (Master generation)

The photolithographic masks described above were used to fabricate three dimensional surface patterns on silicon wafers by photolithography. These wavers then serve as masters for the polymer molding.

To create the three dimensionally patterned surface, three inch (3") and four inch (4") silicon on insulator (SOI) wafers were spincoated with either ma-P 215, ma-P 275 or ma-N 215 (Microresist GmbH, Germany) according to the data sheet of the corresponding resist. The spinning parameters, together with the viscosity of the photoresists, defined the thickness of the resist layer and consequently the depth of the mold. Using the ma-P 215 or the ma-N 215 resists structure heights of ~2 μm could be achieved. For the fluidic structures ma-P 275 resulting in a resist layer of ~7 μm was used.

After baking the coated wafers they were patterned by UV illumination in a mask aligner MA 6 (Karl Suss, Germany) for ~10 sec. depending on resist thickness and type. Subsequently they were developed with a commercial developer (ma-D). Correct pattern formation was confirmed using light microscopy (Figure 66), profilometry (alpha step) and AFM measurements (Figure 67).
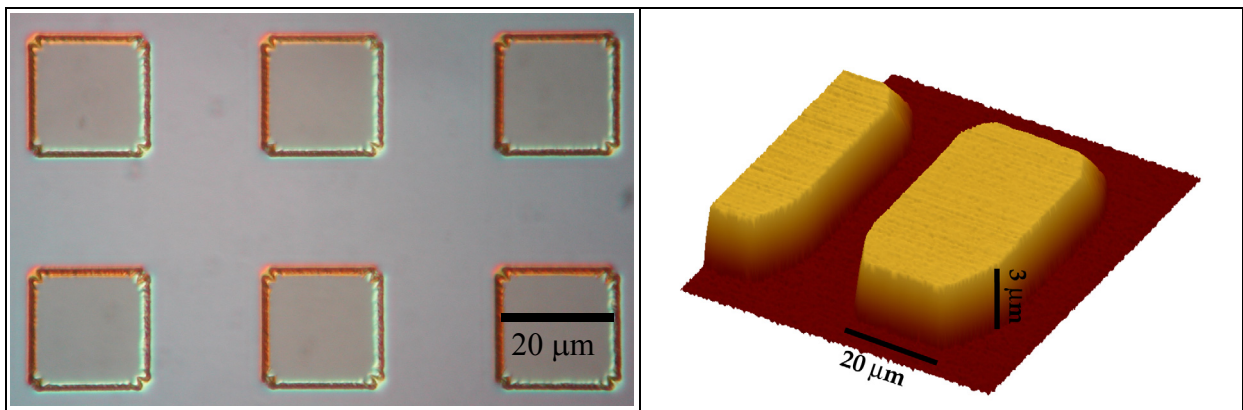
Figure 66: Light microscope image of fabricated photoresist structures. Defects are visible in the corners of the squares where the development process was not fully finished.

Figure 67: AFM image of photoresist after development (3D-image)

4.1.2.1. Elastomeric stamp fabrication

Before using the wafers, fabricated in the previous section, as molding masters they had to be fluorinated in order to render them hydrophobic and making them less prone to elastomer sticking. To achieve this, they were incubated in an desiccator filled with a tri-(chlorosilane) (ABCR, Germany) air mixture.

For fabricating the PDMS stamps the pre-polymer and catalyst of Sylgard 184 (Dow Corning, Midland, MI) are thoroughly mixed in a ratio of 10+1 and are subsequently degassed in an evacuated exsiccator. The well mixed liquid pre-polymer is poured onto the fluorinated silicon masters having either photoresist structures or etched features on their surface and finally the whole is cured at 60°C for 24 hours in an oven (Figure 68A). For the generation of flat, unstructured stamps, PDMS was cured against polystyrene Petri dishes. After curing, the elastomer could be peeled off the master

revealing the three dimensional surface structure (Figure 68B). Stamps could be stored for months in a dust free environment without altering their properties.
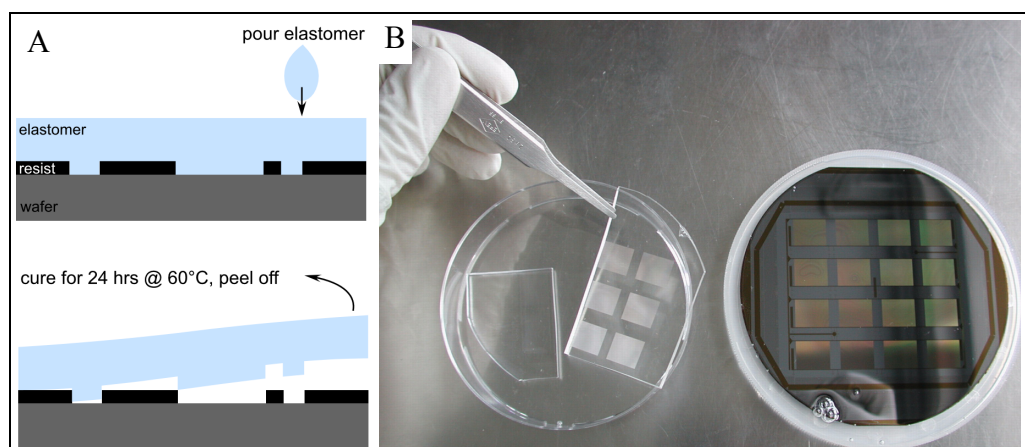
Figure 68: (A) Schematic of stamp fabrication. (B) Already cured piece of elastomer after separation from master and master with elastomer coating.

4.1.3. Microcontact printing of molecules (proteins / DNA)

Stamps were cut in handy pieces such that they could be handled with tweezers. The molecules are diluted in the appropriate buffer solutions to their final concentration as described in the corresponding sections. Depending on the size and shape a volume of between 20 to 100 μL of solution was applied to the stamp surface. Incubation time could vary between a few minutes and over one hour.

After incubation, the stamp was rinsed with DI-water and blown dry under a stream of pure nitrogen. Subsequently the stamp was carefully applied to the target surface and briefly touched to initiate conformal contact formation. Stamps with delicate aspect ratio had to be treated carefully, in order to avoid the collapse of the fragile features. The contact time is generally short, on the order of seconds, but can also be prolonged for special applications.

4.1.4. Microfluidic inking of stamps

Micro-machined micro-fluidic networks made of silicon are used to deliver different probe molecules onto the stamp surface as described in Section 2.1.3.

A flat piece of elastomer is applied to a Si-μFN, which has been treated in an O_2-plasma to render its surface clean and hydrophillic and to promote filling of the channels (Figure 69). Then the channels are filled with the probe solution one after the other using gel loading pipet tips. Where applicable a small percentage of ethanol is added to facilitate the filling of the channels through lowered surface tension. After incubation, the whole μFN is submersed in buffer and the elastomer slab is removed, allowing the buffer to immediately wash away the probe solution still present in the channels. This is

done to prevent adsorption of molecules outside the channels. In the next step the flat elastomer is microcontact printed to the target surface.

Alternatively elastomeric PDMS-µFNs (Figure 65) with pierced inlets are plasma treated (5 sec., 150W) and sealed to a glass surface. By filling the inlet ports with the molecule solution, the target surface is directly patterned. After the incubation time is over, µFNs are lifted while submersed in buffer.
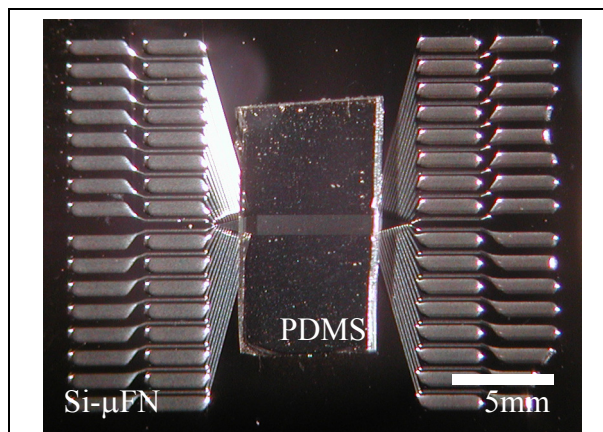
Figure 69: Micrograph of patterning a flat stamp with lines of DNA molecules using a µFN made of silicon.

4.1.5. Chemical modification of stamps and target surfaces

For studying the behavior of molecules on or close to surfaces and for creating surfaces with molecules firmly attached to them, the chemical properties of the surface play a vital role. Thus, in this work a big effort was set into an adequate tailoring of both the stamp- and the target surface.

4.1.5.1. Amino modification of stamps:

For amino modifications of polymer (PDMS) surfaces several recipes can be found in the literature. During the experiments they were evaluated and those working best were chosen for further use.

Method A (APTS):
- PDMS surfaces were treated in an oxygen plasma (pressure 0.8 torr, load coil power 100 W; TePla, Germany) for 3 s.
- The hydrophillic stamps [Delamarche, 2001] were immediately immersed in an aqueous solution of 3% aminopropyltriethoxysilane (APTS, Fluka) adjusted to pH ~6 with acetic acid.
- The solution was heated for 1h to 80 °C under reflux conditions. Freshly silanized PDMS was exhaustively rinsed with DI-water.
- Silanized substrates can be stored several weeks if kept immersed in DI-water.

Method B (APTS and APTMS):
- Stamps are again treated in an oxygen plasma for 10 sec. at ~150 W.
- Then they are incubated in a solution of 95% EtOH, 3% H_2O and 2% APTMS or 2% APTS for 45 min. under constant shaking.
- Subsequently they are washed first in pure ETOH then in degassed DI-water.

- They could be stored in degassed DI-water for 24 hours, after this time they lost the ability to bind molecules via the introduced amine groups.

4.1.5.2. Surface modification of target substrates

Glass or mica surfaces serving as target substrate for printing could in principle be prepared using similar recipes as described for the polymer surfaces. Nevertheless glass surfaces withstand much harsher chemical treatment with organic solvents and thus some of the recipes differed from the ones used before.

To ensure good surface quality all glass substrates (Menzel Gläser, Germany) were subject to a thorough cleaning step. After immersing the substrates in a 10% NaOH solution over night, they were washed with ddH$_2$O, immersed in a 10% HCl solution for 1 hour and washed again with ddH$_2$O. Finally the substrates were blown dry under nitrogen and heated in an oven at 110°C for 15 min.

Two different methods of functionalizing the surfaces were applied:

Method A (APTMS) adopted from Beier et al. [Beier, 1999]
- Wash slides with MeOH.
- Immerse slides in 3% APTMS in MeOH for 15 min. and sonicate meanwhile.
- Wash slides again with MeOH and ddH2O
- Blow dry with nitrogen and bake at 110°C for 15 min.
- Slides could be stored under dry and dust-free conditions and could be kept for several weeks.

Method B (APTS or APTMS)
- Dilute 5% of APTS or APTMS in pure acetone. Incubate clean substrates for 30 min. under constant sonication.
- Rinse with EtOH and finally blow dry with nitrogen and bake at 110°C for 15 min.

4.1.5.3. Activation of reactive surfaces

Binding biological molecules in a controlled manner to a specific surface is a very important task while developing immunological or biochemical assays. Bonds must be strong but may not prevent molecules from freely interacting with their binding partners. All of the crosslinkers were purchased from Pierce (Rockville, USA).

- ***BS***[3]***, EGS*** - These cross-linkers are water-soluble and are diluted to a concentration of 0,5 mg/mL in PBS pH 7.2. Once dissolved the crosslinker solution has to be applied immediately to the amine containing surface to avoid hydrolysis and thereby inactivation. Incubation time lasted between 10 to 20 minutes.

- ***DSS*** - This crosslinker is dissolved first in 50 µl DMSO and then further diluted to a concentration of 0,5 mg/mL in buffer or DI-water. DSS couples to primary amines and is used for DNA coupling to amine surfaces. The incubation lasted for 10 min. and after washing with ddH$_2$O the now activated surface could be exposed to the amine functionalized molecule solution.

- ***GMBS*** - Here the same preparation steps as described for DSS apply, with the difference that this crosslinker links amine and thiol moieties together.

- ***SMCC*** - The procedure is the same as given for GMBS.

- **DMS** - The cross-linker is diluted to a final concentration of 1 mMol in saturated NaHCO3 (1,13mol/l) (that is, 273 mg DMS in 40 mL buffer). Then the surface is incubated for 1hr @ RT, and finally washed with ddH$_2$O and blown dry with nitrogen. After that, the surface is incubated with the solution of the molecules to be bound.

	name	length [Å]	reactive towards	carries a charge on surface
BS3	Bis(sulfosuccinimidyl) suberate	11,4	amine-amine	negative
sulfo EGS	sulfo Ethylene glycol bis[succinimidylsuccinate]	16,1	amine-amine	negative
DSS	Disuccinimidyl suberate	11,4	amine-amine	no
sulfo SMPB	sulfo Succinimidyl 4-[p-maleimidophenyl]butyrate	11,6	thiol-amine	negative
sulfo SMCC	Succinimidyl 4-(N-maleimidomethyl)cyclohexane-1-carboxylate	11,6	thiol-amine	negative
GMBS	(N-[γ -maleimidobutyryloxy]succinimide ester)	6,8	thiol-amine	no
DMS	Dimethylsuberimidate	-	amine-amine	no
s-biot	sulfo-NHS-LC-biotin	22,4	amine-avidin	no

Table 4.5. Selection of cross-linker, employed in this work, listing their essential properties

The molecular properties such as length, flexibility or charge of the cross-linkers strongly affect the binding capacity. It is noteworthy, that a charge introduced on the surface by the crosslinker can hinder binding of certain target molecules completely. For this reason all cross-linkers were tested for the yield of surface attachment. Finally, for best DNA binding, e.g. DSS was chosen.

4.1.6. Analytical instrumentation

In the course of this work a number of different commercial instruments were used. The measurements performed with the instruments followed standard procedures suggested by the manufacturer.

4.1.6.1. Atomic force microscopy (AFM)

The AFM is one of the most important instruments for analyzing surface properties in the micro- and nanometer dimensions. In this work the AFM was extensively used to characterize the surface before and after molecule absorption or binding. Additionally, the formation of solid precipitates and the structure generation by photolithography and etching was monitored.

The atomic force microscope (AFM) scans were performed in air using the non-contact mode on a Dimension 3000/Nanoscope 3a (DI, Santa Barbara, CA) with silicon cantilevers (Ultrasharp Tips, Nanoprobes). For imaging of contact printed molecules freshly cleaved mica was used as molecular flat substrate. In order to ensure equivalent surface conditions as with amine-modified glass, the mica was modified using the same procedure as described for glass in Section 4.1.5.2.

4.1.6.2. Light Microscopy (LM)

To study e.g. the successful binding of molecules to activated surfaces, or to measure the amount of adsorbed molecules to a surface, a fluorescent microscope was extensively used.

Images of fluorophore labeled molecules were acquired with a microscope (Zeiss Axiovert 200 with 40x LD Achroplan objective), equipped with a charge-coupled camera (CCD) cooled to 0 °C (Orca, Hamamatsu). The captured images were analyzed using the SIMPLE PCI software package for this camera. DNA molecules and proteins were labeled red or green using TRITC (λ_{ex}= 552 nm) or FITC (λ_{ex}= 520 nm), respectively.

Darkfield as well as bright-field micrographs of surfaces of structured wafers or μCP-patterned and metal-enhanced surfaces were acquired using a microscope (Waverspec Eclipse ME 600) equipped with long-distance lenses. Images were taken using the same CCD camera.

4.1.6.3. Scanning electron microscopy (SEM)

To image the distribution of single bound colloidal gold particles before silver or gold enhancement a scanning electron microscope XL 30 FEG (Philips) with a beam diameter of ~0,2 μm was used. Molecules were stamped onto clean silicon wafers serving as conductive substrates necessary for SEM measurements. The molecular recognition (detection) was performed with 10-20 nm colloidal gold particle-labeled antibodies. After washing, the probes were imaged using SEM and revealed excellent contrast of the metal particles (e.g. Figure 70) due to a high yield of secondary electrons from the gold particles and a low background of the wafer. Even faint images of adsorbed BSA molecules could be observed on the wafer surface.
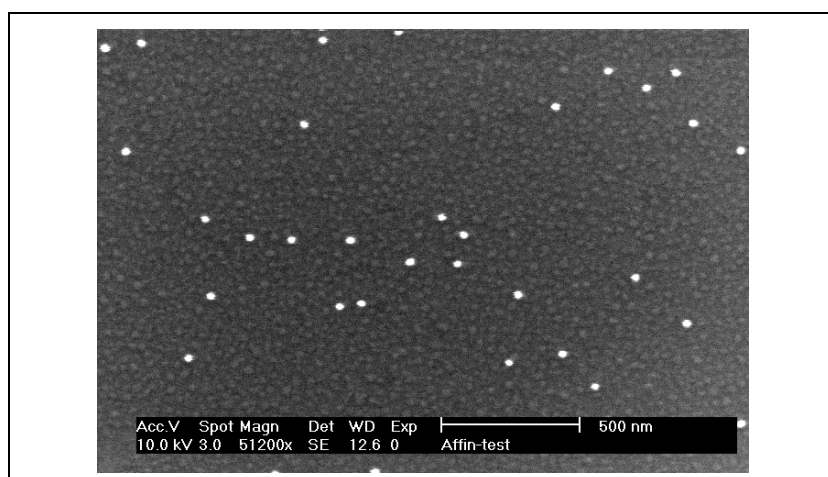
Figure 70: SEM micrograph of surface with bound 20nm gold particles [Roth, 2002]. The faint dots visible on the silicon surface can be attributed to single BSA molecules strongly adsorbed to the surface.

4.1.6.4. Ellipsometry

The thickness of silane layers on the substrates was measured using ellipsometry (EL X-01R, Dr. Riss Ellipsometerbau, Germany). Before, during, and after chemical treatment a series of measurements was done with a fixed angle of incidence for the polarized laser beam. The phase shift and angle of polarization rotation was recorded and by comparison of the measured values with standard curves of known layer thicknesses, the individual layer thickness could be calculated.

4.2. Detailed methods for Ch. 3.1.: The CD-Pickup bio-imager

The setup and basic proof of principle of a low cost bio-assay reader as well as the experimental recipes for the assays performed will be described in this section.

4.2.1. Setup and basic operation of the Pickup Imager

The basic working scheme of the (newly) built instrument has already been described in Section 2.2.2. The apparatus, as it was set up in the laboratory, consisted of an inverted light microscope equipped with a motorized x-y-stage (Figure 71). Above the stage a conventional pickup module from a CD player was mounted on a rigid metal bridge over-spanning the sample stage. The pickup itself was connected to a custom designed electronic control board (inhouse design, J. Grässle). This circuitry controlled the focus position and amplified the measured signal. The output signal is converted by an A/D converter card (NiDAQ, National Instruments) and feed into the computer. Via the output channel of the A/D converter-card, the LabView-based software controlled the focus position using an implemented feedback loop.
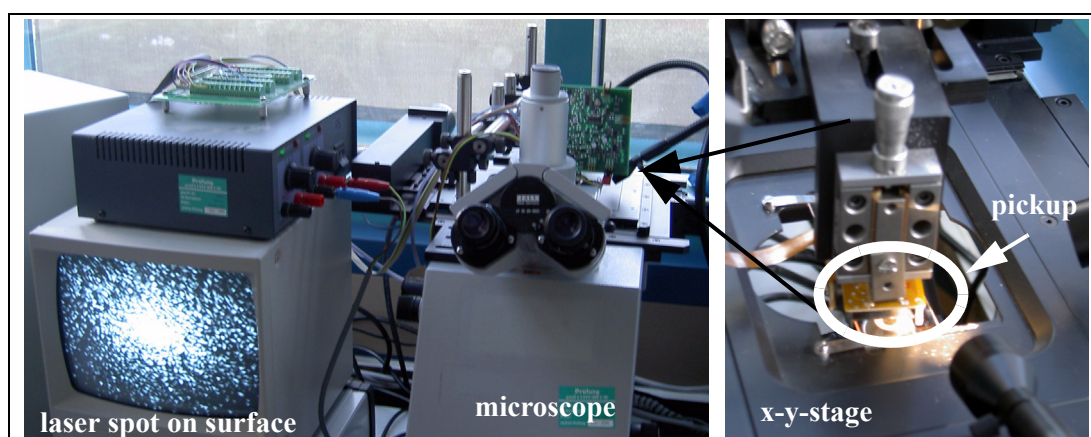
Figure 71: Image of pickup scanner setup. Left: Inverted microscope with scanning table and pickup together with feedback circuitry, power supply and control monitor displaying the laser spot of the pickup on the surface; Right: z-adjustment with pickup module attached above x-y-stage.

The imaging procedure itself is straight forward. First, the assay slide with the precipitate-enhanced pattern is mounted face up on the x-y- sample stage. The electronics, the pickup, the monitor, the

camera and the illumination unit are powered on. Subsequently, the software is started. Once the software is running, the laser is switched off in order to use the eye piece of the microscope or the monitor image to move to the surface area of interest. Because the laser is so bright, leaving it switched on would make it impossible to observe faint surface structures.

Before scanning and imaging the probes surface, the laser beam has to be focused onto the surface. Therefore, the laser is switched on and the automatic focus finding procedure is started. This routine moves the focus of the laser beam from its minimum to its maximum position, using the built in focus coil, while recording the reflected signal. By determining the maximum of the measured signal the software is able to determine the optimal focus position. The adjustment range is roughly 800 μm. If the software could not find an optimal focus position within this range, the surface distance of the pickup module has to be readjusted by hand. Also for proper operation of the focus feedback loop, the surface of the probe has to have a reflectivity of at least ~4%, otherwise the feedback is not able to focus correctly. Once the focus position is set the scan can be started.

The pickup output delivers a RF-signal, which is the sum of the currents from the 4-quadrant detector. The bandwidth of this RF-signal is around *1 MHz* for audio CD players, and can be above *100 MHz* for CD-ROM or DVD pickups. This bandwidth limits the maximum possible scan speed for a given spatial resolution. For example, to get a resolution of 1 μm at a bandwidth of *1MHz*, the maximum scan speed is: $v_{scanmax}=1\ \mu m \times 1MHz/2=0.5\ m/s$. In the set-up chosen, a 12bit data acquisition card with a sampling rate of *200 ks/s* is used. This choice limits the bandwidth of the system to *100kHz*, which still results in an impressive scan speed of *50 mm/s* without degradation in resolution. Nevertheless, to avoid vibrations and thus image artefacts, scan speed was chosen to be even lower, on the order of *1 mm/s*.

4.2.1.1. Software interface and data acquisition with the CD-pickup imager

The graphical user interface (GUI) and control software for the imager was written in LabView (National-Instruments, USA) running on any Windows based PC. The scan table control (Merzhäuser, Germany) is connected to the PC via an RS232 interface. To link the external electronic board to the PC a multifunction IO-PCI board, PCI-MIO-16-E-4 (National-Instruments, USA) with 16 multiplexed analog-digital-converter inputs, 2 digital-analog-converter outputs and 8 configurable digital IOs was employed.

The software controls the entire instrument and records the acquired data. It determines the operating point of the auto-focus servo, displays the acquired RF-signal, and stores the data on hard disc in an uncompressed proprietary binary or ASCII file format or compressed in the standard JPEG file format. The GUI is designed to provide easy handling and simple setup of the scanning parameters

(Figure 72). The scanning parameters that can be set are e.g. the lateral resolution or step size, the sampling rate, the scan area, the number of lines to be acquired, the offset, and the filename and type with which the data is stored.

The scanning is done line-by-line in forward or backward direction. After each step in x-direction, one or more samples of the RF-signal are acquired. If more than one sample per step is acquired, the average of these samples is stored as one data-point. All line scans are accumulated and displayed in real-time in a color-intensity chart. After finishing the scan procedure the data is stored on hard disc in the selected file format.
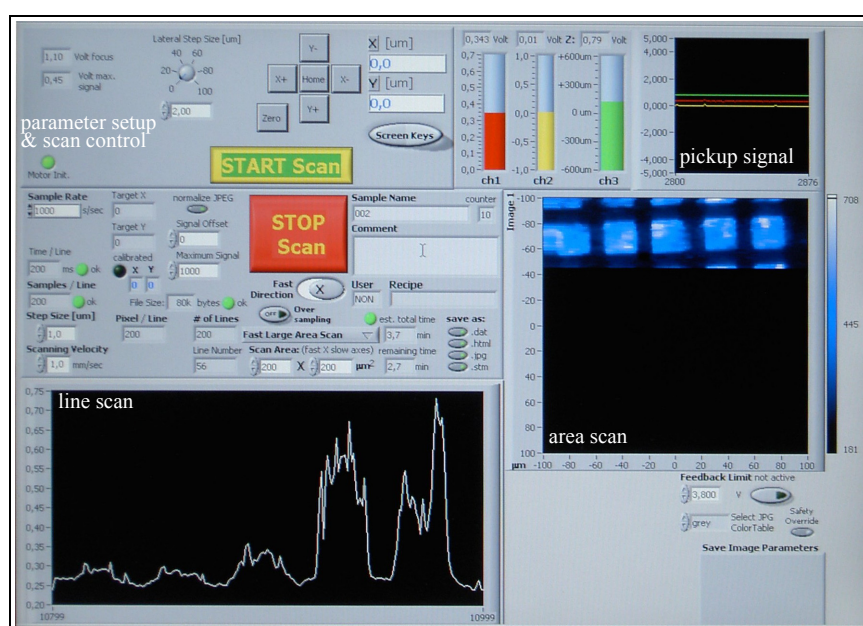
Figure 72: Screenshot of the pickup software while acquiring an image of a patterned surface.

4.2.2. Immunoassay

The biological model assays that were set up to test the functionality of the CD-pickup imager had to be designed such that they were highly reproducible to be able to thoroughly test the instrument but still not be to complex to be repeated many times. Another prerequisite was that the assays being chosen are similar to assays used in clinical diagnostics to prove the applicability of the detection system for ever day use.

For this reason two test assay systems were chosen: A simple two molecule-assay consisting of biotinylated BSA (bBSA) and the matching anti-biotin antibody conjugated to colloidal gold. The bBSA is patterned onto the surface in different ratios from 0,01% bBSA diluted in BSA (1mg/mL) to 100% bBSA. Using these dilutions, the detection properties of different densities of bound colloidal gold particles after signal enhancement can be nicely measured and compared to simulated results.

A second, clinically more relevant assay was implemented as a sandwich immunoassay for C-reactive protein (CRP antigen, HyTest, Turku Finland). First, a monolayer of the capture antibody for CRP (anti-CRP Clone 5, HyTest, Turku Finland) was patterned onto the substrate surface by μCP. After passivating the surface by incubation with 1 mg/mL BSA solution, different concentrations of CRP ranging from 0.1 to $1 \cdot 10^5$ ng/mL diluted in 1 mg/mL BSA are applied to the test areas and incubated for 45 min. After rinsing, the bound antigens were detected with a second antibody (anti-CRP Clone 7) diluted to 0.01 mg/mL in a BSA solution for 45 min. The second antibody carried a biotin label and was bound by an anti-biotin antibody conjugated to colloidal gold used in the previous experiments. Following signal enhancement by autometallography, the immuno-reacted slides were measured using the pickup imager.

4.2.3. Signal enhancement

The fine tuning of the signal enhancement procedure is of great importance for obtaining accurate and consistent results from the immuno-assays performed. Particular effort was set on the reduction of unspecific background, which has a direct impact on the quality of the data.

In this section the biochemical protocols for the signal enhancement of bioassays with gold or silver precipitation or alternatively using enzymatic conversion of label will be described.

4.2.3.1. Gold or silver enhancement

After blocking the slide surface with a 1% BSA in PBS pH 7.2 solution to prevent unspecific reactions the biotinylated molecules present on the surface were reacted for 45 minutes with an anti-biotin antibody conjugated to 5 nm colloidal gold particles (British BioCell) diluted 1:100 in 1% BSA.

A commercial silver enhancement solution (Sigma, SE-100) to grow elemental silver particles was used as recommended by the supplier. The provided solutions A and B were mixed in a ratio 1:1 and applied to the surface carrying the gold particle-labeled pattern. The development of silver particles was monitored under a microscope. Probes were incubated for an average time of 15 min. To stop the reaction the probes were rinsed with DI-water.

Alternatively to silver, a gold enhancement kit (Nanoprobes, GoldEnhanceLM) was employed. Here, solutions A and B of this kit were mixed in a volume ratio of 1:1 and pre-incubated for 5 min. Subsequently the same amounts of solution C and D were added. The mixed solution was then applied to the substrate surface and covered with a plastic coverslip. Incubation time ranged from 10 to 15 minutes and the reaction was stopped by rinsing with DI-water.

4.2.3.2. Signal enhancement using alkaline phosphatase

As an alternative to metal enhancers for the signal amplification, an enzymatic detection procedure employing an alkaline phosphatase (AP)-streptavidin conjugate (Sigma-Aldrich, USA) was tested. AP was diluted 1:50 from the 1mg/mL stock solution in 30 mM Tris-HCl (pH 8.1) buffer. To equilibrate the surface, the probe was first rinsed with the dilution buffer (Tris-HCl) twice, then it was incubated with the AP solution for 45 minutes, followed by a wash step with the dilution buffer.

The signal generating step was performed by letting the surface react with the Elf 97 (Molecular Probes) substrate diluted in the same buffer (1:10) for one hour. Alkaline phosphatase cleaves the phosphate group of the soluble ELF substrate causing it to precipitate at the site of enzyme activity. Rinsing the probes surface with DI-water finally removed the remaining unprecipitated substrate, and after blowing the probe dry with nitrogen, it was ready for imaging.

4.2.3.3. Signal enhancement using Horseradish Peroxidase

Analogous to alkaline phosphatase, horseradish peroxidase was used to precipitate a reporter substrate.

The enzyme is conjugated to the protein streptavidin (500 u/mL stock, Roche, diluted 1:500 in PBS pH 7.4). After incubating the probe surface with the enzyme solution for 45 minutes the probe is washed in PBS buffer. Then, the surface was treated with a solution of DAB/Co substrate (Sigma, prepared as recommended by the manufacturer). Enzymatic action during incubation turned the DAB/Co substrate into a dark insoluble precipitate. After 1 hour of reaction, the probe was rinsed with PBS buffer, then with DI-water, and subsequently blown dry with nitrogen. At that stage the enhanced assay was ready for imaging.

4.3. Detailed methods for Ch. 3.2.: Enzyme-assisted-inverse μCP

For the development of this novel technique established methods from different research field had to be combined. This section summarizes the main procedures in brief.

4.3.1. Preparation of gold substrates

Gold surfaces for patterning with alkane thiols were fabricated by thermal evaporation of a 1nm thick titanium layer onto glass slides or Si wafers, serving as adhesion promoter, immediately followed by evaporation of a 15 nm layer of gold. Substrates were cleaned in ethanol and DI-water prior to evaporation. The coated slides could be stored in a dust free environment for several months.

4.3.2. Microcontact printing of alkane thiols

Two different alkanethiols were used for μCP: Eicosanethiol (ECT) is a thiol with a C_{20}-alkyl chain, Hexadecanethiol (HDT) consists of a C_{16} backbone and a thiol group. Both compounds were obtained from M. Geissler, IBM-Research, Zürich.

Patterning procedure
- Alkanethiols are diluted in EtOH at a concentration of approximately 0.5 mM. The solution can be kept for a maximum of one week.
- Stamps are inked for a few minutes. After incubation stamps are immediately blown dry with nitrogen without any rinsing step.
- Then stamps are applied to the gold surface for a few seconds.
- After removal of the stamp the patterned gold surface is ready for etching or further processing.

4.3.3. Etching procedure for thin gold films

The etch bath consisted of a 0.1 mM KCN solution buffered at pH 11 with NaOH. (Note: lower pH could result in extremely hazardous fumes!).

Gold substrates having a patterned alkanethiol layer as etch stop are gently immersed into the etching solution (wear protective clothing!). Dissolving of the unprotected gold then takes place within a few seconds to a few minutes. The etch rate is about 0.05 nm/sec. Stirring the solution speeds up the reaction and increases etch selectivity. Once all unprotected gold areas are etched away the substrate is removed from the solution and is thoroughly washed with DI-water. To achieve best results it is important to constantly monitor the progress of the etching and to ensure that no patterned structures are underetched.

4.3.4. Enzymatic digestion of surface bound proteins

A dense monolayer of a mixture of proteins (5% casein, 5% FCS, 1% BSA, or 1% cold water fish-gelatin) is contact-printed onto a gold-covered glass slide. After removing the stamp, the whole gold surface is immersed in a 0.5 mM solution of ECT for 10 to 20 seconds. The protease (protease K or pronase E) is diluted in a sodium phosphate buffer (150 mM sodium phosphate, 10 mM HCl, pH 7.2) to a concentration of 1mg/mL. The surface is incubated with the protease solution for at least 4 hours at room temperature. Finally the surface is rinsed with DI-water and etched for about 12 minutes under constant optical control in an etch bath containing 0.1 mM KCN buffered with NaOH at pH 9. Additionally 1-octanole can be added as defect healing reactant [Geissler, 2002]. This increases the overall selectivity of the etch process.

4.4. Detailed methods for Ch.3.3: The stamp aligner

To successfully create arrays of molecules by overlay printing a special tool, the stamp aligner, was built. This section describes the setup of this tool as well as the experimental procedures to create the individual arrays.

4.4.1. Design of the stamps

To create well aligned arrays of contact printed molecules, a universal stamp (Figure 73) and an appropriate surface alignment pattern (Figure 74) was designed such that this universal stamp pattern could be used for any of the molecules to be stamped. For reasons of simplicity the array was chosen to be one dimensional, that is, representing only a linear array of dots. By successive positioning the stamp over the correspondingly shifted alignment mark it is possible to create an array of molecule spots next to each other.
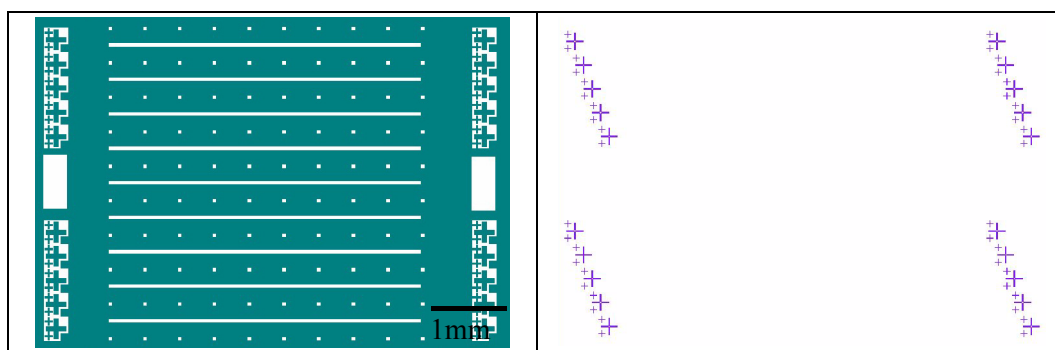
Figure 73: Design pattern for a stamp with integrated alignment structures. Dark areas will be recessed on the final PDMS stamp.

Figure 74: Design pattern for the appropriate alignment marks for the stamps from Figure 73.

4.4.2. The alignment tool setup

Handling and precise positioning of a patterned stamp in the micrometer range onto a target surface is a very demanding task. Therefore, a tool was developed that facilitated the positioning of the stamps on an arbitrary flat surface with a precision of a few micrometers. An important prerequisite for such a tool is its capability of exerting full control over the sample in all three spatial directions as well as tilt and rotation.

The constructed alignment tool consisted of a x-y-z stage (Luigs & Neumann, Germany) that is mounted on top of a x-y stage (Merzhäuser, Germany) on an inverted fluorescence microscope. To give the sample additional degrees of freedom, a rotation table and a device to adjust for stamp tilt and angle were implemented (Figure 75). This allowed for the easy adjustment of the relative posi-

tion of the stamp and the substrate under constant optical control. The stamp itself was held in place by applying a vacuum to the vacuum chuck.
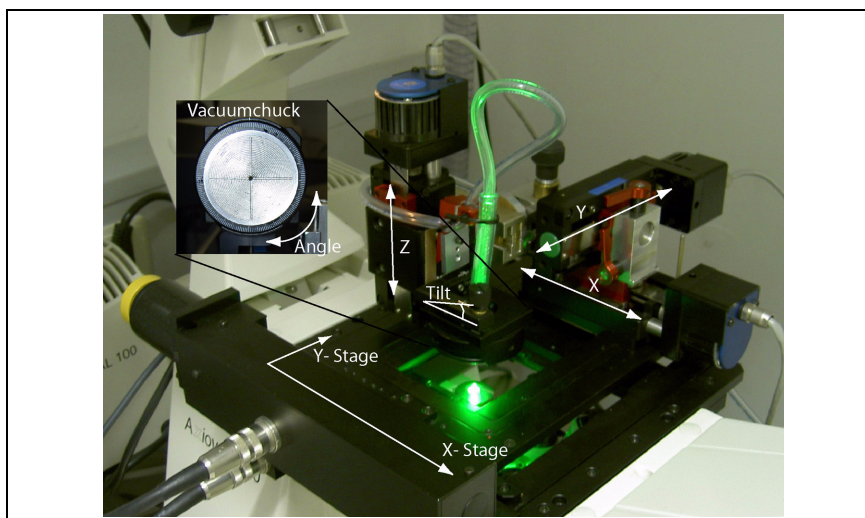
Figure 75: Setup of the alignment apparatus, including inverted microscope, x-y stage, x-y-z-stage and vacuum chuck as probe holder.

4.4.3. Procedure for the aligned printing

First, the stamp with the appropriate alignment and array pattern (4.4.1) was incubated with a solution of the desired molecules. After washing and drying, the stamp was placed onto the sample holder with vacuum switched on. The sample stage was brought close to contact with the target surface. The target surface itself carried the alignment marks, either made of gold structures or of previously patterned fluorophore labeled marker proteins.

After approaching the target surface to a distance of only a few micrometers distance between the stamp and the target surface, it was possible to observe both surfaces at the same time from below with the inverted microscope. It was then possible to adjust the position of the stamp relative to the target surface, such that both alignment marks, the ones on the stamp and those on the surface were well aligned. Lowering the sample holder further finally brought the stamp in full contact with the surface. By switching of the vacuum, the stamp was released from the sample holder. After printing, the stamp could be lifted off the surface by hand, leaving the first printed layer of molecules behind. This procedure was then repeated for the other stamps carrying different molecules. By aligning to the appropriately shifted alignment marks, the array was built step by step.

4.5. Detailed methods for Ch.3.4.: Microcontact printing of DNA

In the following section additional experimental procedures for microcontact printing DNA are described. These procedures, together with the ones outlined in the previous chapters about physico-

chemical methods of surface modification build the toolbox that allowed to successfully develop this novel soft-lithographic technique.

4.5.1. DNA molecules used for the experiments

DNA oligonucleotides (oligos) were purchased from various vendors (MWG Biotech, ROTH, and IBA GmbH Göttingen). They all had lengths of between 18 and 25bp, were HPLC-purified, and modified by the manufacturer when necessary. Oligos used for coupling to a surface were modified with a 5'-amino C_6 linker[23]. Fluorescent labels were attached internally either as fluorescein-isothiocyanate (FITC) or as tetramethylrhodamine (TRITC). Probes used for immunolabeling were 5'-biotin labeled. To obtain DNA fragments of varying length, different sets of primers were defined and used in PCR reactions. PCR was performed according to standard procedures [Maniatis, 1989]. The composition of the PCR mix is given in Table 4.6. The PCR amplification included 40 cycles of denaturing, annealing and extension (Table 4.7.). The temperatures were calculated using the GC-rule. Final products were purified using a QIAquick PCR purification kit (Qiagen). The desired fragment length was confirmed by gel electrophoresis.

10x buffer	10µl
MgCl$_2$	10µl
dNTP mix (à 10mM)	10µl
upper Primer	2µl
lower primer	2µl
Taq polymerase	1µl
template (10µg/µl)	2µl
H$_2$O	71µl

Table 4.6. PCR mixture

1.	2'@ 94°C	
2.	45"@ 94°C	
3.	30"@ 48°C	40x
4.	1'@ 72°C	
	repeat step 2.-4. 40x	
5.	5'@ 72°C	

Table 4.7. Cycle definition for PCR

Gel electrophoresis was performed in 1.5% agarose in 1xTAE buffer gel (70mL/gel). The gels were loaded with 100µl of the PCR-product, 20µl 6x running buffer, and 3µl of 1:100 diluted SYBRGreen to mark the respective fragments. A separate lane was loaded with a 50bp DNA ladder (dilution was 10µl+1µl SYBR Green). Then the samples were run for 1h at 120V.

---

23) A six carbon atoms long space is introduced at the 5' end of the molecule to increase the distance of the actual sequence from the surface and aid binding of other molecules or enzymes.

4.5.2. Microcontact printing of DNA

The basic principle of this procedure did not differ much from the established contact printing of proteins. What had to be considered, however, were the requirements for the surface and the dilution buffer, as described in theory in Section 2.1.6.

DNA samples (oligonucleotides or PCR products) were diluted 1:10 or 1:100 from stock (100 pmol/mL for oligonucleotides) in DI-water (carbonated, pH 5.2) or any other non-amine-containing buffer with pH 5-7. The stamps with amine-grafted surface were prepared as described in Section 4.1.5.1. and incubated with 10 to 40 mL of sample solution for 45 min., rinsed thoroughly with DI-water, and finally blown dry with nitrogen. The stamp is microcontact-printed onto the substrate surface and left in place for an average contact time of 15 s. After lifting the stamp, it is important not to treat the surface with any buffer of pH 7 or higher because this would destroy the ionic interaction between the DNA fragments and the surface and wash the already adsorbed molecules away.

4.5.3. DNA Array spotting and printing

Stamps, as well as microarray glass slides (Corning, GAPS slides) were spotted using a microarray spotter (sciFLEXXARRAYER, Scienion) equipped with one piezo nozzle. PCR products were taken from the Amersham ScoreCard kit and diluted 1:10 in MES buffer pH 7 to a concentration of 20 ng/mL, which amounts to roughly 0.075 pmol/mL. In order to concentrate enough DNA onto the surface of the stamp, an average of 30 single drops of 100 pl was deposited by the piezo needle at each site. After spotting onto the stamps, they were microcontact-printed several times onto different conventional microarray glass slides. Stamped slides were treated identically as the directly spotted slides (control). The spotted probes were hybridized with the spike mix kit from Amersham according to the manufacturer's protocols.

4.5.4. Postprocessing of printed or spotted DNA slides

Experiments showed that it was useful to post process slides with contact-printed or spotted DNA molecules in order to increase the binding of DNA to the surface. Passivation of the charged surface had the effect of reduced background. The following procedure was derived from protocols published by P. Brown [Brown, 2003].

Stamped or spotted slides were rehydrated by incubating them in a hybridization chamber with 1x SSC for 5 min. Then the samples were heated to 70-80°C for 3 sec. and blown dry with nitrogen. In order to link the electrostatically adsorbed DNA molecules covalently to the substrates surface a UV crosslinker (Stratalink) set to 650 mJ was employed. Alternatively, target DNA, if aminated, was

cross-linked using bis-sulfoxisuccinimidyl subberat (BS[3], Pierce). For this purpose the cross-linker was diluted to a concentration of 0.5 mg/mL in MES buffer (pH 6) and the DNA modified slides were incubated for 30 minutes with this solution followed by a thorough rinsing step. After crosslinking, 5.5 g of succinic anhydride (Sigma-Aldrich, USA) were dissolved in 325mL 1-methyl-2-pyrolidinone. Immediately after succinic anhydride dissolved, 25 mL sodium borate (1M, pH 8) was added and after thoroughly mixing, the solution was poured into an empty slide chamber. Then slides were dipped into the solution several times and incubated on an orbital shaker for 15-20 min. Finally the slides were immersed in 95°C water for 2 min. and blown dry.

4.5.5. Hybridization of oligonucleotides and PCR-products

Hybridization of probe DNA to the target DNA (immobilized DNA) was performed according to common protocols used in microarray technology [Brown, 2003]. The slides were pre-hybridized in a solution of 6xSSC (saline sodium citrate, containing 1% bovine serum albumin, BSA and 0.5% sodium dodecyl sulfate, SDS), and finally rinsed with DI-water. Hybridization probes together with salmon sperm 1μg/μl DNA were dissolved 1:10 in hybridization buffer (Table 4.9.), denatured at 95°C for 2 min., spread onto the slide, and covered with a coverslip to achieve a uniform hybridization reaction. Subsequently, the sealed slides were put to a hybridization oven at 42 to 48°C for 12 h. After hybridization, slides were stringently washed in SSC buffers of decreasing ionic strength, 10 min. at a time, under constant shaking (see Table 4.10.).

6x	SSC
0,5%	SDS
1%	BSA

Table 4.8. Pre-hybridization buffer

50 μl	2% SDS on H_2O --> 0.1% SDS
250 μl	20x SSC --> 5x SSC
500 μl	1x DMF --> 50%
100 μl	10x Denhardt solution --> 1x
100 μl	H_2O

Table 4.9. Hybridization buffer (1mL)

I:	1x SSC / 0.03% SDS	(190 mL H_2O+ 10 mL 20x SSC + 0.6 mL 10% SDS)
II:	0.2x SSC	(198mL H_2O / 2mL 20x SSC)
III:	0.05x SSC	(200mL H_2O / 0.5 mL 20x SSC)

Table 4.10. Wash solutions: each 200mL

4.5.6. Scanning of DNA arrays

The readout of the hybridized slides was done using a microarray scanner (GenePix 4000B, Axon Instruments) in two-color mode for Cy3/TRITC and Cy5. The gain of the photomultiplier was set to 500. This value was only lowered in the case of saturating signal intensity.

In order to calibrate the microarray scanner a calibration curve with known amounts of DNA adsorbed to the surface was recorded. The results are shown in the experimental part (Figure 53). Unfortunately the elastomeric stamps could not be imaged with the slide scanner due to mechanical reasons. Thus, slides were additionally imaged using an inverted fluorescent microscope to compare the intensities with data obtained from imaging the stamp surfaces.

4.6. Detailed methods for Ch. 3.5.: PCR on stamp

The development of this novel method called for a thorough testing of a number of cross-linking and surface modification chemistries. The window of the experimental conditions was found rather narrow for establishing a successful procedure. The following sections describe the experimental protocols established in the process of developing the new technique.

4.6.1. Crosslinking of the ssDNA to the stamp surface

For the immobilization of the first strand (template) of ssDNA several chemical methods were tested. Using the cross-linking molecule disuccinimidyl suberate (DSS) turned out to give the best reproducible results. Thus, the stamps surface was first amine-grafted as described in Section 4.1.5.1. and then activated by modifying the amine groups with the cross-linker DSS (Section 4.1.5.3.). The amino-modified DNA oligonucleotides that served as template first strand, were diluted to 0,01 µM in PBS pH 7.2 containing 0,1 M Mg^{2+}. The target stamp surface was then incubated for 1-2 hours with the diluted oligo solution and subsequently washed with DI-water. At that stage, the stamp is ready for hybridization or alternatively, for PCR reaction.

4.6.2. Hybridization on stamp

As a first proof of principle test, an oligonucleotide that was exactly complementary to the first fragment immobilized on the surface of the stamp was designed and let hybridize on the surface. Hybridization conditions and buffers were equivalent to those described in Section 4.5.5. Hybridization was performed in a hybridization oven set to 42°C with high humidity to prevent evaporation. After hybridization the stamps were washed with DI-water and blown dry.

4.6.3. PCR on stamp

The "PCR reaction" used here, is only one elongation step with the subsequent cycling steps omitted. The reaction mixture, nevertheless, is the same as described previously (Section 4.5.1.). To elongate the immobilized first strand on the stamp, the surface was incubated at 42°C with the appropriate primer oligonucleotide diluted in hybridization buffer. After thoroughly rinsing the surface, the PCR buffer containing dNTPs, polymerase enzymes and $MgCl_2$ was added to the stamp surface. To initiate the elongation reaction the stamp was put to a thermocycler set to 48 °C for 5 minutes, then the stamp was removed, washed carefully with hybridization buffer and blown dry.

4.6.4. Microcontact printing of the hybridized second ssDNA

Several procedures for the separation of the two complementary strands have been tested. The successful procedure proved to be the following:

Amino modified glass slides (Section 4.1.5.) were used as substrates because the target surface had to be of positive charge in order to attract and retain the second strand ("copy") DNA. It was observed, that a transfer of molecules under dry conditions is not, or only with minor quality, possible. Hence, the microcontact-printing step was performed in the presence of buffer solution between the contact areas (that is, the stamping is performed while surface and stamp are submersed in liquid). To insure good contact of the two surfaces, a weight (~25g) was applied to the stamp. Furthermore, the temperature was elevated to facilitate unbinding and transfer of the molecules. At 70°C a good transfer was observed. Stamps were applied for 15 min. to the target surface in an incubation chamber, thereby keeping the ambient humidity high (95%) to prevent drying of the contact buffer. After incubation, the stamp was lifted from the substrate and could be reloaded by hybridization or a new elongation cycle.

4.7. Chemicals and biomolecules

4.7.1. Silanes

	name	functional group	length [nm]
APTS	Amino-propyl-tri-ethoxy-silane (Sigma-Aldrich)	amine	1.05
APTMS	Amino-propyl-tri-methoxy-silane (Sigma-Aldrich)	amine	0.9
MPTMS	Mercapto-propyl tri methoxy-silane (ABCR, Karlsruhe)	thiol	1.2

Table 4.11. Properties of silanes used to graft on surfaces.

4.7.2. Chemical reagents

name	comment	supplier
Methyl-Pyrolidi-none	used to block surface interactions	Sigma
Succinic anhydride	used to block surface interactions	Sigma
SSC	saline sodium citrate buffer	Sigma
SDS	sodium dodecyl sulfate	Sigma
Au Enhancement Kit	mix solutions A+B+C+D in a ratio 1:1:1:1	Nanoprobes
Ag Enhancement Kit	mix solution A+B 1:1	Sigma
Mica	atomically flat substrate used for AFM images	
Poly-L-Lysin	used to coat glass slides	Sigma
Anti-biotin colloi-dal gold	anti-biotin antibody conjugate 1nm colloidal gold parti-cles	British Bio Cell
BSA	Bovine Serum Albumin, prevents unspecific adsorption	Sigma
biotin BSA	used to simulate binding events	Pierce
glass slides	glass slides for microscopy	Menzel
PDMS	poly-(dimethylsiloxane)	Corning
Anti-rabbit anti-body	polyclonal antibody to rabbit raised in goat	Sigma
Anti-CRP anti-body	clone 5 and 7 were used to capture and detect antigen CRP	HyTest, Turku Finland
CRP- antigen	human C-reactive protein (CRP)	HyTest, Turku Finland
salmon sperm DNA	DNA from salmon testes, used for blocking unspecific interaction on DNA microarrays	Sigma

Table 4.12. Other chemical and biological reagents used.

4.7.3. DNA Oligomers

For the experiments described above a variety of DNA oligomers with different sequences was used. They were all designed using the Software "DNA-MAN" (Lynnon BioSoft, USA) such that hairpins or self-pairing was prevented. These sequences were ordered from major DNA vendors and purified by HPLC. The probe concentration of the individual probes was 100 pmol/μL in H_2O.

name	sequence 5´-3´	label 1	label 2	comment
RS1	CCG CTC GCG CTA CTG TAC CGA	5´-biotin	3´ FAM	various
RS2	TGA TAT CGA ATT CCX GCA GCC CGG	5´-C12 amino	pos 15 FAM	Complementary to RS3.
RS3	CCG GGC TGC AGG AAT TCG AXA TCA	5´-thiol group	pos 20 TAMRA	various
RS4	XGA TAT CGA ATT CCY GCA GCC CGG	5´-dTNH2	pos 15 FAM	Complementary to RS3.
BS50	CGG CCG CTC TAG AAC TAG T	--	--	50 bp PCR fragment with RS 2/4, Bluescript vector template
BS50BIO	CGG CCG CTC TAG AAC TAG T	5´-biotin	--	50 bp PCR
BS100	ACC ATG ATT ACG CCA AGC T	--	--	100 bp PCR
BS100BIO	ACC ATG ATT ACG CCA AGC T	5´-biotin	--	100 bp PCR
BS200	CTC ACT CAT TAG GCA CCC CA	--	--	200 bp PCR
BS200BIO	CTC ACT CAT TAG GCA CCC CA	5´-biotin	--	200 bp PCR
BS500	AAC GCC AGC AAC GCG GCC T	--	--	500 bp PCR
BS500BIO	AAC GCC AGC AAC GCG GCC T	5´-biotin	--	500 bp PCR
BS500 BIO	AAC GCC AGC AAC GCG GCC T	5´-biotin	--	500 bp PCR
BS500 UPPER	AGG CCG CGT TGC TGG CGT TT	--	--	Complementary to BS500 and BS500 BIO
RS2 BIO	TGA TAT CGA ATT CCT GCA GCC CGG	5´-biotin	--	Complementary to RS3 and RS3BIO
RS3 BIO	CCG GGC TGC AGG AAT TCG ATA TCA	5´-biotin	--	Complementary to RS2, RS4 and RS2BIO
BSUPPER	TGA TAT CGA ATT CCT GCA GCC CGG	--	--	Same sequence as RS2/RS4
cRS1-P	TCG GTA CAG TAG CGC GAG CGG	5´ phosphate	pos 11 FAM	test surface modification
MATT1	GAT CAG ATA TCG GTA CAG TAG CGC GAG CGG	5' amino	--	complementary to MATT3, same sequence as SEL1 10-30
M1-NH2-bio	AAAAAAAAAA GAT CAG ATA TCG GTA CAG TAG CGC GAG CGG	5' C6 amino	3' biotin	test surface modification
M1-SH-bio	AAAAAAAAAA GAT CAG ATA TCG GTA CAG TAG CGC GAG CGG	5' SH	3' biotin	test surface modification
MATT1-SH	GAT CAG ATA TCG GTA CAG TAG CGC GAG CGG	5' SH	--	test surface modification
PRIM1	CCG CTC GCG C	5' biotin	--	used for PCR on stamp

Table 4.13. List of oligonucleotides used in the experiments.

MATT2	GAT CAG ATA TCG	5' FAM	--	used for PCR on stamp
MATT3	CCG CTC GCG CTA CTG TAC CGA TAT CTG ATC	5' biotin	--	complementary to MATT1, same sequence as RS1 1-21 position; used for PCR on stamp
SEL1	TCG GTA CAG TAG CGC GAG CGG	5' DIG	--	complementary to RS1
SL+1	ACCATGATTACGC-CAAGCT	5' C6 amino	pos 11 FAM	compl. to SL-1; used for PCR on stamp
SL-1	TTTCGTTCCACT-GAGCGTCA	5' C6 amino	3' TAMRA	compl. to SL+1; used for PCR on stamp
SL500	CTCACCGTCTTTCAT-TGCCA	5' biotin	pos 8 TAMRA	anneals only to pBC KS+ Vector, so it is wrong Primer for PCR
SL500x no	GGAACCGGAGCTGAAT-GAAG	--	--	same as SLx500bio
SL500x bio	GGAACCGGAGCTGAAT-GAAG	5' biotin	pos 12 TAMRA	500 bp fragment with sl1
SL500x upper	CTTCATTCAGCTCCGGT-TCC	5' C6 amino	--	comp to SLx500
H1_x	GAT CAG ATA TCG GTA CAG TAG CGC GAG CGG	5' C6 amino	3' FAM 5/6	Same sequence as MATT1
P1_x	CCG CTC GCG C	5' TAMRA	--	same sequence as PRIM1
SH-BMBF1	TCTCCGAATCATTTATAA-CATAGTTCAACAGGT-TGAGGAAAACTGAATTA	5' SH	3' TAMRA	for immobilization on gold

Table 4.13. List of oligonucleotides used in the experiments.

5. Conclusion and Outlook

One goal of this thesis was to establish a novel biomedical assay detection device. In the course of the work it was proven that a standard compact disc (CD) pickup taken from a music CD player can be employed to detect and quantify biomolecular binding events. The CD pickup tracked growing silver grains during an autometallographic reaction initiated by the binding of colloidal gold-labeled ligands to immobilized receptor molecules. The surface density of receptors was chosen to be low allowing for discrimination among individual binding events. Surfaces were characterized by atomic force microscopy and electron microscopy. Titration of the ligand solution resulted in a clear sigmoid correlation between the number of silver or gold grains created on the surface and the concentration of analytes applied. The system's optical resolution was shown to be in the sub-micrometer range, allowing the detection of individual silver grains. In a sandwich-type ELISA experiment the feasibility of measuring the concentration of target molecules (C-reactive Protein, CRP) in an applied test solution, with a dynamic range of at least four orders of magnitude, was demonstrated. Results were readily comparable with those obtained by commercially available ELISA kits. Integrated in a biochemical or diagnostic assay system, this novel tool has the potential to be developed into an expedient extension of the diagnostic readout devices on the market. By making use of low-cost parts for the device and using mass fabrication methods such as injection molding for substrate carriers, this system should outperform any currently available diagnostic system.

A further goal was to establish new ways of fabricating arrays of biomolecules on flat surfaces. This was achieved building an alignment device such that molecule pattern could be overlay contact-printed. It could be shown that the alignment tool built from simple commercially available components satisfied the requirements for producing arrays of DNA molecules or proteins by overlay microcontact printing for research purposes. In a set of experiments, sample arrays in the form of lined-up molecule dots were fabricated. To prove the principle feasibility four separate stamps were first inked with four different solutions of molecules and then printed to a substrate surface, such that the patterns on the stamps together constitute an array of 400 molecule spots. The expansion of this method to overlay print more different molecules is easily possible by changing the design of the stamps slightly. The effort of creating these molecule arrays scales linearly with the number of probes within the array. However, by using combinatoric inking pads it should be possible to further reduce the effort. The positioning resolution that has been achieved with this tool was approximately 4 ± 2 µm. For the needs of this project, the achieved resolution was completely sufficient and if necessary could even be further improved by increasing the mechanical stability of the setup.

While developing the alignment device a new way to create alignment structures had to be found. This led to the development of the novel technique termed "Enzyme-Assisted Microcontact Printing" (EAI-µCP). With adoption of this novel method, a gap in the toolbox of microcontact printing could be closed. It is now possible to pattern surfaces with two dimensional structures of high aspect ratio etched into noble metals. In the process of developing the biotest platform, this printing method opened up a pathway to create arrays of overlay microcontact printed molecules where EAI-µCP was used to create alignment marks that were compatible in size to those integrated on the stamp surface. With this trick, problems resulting from the intrinsic shrinking of the elastomer upon curing were circumvented. However, it must be stated, that the entire process of alignment mark generation is time-consuming and a method that limits or suppresses the shrinkage of the elastomer might be more favorable for commercial array production.

The successful extension of microcontact printing to the field of DNA and charged polymers constituted another major part of this work. New protocols have been developed that make µCP of DNA as simple as it is for proteins. Experiments performed in the course of this thesis showed that a complete DNA microarray can be printed several times from a once inked stamp, which in future could help save time and costs for microarray production. The usability of arrays produced with µCP of DNA is corroborated by identical experimental results generated from "cloned" arrays and conventionally spotted arrays. Microcontact printing of DNA could assist the transition from sequential array fabrication in a spot by spot fashion to the production of complete arrays in a one step, book printing type fabrication. This would allow to reduce production costs dramatically and in turn increase the general acceptance of such high density arrays on the non-research market.

A further goal was to develop µCP of DNA into a more intelligent surface patterning method for DNA array fabrication. This was achieved by combining µCP with the well-established method of enzymatic DNA amplification (PCR). This novel technology was termed "PCR-on-stamp". With the experiments performed in this thesis, it was demonstrated that it is indeed possible to transfer one strand of previously attached double stranded DNA from an elastomer stamp to a target surface, leaving the other strand firmly attached to the stamp surface. The transfer can then be repeated after reloading the stamp again by either hybridizing DNA molecules directly from a solution or by performing solid-phase PCR on the elastomer surface. Further experiments are necessary to prove full functionality of the method, but at the time of writing no major obstacles seemed to interfere with the envisioned goal of successive array printing. Fine tuning and further engineering will help to complete the protocols. The such created, DNA modified, surfaces could be used either the way they are for genetic testing (e.g. as microarrays) or to serve as template surface for localized surface modifi-

cation with DNA tagged biomolecules. PCR-on-stamp could help to meet the markets demand for such cheap and functionalized surfaces.

In conclusion, this thesis presents a set of methods and technologies, which constitute a complete diagnostic assay system. Described was a method for creating test substrates consisting of arrayed molecules suitable for analysis by use of the novel assay readout device, the CD-Pickup imager. Subsequently the method of µCP of proteins was further developed to use DNA as ink. And finally, a novel method for the intelligent fabrication of DNA arrays was developed and presented.

6. Appendix

6.1. Calculation of the adsorption rate

The rate equation for the surface density D_s can be expressed as:

$$\frac{\partial}{\partial t}D_s(t) = k_a C(t) D_{free}(t) - k_d D_s(t) \tag{30}$$

with the association and dissociation rate constants k_a and k_d, the concentration of free sites on the surface $D_{free}(t)$ and the bulk protein concentration $C(t)$. $D_{free}(t)$ and $C(t)$ can be rewritten as:

$$C(t) = C_0 - D_s(t)$$
$$D_{free}(t) = D_{0free} - D_s(t) \tag{31}$$

Assuming $C_0 \gg D_s(t)$ which is valid for high protein concentrations in solution

$$C(t) \approx C_0 \tag{32}$$

Combining Eq. 30 and Eq. 31 the solution for the homogeneous differential equation can be determined to be

$$D_s(t) = K e^{-(k_a C_0 + k_d)t} \tag{33}$$

The solution of the inhomogeneous differential equation can then immediately be calculated and by setting $t=0$ the integration constant K can be determined:

$$D_s(t) = K e^{-(k_a C_0 + k_d)t} + \frac{k_a C_0 D_{0free}}{k_a C_0 + k_d} \tag{34}$$

$$\text{with } D_s(t=0) = K + \frac{k_a C_0 D_{0free}}{k_a C_0 + k_d} = 0 \tag{35}$$

Thus, one gets as final solution to the differential equation Eq. 30 an exponentially growing function showing saturation behavior.

$$\begin{aligned} D_s(t) &= -\frac{k_a C_0 D_{0free}}{k_a C_0 + k_d} e^{-(k_a C_0 + k_d)t} + \frac{k_a C_0 D_{0free}}{k_a C_0 + k_d} \\ &= \frac{k_a C_0 D_{0free}}{k_a C_0 + k_d}(1 - e^{-(k_a C_0 + k_d)t}) \end{aligned} \tag{36}$$

6.2. Calculation of the interaction free energy

The interaction free energy for a sphere in close vicinity to a charged plate is derived using the linearized Poisson-Boltzmann equation, which states for the potential ψ in the system defined in Section 2.1.6.4.:

$$\Delta\psi = \kappa^2\psi \quad \text{outside the sphere and the plane} \tag{37}$$

$$\Delta\psi = \kappa^2\psi - \frac{\rho}{\varepsilon_r\varepsilon_0} \quad \text{inside the sphere} \tag{38}$$

where κ is the Debye Hückel parameter, ε_r and ε_0 are the permittivities in medium or vacuum, respectively. The boundary conditions for such a system are:

$$\psi \text{ and } \frac{\partial\psi}{\partial n} \quad \text{are continuous at the sphere's surface} \tag{39}$$

where n is the normal coordinate perpendicular to the surface. Assuming the surface charge density σ_P on the plate to be constant (instead of a constant surface potential, which would be the case for a metal plate),

$$\frac{\partial\psi}{\partial n} = -\frac{\sigma_P}{\varepsilon_r\varepsilon_0} = const \quad \text{on the surface of the plate.} \tag{40}$$

The solution to Eq. 37 and Eq. 38 can be written as a superposition of the potential created by the sphere ψ_s and the potential created by the plate ψ_p alone, adding an interaction term ψ_I that satisfies the boundary condition Eq. 40, thus

$$\psi_{tot} = \psi_s + \psi_p + \psi_I. \tag{41}$$

ψ_p and ψ_s can easily be solved using Eq. 37 and Eq. 38 with z perpendicular to the plate surface and r being the radius of the sphere:

$$\psi_p(z) = \psi_{p0}e^{-\kappa z} \tag{42}$$

$$\psi_s(r) = \psi_{s0}\frac{a}{r}e^{-\kappa(r-a)} \tag{43}$$

ψ_{s0} is derived by using boundary condition Eq. 40 together with Eq. 43 and ψ_{p0} can be determined using Eq. 42 and Eq. 40 (adapted from Ohshima et al. [Ohshima, 1993])

$$\psi_{s0} = \frac{1}{\varepsilon_r\varepsilon_0\kappa a}e^{-\kappa a}\int_0^a r\rho(r)\sinh(\kappa r)dr \tag{44}$$

$$\psi_{p0} = \frac{\sigma}{\varepsilon_r \varepsilon_0 \kappa} \tag{45}$$

Assuming an isotropic charge distribution in the sphere one can solve the integral and obtains for the potential on the sphere surface:

$$\psi_{s0} = \frac{1}{\varepsilon_0 \varepsilon_r} \frac{q}{4\pi a} \frac{\sinh(\kappa a)}{\kappa a} e^{-\kappa a} \tag{46}$$

ψ_I is derived in the next step by using the method of image charges.

By placing an image sphere S' with radius a at a symmetric position with respect to sphere S behind the plate (Figure 13) it is possible to simplify the given mathematical problem. The z coordinate of S' is $z=-d$. Considering the derivatives of the potentials of S and S' it can be stated that they cancel each other out at the place of the plate ($z=0$). Thus the value of the derivative of the interaction potential is always equal to Eq. 40 and ψ_I is given by (note the '+' sign):

$$\psi_I = +\psi_{s0}\frac{a}{r'}e^{-\kappa(r'-a)} \tag{47}$$

Hence the solution to the Poisson Boltzmann equation is at any point Q outside of S and P where r and r' are the distances to the center of the respective spheres:

$$\psi_{tot}(Q) = \psi_s + \psi_p + \psi_I = \psi_{p0}e^{-\kappa z} + \psi_{s0}\frac{a}{r}e^{-\kappa(r-a)} + \psi_{s0}\frac{a}{r'}e^{-\kappa(r'-a)} \tag{48}$$

where ψ_{p0} and ψ_{s0} are only factors, that can be derived from the boundary conditions.

With this solution for the total potential it is possible to attempt the calculation of the interaction energy of a sphere and a charged surface.

List of Figures

List of Tables

Bibliography

Adamson, A. W., Gast, A. P., 6th ed.; Wiley Interscience, **1997**. *Physical Chemistry of Surfaces.*

Adessi, C., Matton, G., Ayala, G., et al. <u>Nucleic Acids Res</u> **2000**, *28*, E87. *Solid phase DNA amplification: characterisation of primer attachment and amplification mechanisms*

Aizenberg, J., Black, A. J., Whitesides, G. M. <u>Nature</u> **1999**, *398*, 495-498. *Control of crystal nucleation by patterned self-assembled monolayers*

Alberts, B., Bray, D., Lewis, J., et al.; Garland Publishing, **1994**. *Molecular Biology of the Cell.*

Albrecht, C., Blank, K., Lalic-Multhaler, M., et al. <u>Science</u> **2003**, *301*, 367-370. *DNA: A programmable force sensor*

Bain, C. D., Whitesides, G. M. <u>Science</u> **1988**, *240*, 62-63. *Molecular-level control over surface order in self-assembled monolayer films of thiols on gold*

Baum, M., Bielau, S., Rittner, N., et al. <u>Nucleic Acids Research</u> **2003**, *31*. *Validation of a novel, fully integrated and flexible microarray benchtop facility for gene expression profiling*

Beier, M., Hoheisel, J. D. <u>Nucleic Acids Res</u> **1999**, *27*, 1970-1977. *Versatile derivatisation of solid support media for covalent bonding on DNA-microchips*

Bernard, A., Delamarche, E., Schmid, H., et al. <u>Langmuir</u> **1998**, *14*, 2225-2229. *Printing patterns of proteins*

Bernard, A., Renault, J. P., Michel, B., Bosshard, H. R., Delamarche, E. <u>Advanced Materials</u> **2000**, *12*, 1067-1070. *Microcontact printing of proteins*

Bernard, A., Fitzli, D., Sonderegger, P., et al. <u>Nat Biotechnol</u> **2001a**, *19*, 866-869., *Affinity capture of proteins from solution and their dissociation by contact printing*

Bernard, A., Michel, B., Delamarche, E. <u>Anal Chem</u> **2001b**, *73*, 8-12., *Micromosaic immunoassays*

Biebuyck, H. A., Larsen, N. B., Delamarche, E., Michel, B. <u>IBM J.Res.Develop.</u> **1997**, *41*, 159-170. *Lithography beyond light: Microcontact printing with monolayer resists*

Bietsch, A., Michel, B. <u>Journal of Applied Physics</u> **2000**, *88*, 4310-4318. *Conformal contact and pattern stability of stamps used for soft lithography*

Blossey, R., Bosio, A. <u>Langmuir</u> **2002**, *18*, 2952-2954. *Contact line deposits on cDNA microarrays: A "twin-spot effect"*

Bockelmann, U., EssevazRoulet, B., Heslot, F. <u>Physical Review Letters</u> **1997**, *79*, 4489-4492. *Molecular stick-slip motion revealed by opening DNA with piconewton forces*

Bockelmann, U., Thomen, P., Essevaz-Roulet, B., Viasnoff, V., Heslot, F. <u>Biophysical Journal</u> **2002**, *82*, 1537-1553. *Unzipping DNA with optical tweezers: high sequence sensitivity and force flips*

Bohren, C. F., D.R., H.; Wiley-Interscience: New York, **1983**. *Absorption and Scatterin of Light by Small Particles.*

Branch, D. W., Corey, J. M., Weyhnmeyer, J. A., Brewer, G. J., Wheeler, B. C. Med.Biol.Eng.Comput. **1998**, *36*, 135-141. *Microstamp patterns of biomolecules for high-resolution neuronal networks*

Breslauer, K. J., Frank, R., Blocker, H., Marky, L. A. Proceedings of the National Academy of Sciences of the United States of America **1986**, *83*, 3746-3750. *Predicting DNA Duplex Stability from the Base Sequence*

Brown, P. O., http://cmgm.stanford.edu/pbrown/protocols/index.html, **2003**, *Experimental Protocols*,

Burgin, T., Choong, V.-E., Maracas, G. Langmuir **2000**, *16*, 5371-5375. *Large area submicrometer contact printing using a contact aligner*

Burns, M. A., Johnson, B. N., Brahmasandra, S. N., et al. Science **1998**, *282*, 484-487. *An integrated nanoliter DNA analysis device*

Caelen, I., Bernard, A., Juncker, D., et al. Langmuir **2000**, *16*, 9125-9130. *Formation of gradients of proteins on surfaces with microfluidic networks*

Calonder, C., Van Tassel, P. R. Langmuir **2001**, *17*, 4392-4395. *Kinetic regimes of protein adsorption*

Carre, A., Birch, W. The 25th Annual Meeting of the Adhesion Society **2002**, 50-52. *Interfacial Interactions Between DNA Molecules and Aminated Glass Substrates*

Carre, A., Lacarrriere, V., Birch, W. Journal of Colloid and Interface Science **2003**, *260*, 49-55. *Molecular interactions between DNA and an aminated glass substrate*

Chan, V., Graves, D. J., Fortina, P., McKenzie, S. E. Langmuir **1997**, *13*, 320-329. *Adsorption and surface diffusion of DNA oligonucleotides at liquid/solid interfaces*

Crowe, J. S., Cooper, H. J., Smith, M. A., et al. Nucleic Acids Research **1991**, *19*, 184-184. *Improved Cloning Efficiency of Polymerase Chain-Reaction (Pcr) Products after Proteinase-K Digestion*

Danscher, G., Hacker, G. W., Grimelius, L., Norgaard, J. O. R. Journal of Histotechnology **1993**, *16*, 201-207. *Autometallographic Silver Amplification of Colloidal Gold*

de Wildt, R. M. T., Mundy, C. R., Gorick, B. D., Tomlinson, I. M. Nature Biotechnology **2000**, *18*, 989-994. *Antibody arrays for high-throughput screening of antibody-antigen interactions*

Delamarche, E., Michel, B., Biebuyck, H. A., Gerber, C. Adv.Mat. **1996a**, *8*, 719-729. *Golden interfaces: The surface of self-assembled monolayers*

Delamarche, E., Michel, B. Thin Solid Films **1996b**, *273*, 54-60. *Structure and stability of self-assembled monolayers*

Delamarche, E., Bernard, A., Schmid, H., Michel, B., Biebuyck, H. Science **1997**, *276*, 779-781., *Patterned delivery of immunoglobulins to surfaces using microfluidic networks*

Delamarche, E., Bernard, A., Schmid, H., et al. Journal of the American Chemical Society **1998**, *120*, 500-508. *Microfluidic networks for chemical patterning of substrate: Design and application to bioassays*

Delamarche, E., Geissler, M., Bernard, A., et al. Advanced Materials **2001**, *13*, 1164-1167. *Hydrophilic poly (dimethylsloxane) stamps for microcontact printing*

Delamarche, E., Geissler, M., Wolf, H., Michel, B. J Am Chem Soc **2002**, *124*, 3834-3835., *Positive microcontact printing*

Diamandis, E. P., Christopoulos, T. K.; Academic Press: San Diego, CA, **1996**. *Immunoassays.*

DiMilla, P. A., Folkers, J. P., Biebuyck, H. A., et al. J.Am.Chem.Soc. **1994**, *116*, 2225-2226. *Wetting and protein adsorption of self-assembled monolayers of alkanethiolates supported on transparent films of gold*

Drmanac, R., Drmanac, S. Methods Mol. Biol., **2001**, *170*, 39-51.

Eckert, R., Jeney, S., Horber, J. K. H. Cell Biology International **1997**, *21*, 707-713. *Understanding intercellular interactions and cell adhesion: Lessons from studies on protein-metal interactions*

EssevazRoulet, B., Bockelmann, U., Heslot, F. Proceedings of the National Academy of Sciences of the United States of America **1997**, *94*, 11935-11940. *Mechanical separation of the complementary strands of DNA*

Fang, Y., Hoh, J. H. Nucleic Acids Research **1998**, *26*, 588-593. *Surface-directed DNA condensation in the absence of soluble multivalent cations*

Florin, E.-L., Moy, V. T., Gaub, H. E. Science **1994**, *264*, 415-417. *Adhesion force between individual ligand-receptor pairs*

Fodor, S. P. A., Read, J. L., Pirrung, M. C., et al. Science **1991**, *251*, 767-773. *Light-directed, spatially addressable parallel chemical synthesis*

Folch, A., Schmidt, M. A. JMEMS **1998**, *XXX*, 00. *Wafer-level in-registry microstamping*

Fragneto, G., Su, T. J., Lu, J. R., Thomas, R. K., Rennie, A. R. Physical Chemistry Chemical Physics **2000**, *2*, 5214-5221. *Adsorption of proteins from aqueous solutions on hydrophobic surfaces studied by neutron reflection*

Fritzsche, W. J Biotechnol **2001**, *82*, 37-46., *DNA-gold conjugates for the detection of specific molecular interactions*

Fu, A. Y., Chou, H. P., Spence, C., Arnold, F. H., Quake, S. R. Analytical Chemistry **2002**, *74*, 2451-2457. *An integrated microfabricated cell sorter*

Geissler, M., Schmid, H., Bietsch, A., Michel, B., Delamarche, E. Langmuir **2002**, *18*, 2374-2377. *Defect-tolerant and directional wet-etch systems for using monolayers as resists*

Geissler, M., Wolf, H., Stutz, R., et al. Langmuir **2003**, *19*, 6301-6311. *Fabrication of metal nanowires using microcontact printing*

Gilson, M., http://www.biophysics.org/btol/img/Gilson.M.pdf, **2000**, *Introduction to continuum electrostatics. with molecular applications,*

Gopel, W. Sens.Actuators A **1996**, *56*, 83-102. *Ultimate limits in the miniaturization of chemical sensors*

Grandbois, M., Beyer, M., Rief, M., Clausen-Schaumann, H., Gaub, H. E. <u>Science</u> **1999**, *283*, 1727-1730. *How strong is a covalent bond ?*

Hacia, J. G., Brody, L. C., Chee, M. S., Fodor, S. P., Collins, F. S. <u>Nat Genet</u> **1996**, *14*, 441-447. *Detection of heterozygous mutations in BRCA1 using high density oligonucleotide arrays and two-colour fluorescence analysis*

Hacker, G. W., Polak, J. M., Springall, D. R., et al. <u>Mikroskopie</u> **1985**, *42*, 318-325. *Immunogold-Silver Staining (Igss) - a Review*

Hacker, G. W., Danscher, G. <u>Cell Vision 1</u> **1994**, *2*, 102-109. *Recent advances in immunogold-silver staining (IGSS) – autometallography.*

Hacker, G. W., Zehbe, I., Hainfeld, J. F., et al. <u>Cell Vision 3</u> **1996**, *3*, 209-215. *High performance in situ hybridization and in situ PCR.*

Harrington, C. A., Rosenow, C., Retief, J. <u>Curr Opin Microbiol</u> **2000**, *3*, 285-291. *Monitoring gene expression using DNA microarrays*

Hermanson, G. T.; Academic Press, **1996**. *Bioconjugate Techniques*.

Irving, R. A., Hudson, P. J. <u>Nature Biotechnology</u> **2000**, *18*, 932-933. *Proteins emerge from disarray*

Israelachvili, J., 2nd edition ed.; Academic Press, **2000**. *Intermolecular & Surface Forces*.

James, C. D., Davis, R. C., Kam, L., et al. <u>Langmuir</u> **1998**, *14*, 741-744. *Patterned protein layers on solid substrates by thin stamp microcontact printing*

James, C. D., Davis, R., Meyer, M., et al. <u>IEEE Trans Biomed Eng</u> **2000**, *47*, 17-21., *Aligned micro-contact printing of micrometer-scale poly-L-lysine structures for controlled growth of cultured neurons on planar microelectrode arrays*

Jehanli, A., Hough, D. <u>Molecular Immunology</u> **1985**, *22*, 557-566. *Pronase and Proteinase-K Digestion of Human Immunoglobulin-M*

Juncker, D., Schmid, H., Bernard, A., et al. <u>Journal of Micromechanics and Microengineering</u> **2001**, *11*, 532-541. *Soft and rigid two-level microfluidic networks for patterning surfaces*

Kuhn, K. J., <u>http://www.ee.washington.edu/conselec/CE/kuhn/cdrom/95x8.htm</u>, **2001**, *CD/ROM -- An extension of the CD audio standard*,

Kumar, A., Biebuyck, H. A., Abbott, N. L., Whitesides, G. M. <u>Journal of the American Chemical Society</u> **1992**, *114*, 9188-9189. *The Use of Self-Assembled Monolayers and a Selective Etch to Generate Patterned Gold Features*

Kumar, A., Whitesides, G. M. <u>Appl.Phys.Lett.</u> **1993**, *63*, 2002-2004. *Features of gold having micrometer to centimeter dimensions can be formed through a combination of stamping with an elastomeric stamp and an alkanethiol "ink" followed by chemical etching*

Kumar, A., Biebuyck, H. A., Whitesides, G. M. <u>Langmuir</u> **1994**, *10*, 1498-1511. *Patterning Self-Assembled Monolayers - Applications in Materials Science*

Kumar, A., Abbott, N. L., Kim, E., Biebuyck, H. A., Whitesides, G. M. Accounts of Chemical Research **1995**, *28*, 219-226. *Patterned Self-Assembled Monolayers and Mesoscale Phenomena*

La Clair, J. J., Burkart, M. D. Organic & Biomolecular Chemistry **2003**, *1*, 3244-3249. *Molecular screening on a compact disc*

Lagally, E. T., Medintz, I., Mathies, R. A. Analytical Chemistry **2001**, *73*, 565-570. *Single-molecule DNA amplification and analysis in an integrated microfluidic device*

Lander, E. S., Linton, L. M., Birren, B., et al. Nature **2001**, *409*, 860-921. *Initial sequencing and analysis of the human genome*

Lange, S. A., Benes, V., Kern, D. P., Horber, J. K., Bernard, A. Anal Chem **2004**, *76*, 1641-1647. *Microcontact printing of DNA molecules*

Larsen, N. B., Biebuyck, H. A., Delamarche, E., Michel, B. J.Am.Chem.Soc. **1997**, *119*, 3017-3026. *Order in microcontact printed self-assembled monolayers*

Lipshutz, R. J., Fodor, S. P., Gingeras, T. R., Lockhart, D. J. Nat Genet **1999**, *21*, 20-24. *High density synthetic oligonucleotide arrays*

Lockhart, D. J., Dong, H., Byrne, M. C., et al. Nat Biotechnol **1996**, *14*, 1675-1680. *Expression monitoring by hybridization to high-density oligonucleotide arrays*

Maniatis, T., Sambrook, J., Fritsch, E. F.; Cold Spring Harbor Laboratory, **1989**. *Molecular Cloning: A Laboratory Manual.*

Michel, B., Bernard, A., Bietsch, A., et al. Ibm Journal of Research and Development **2001**, *45*, 697-719. *Printing meets lithography: Soft approaches to high-resolution printing*

Michel, B., http://www.unternehmen.com/Bernhard-Michel/MieCalc/index.html, **2002**, *MieCalc - frei konfigurierbares Programm für Streulichtberechnungen (Mie-Theorie)*,

Mrksich, M., Chen, C. S., Xia, Y., et al. Proc Natl Acad Sci U S A **1996**, *93*, 10775-10778., *Controlling cell attachment on contoured surfaces with self-assembled monolayers of alkanethiolates on gold*

Mullis, K. B. Patent **1985**. *Process for Amplifying Nucleic Acid Sequences Polymerase Chain Reaction*

Mullis, K. B. Scientist **2003**, *17*, 11-11. *The first polymerase chain reaction*

Norde, W. Advances in Colloid and Interface Science **1986**, *25*, 267-340. *Adsorption of Proteins from Solution at the Solid-Liquid Interface*

Ohshima, H., Kondo, T. Journal of Colloid and Interface Science **1993**, *157*, 504-508. *Electrostatic Interaction of an Ion-Penetrable Sphere with a Hard Plate - Contribution of Image Interaction*

Papra, A., Bernard, A., Juncker, D., et al. Langmuir **2001**, *17*, 4090-4095. *Microfluidic networks made of poly(dimethylsiloxane), Si, and Au coated with polyethylene glycol for patterning proteins onto surfaces*

Prime, K. L., Whitesides, G. M. J.Am.Chem.Soc. **1993**, *115*, 10714-10721. *Adsorption of proteins on surface containing end-attached oligo(ethylene oxide): A model system using self-assembled monolayers*

Reichert, J., Csaki, A., Kohler, J. M., Fritzsche, W. Anal Chem **2000**, *72*, 6025-6029., *Chip-based optical detection of DNA hybridization by means of nanobead labeling*

Renault, J. P., Bernard, A., Juncker, D., et al. Angewandte Chemie-International Edition **2002**, *41*, 2320-2323. *Fabricating microarrays of functional proteins using affinity contact printing*

Rogers, J. A., Bao, Z., Baldwin, K., et al. Proc Natl Acad Sci U S A **2001**, *98*, 4835-4840., *Paper-like electronic displays: large-area rubber-stamped plastic sheets of electronics and microencapsulated electrophoretic inks*

Röhr, C., http://ruby.chemie.uni-freiburg.de/Vorlesung/silicate_0.html, **1999**, *Silicatchemie*,

Roth, G. Diploma Thesis, *Protein-Protein Interaktion an Mikrostrukturen* University Tübingen, **2002**.

Saiki, R. K., Scharf, S., Faloona, F., et al. Science **1985**, *230*, 1350-1354. *Enzymatic Amplification of Beta-Globin Genomic Sequences and Restriction Site Analysis for Diagnosis of Sickle-Cell Anemia*

Schena, M., Shalon, D., Davis, R. W., Brown, P. O. Science **1995**, *270*, 467-470. *Quantitative monitoring of gene expression patterns with a complementary DNA microarray*

Schena, M., Heller, R. A., Theriault, T. P., et al. Trends Biotechnol **1998**, *16*, 301-306. *Microarrays: biotechnology's discovery platform for functional genomics*

Schena, M. Molecular Biochip Technology; Eaton Publishing, **2000**. *Molecular Biochip Technology*.

Schober, A., Gunther, R., Schwienhorst, A., Doring, M., Lindemann, B. F. Biotechniques **1993**, *15*, 324-329. *Accurate high-speed liquid handling of very small biological samples*

Schulze, A., Downward, J. Nat Cell Biol **2001**, *3*, E190-195. *Navigating gene expression using microarrays--a technology review*

Shalon, D., Smith, S. J., Brown, P. O. Genome Res **1996**, *6*, 639-645. *A DNA microarray system for analyzing complex DNA samples using two-color fluorescent probe hybridization*

Singh-Gasson, S., Green, R. D., Yue, Y. J., et al. Nature Biotechnology **1999**, *17*, 974-978. *Maskless fabrication of light-directed oligonucleotide microarrays using a digital micromirror array*

Singhvi, R., Kumar, A., L¢pez, G. P., et al. Science **1994**, *264*, 696-698. *Engineering cell shape and function*

Smith, S. B., Cui, Y., Bustamante, C. Science **1996**, *271*, 795-799. *Overstretching B-DNA: The elastic response of individual double-stranded and single-stranded DNA molecules*

Southern, E., Mir, K., Shchepinov, M. Nat Genet **1999**, *21*, 5-9. *Molecular interactions on microarrays*

St. John, P. M., Craighead, H. G. Appl.Phys.Lett. **1996**, *68*, 1022-1024. *Microcontact printing and pattern transfer using trichlorosilanes on oxide substrates*

St. John, P. M., Davis, R., Cady, N., et al. <u>Anal Chem</u> **1998**, *70*, 1108-1111., *Diffraction-based cell detection using a microcontact printed antibody grating*

Stroock, A. D., Dertinger, S. K. W., Ajdari, A., et al. <u>Science</u> **2002**, *295*, 647-651. *Chaotic mixer for microchannels*

Taton, T. A., Mirkin, C. A., Letsinger, R. L. <u>Science</u> **2000**, *289*, 1757-1760., *Scanometric DNA array detection with nanoparticle probes*

Thorsen, T., Maerkl, S. J., Quake, S. R. <u>Science</u> **2002**, *298*, 580-584. *Microfluidic large-scale integration*

Török, P., Higdon, P. D., Juskaitis, R., Wilson, T. <u>Optics Communications</u> **1998**, 335-341. *Optimising the image contrast of conventional and confocal optical microscopes imaging finite sized spherical gold scatterers*

Vainrub, A., Pettitt, B. M. <u>Chemical Physics Letters</u> **2000**, *323*, 160-166. *Thermodynamics of association to a molecule immobilized in an electric double layer*

Vansant, E. F., VanDerVoort, P., Vrancken, K. C. In *Characterization and Chemical Modification of the Silica Surface*; Elsevier Science Publ B V: Amsterdam, 1995; Vol. 93, pp 3-30.

Venter, J. C., Adams, M. D., Myers, E. W., et al. <u>Science</u> **2001**, *291*, 1304-+. *The sequence of the human genome*

Verwey, E. J. W., Overbeek, J. T. G.; Elsevier: Amsterdam, **1948**. *Theory of the Stability of Lyophobic Colloids.*

Watson, A., Mazumder, A., Stewart, M., Balasubramanian, S. <u>Curr Opin Biotechnol</u> **1998**, *9*, 609-614. *Technology for microarray analysis of gene expression*

Xia, Y., Whitesides, G. <u>Angewandte Chemie Int. Ed.</u> **1998**, *37*, 550-575. *Soft Lithography*

Acknowledgements

First of all, my special thanks go to Dr. André Bernard for his continuos and enduring support through all the "up's" and "down's" of this work. Without him and without his encouragement this work would not have been possible. Furthermore, I would like to thank him for holding up the research environment which helped me to finish my experiments and for his endurance in proof-reading this thesis. Besides his professional guidance, I would also like to thank him for the exciting and inspiring times we had in these three years. I really enjoyed the time, both professionally and privately.

I am greatly indebted to Prof. Dr. Dieter Kern for giving me the opportunity to join his group in the department of Applied Physics at the University of Tübingen as a Ph.D. student. Furthermore, I would like to thank him for his continuous and uncomplicated support and the possibility to use the exciting cleanroom facilities of the university.

I would like to express my gratitude to Prof. Dr. Heinrich Hörber from Wayne State Medical University, USA for his idea to actually start this Ph.D. while working in a start-up company. His suggestion was the beginning of three very exiting years. For the opportunity to finish the Ph.D. in time, after "wild" times, I am deeply in his dept. Without him it would have been hard to accomplish this thesis.

I wish to express my gratitude to Prof. Dr. Stefan Dübel for agreeing to serve as co-examiner for this thesis, for proof-reading manuscripts, and for very inspiring discussions.

My sincere thanks go to Dr. Vladimir Benes and Dr. Christian Boulin for making it possible to finish my Ph.D. at EMBL-Heidelberg. I consider this opportunity as an honour which was not self-evident. I also would like to express my gratitude to Dr. Benes for the warm welcoming in his group at EMBL as if my being there was planned.

The whole *indigon team* deserves a very big "Thank You All". Matthias Kolleck, Dr. Manfred Wick, Beate Breitinger, Andreas Vetter, Constanze Sinner, Dr. Silke Wittemann, Dr. Thilo Lacoste, Dr. Susanne Kopta, and Yvonne Ott contributed a great deal to the results of this work. Together we experienced what it means to work in a start-up company in the New Economy Age. I definitely enjoyed the time with you all.

I would also like to thank the whole *Kern group* at the University of Tübingen for accepting me as external Ph.D. student. I very much appreciated the help of Ralf Stiefel and Bertram Herzog with all the misbehaving "technology" in the cleanroom and elsewhere.

Furthermore, I am grateful to the whole *Gencore group* at EMBL-Heidelberg Dr. Jürgen Zimmermann, Sabine Schmidt, Richard Carmouche, Tommy Ivacevic, David Ibberson, Jos de Graaf, Ti Bach Nga Ly, Susanne Schneider, Dr. Monika Benesova, Dr. Angela Relogio and François Pouthas for giving me such a good time at EMBL. It was a pleasure for me to work and dine with you guys.

I appreciated the help of Florian Rammrath from Hamamatsu, Germany, with the camera software and would like to thank him for letting me use the camera software free of charge. This was a generous gesture.

I am also grateful to Genie and Wayne Sorensen for their effort in proof-reading this thesis "on the spot".

Foremost, I am deeply indepted to Heike Quader for giving me three wonderful years, which I enjoyed so much. Whenever I lost focus she encouraged me and helped me to continue the work. Together we enjoyed wonderful times. I just want to say: Thank you for being you.

And last but not least, I wish to thank my family Stefanie, Peter and Philipp Lange for just being there and being the way they are. Furthermore, I would like to thank Karin Beth for consulting concerning layout.

I would also like to express my gratitude to all of my friends who gave me the necessary support over all these years and to all the people that I unintentionally forgot to mention.

Heidelberg, April 2004

Curriculum Vitae

Personal

Name: Sebastian A. Lange

Address: Hagenstraße 6
69126 Heidelberg
Germany

Date of Brith: 17.02.1974

Place of Birth: Tübingen, Germany

Nationality: German

Education

1981 - 1984   Primary school in Tübingen, Germany

1984 - 1993   Secondary school at the **Amos Comenius Gymnasium** Bonn, Germany, graduated with "Abitur".

1994 - 2000   Diplomastudy of Physics at the **University of Heidelberg**, Germany

                     Master's thesis at the **European Molecular Biology Laboratory (EMBL)** and **Max Planck Institut for.med. Research** in Heidelberg under the supervision of Prof. J.K.H. Hörber; "*Measurement of specific molecular interaction forces in the single molecule experiment performed with the atomic force microscope*". Graduated with Master's degree in physics.

1997 - 1998   Study at the **University of Massachusetts at Amherst (UMASS)**, USA.

1998 - 1999   Research assistant at the University Heidelberg, Department of Applied Physics

2001 - 2004   PhD at the **University of Tübingen, Department of Applied Physics** and at the **European Molecular Biology Laboratory (EMBL) at Heidelberg, Cell Biology and Biophysics Programm** under the supervision of Professor D. Kern and Dr. A. Bernard. Thesis title: "*Softlithography applied to the construction of a low-cost bioassay system*".

2001 - 2002   Research assistant at **LifeBits AG**, Tübingen.

2002 - 2004   Cofounder and research associate of **Indigon GmhH**, Tübingen.

Publications and Posters

Lange, S. A., Benes, V., Kern, D. P., Horber, J. K., Bernard, A. <u>Anal Chem</u> **2004**, *76*, 1641-1647. *Microcontact printing of DNA molecules*

Lange, S.A., Benes, V., Kern, D. P., Horber, J. K., Bernard, A.; *Microcontact Printing of DNA*; 3. Biosensor Symposium; Potsdam; 2003; Poster

Academic teachers

Prof. D. Kern, Dr. A. Bernard, Prof. J.K.H. Hörber, Prof. D. Manstein, Prof. D. Dübel, Prof. J. Bille, Prof. D. Gromes, Prof. D. Schwalm, Prof. R.H.A. Fink, Prof. S. Hunklinger, Prof. A. Brandis, Prof. H.J. Keller, Prof. H.G. Dosch

Selbständigkeitserklärung

Hiermit erkläre ich, daß ich diese Arbeit selbständig, und nur mit den angegebenen Hilfsmitteln angefertigt habe. Alle Stellen, die dem Wortlaut oder dem Sinne nach anderen Werken entnommen sind, habe ich durch Angabe der Quellen kenntlich gemacht. Weiterhin versichere ich, daß die vorliegende Arbeit bisher nirgendwo in dieser oder ähnlicher Form für ein anderes Promotionsverfahren eingereicht wurde.

Sebastian Lange